

**PERFORMANCE OF SHAPE MEMORY ALLOY REINFORCED
CONCRETE FRAMES UNDER EXTREME LOADS**

by

Moniruzzaman Moni

B.Sc., Bangladesh University of Engineering & Technology, 2004

A THESIS SUBMITTED IN PARTIAL FULFILLMENT
OF THE REQUIREMENTS FOR THE DEGREE OF

MASTER OF APPLIED SCIENCE

in

The College of Graduate Studies
(Civil Engineering)

THE UNIVERSITY OF BRITISH COLUMBIA
(Okanagan)

MAY 2011

© Moniruzzaman Moni, 2011

ABSTRACT

Reinforced concrete (RC) frame structures are commonly used in various parts of the world for resisting lateral loads. Over the last few decades, the influence of extreme loads on structures has received much attention by researchers and practicing engineers. In RC structures steel is mainly used as reinforcing material where its major setback is associated with a high residual deformation after yielding during an extreme load event, which may often result in structural collapse or substantial damages to the structure. Superelastic shape memory alloy (SMA) is a special material, which has the ability to undergo large deformation and recover its shape upon unloading. In the present study, a numerical investigation has been carried out to determine the potential application of SMA rebar in improving the performances of reinforced concrete (RC) frames under extreme loads.

Nine RC ductile moment-resisting frames of different stories (3, 6 and 8) designed as per CSA A23.3 located in western Canada are taken into consideration. For each storey type, three different reinforcement detailings have been considered, namely: i) steel reinforcement only (Steel RC); ii) SMA rebar used in the plastic hinge region of the beams and steel rebar in other regions (Steel-SMA RC); and iii) the beams fully reinforced with SMA rebar (SMA RC). For all 3 cases, the columns were reinforced with steel rebars. Nonlinear static pushover analyses, nonlinear incremental dynamic and linear dynamic time history analyses were performed on these buildings to determine the overstrength factor (R_o), ductility reduction factor (R_d) and the response modification factor (R) of the considered buildings. In addition, the supply and demand of the ductility reduction factor were also compared with different frame types. The results indicated that the code proposed response modification factors can be used for the SMA and Steel-SMA RC frames. Seismic vulnerability of the considered frames are also evaluated in terms of peak global roof drift, maximum inter-story drift, maximum residual roof drift and maximum residual inter-storey drift, which are considered as critical response parameters. In addition, the progressive collapse performances of the considered frames have been evaluated as per the General Service Administration (GSA, 2003) guideline by performing linear and nonlinear static and dynamic, analyses. The results showed that the performance of the Steel RC frame is better compared to that of the SMA RC frame under progressive collapse.

TABLE OF CONTENTS

ABSTRACT.....	ii
TABLE OF CONTENTS	iii
LIST OF TABLES	vi
LIST OF FIGURES.....	viii
LIST OF NOTATIONS.....	xiii
ACKNOWLEDGEMENTS	xv
CHAPTER 1 : INTRODUCTION AND THESIS ORGANIZATION	1
1.1 GENERAL	1
1.2 OBJECTIVES OF THE STUDY	3
1.3 SCOPE OF THE RESEARCH.....	3
1.4 THESIS ORGANIZATION	5
CHAPTER 2 : LITERATURE REVIEW.....	8
2.1 GENERAL	8
2.2 SPECIAL PROPERTIES OF SMA.....	10
2.2.1 Shape memory effect (<i>SME</i>).....	10
2.2.2 Superelasticity or pseudo elasticity (<i>PE</i>).....	11
2.2.3 Characteristics under repetitive or cyclic loading	12
2.3 MECHANICAL PROPERTIES OF SMAs.....	15
2.3.1 Behavior under tension and compression.....	15
2.3.2 Torsion and shear behaviour.....	18
2.4 CONSTITUTIVE MATERIAL MODELLING OF SMAs.....	18
2.4.1 Phenomenological modelling	19
2.4.2 Thermodynamics-based modelling.....	20
2.5 USES OF SMAs	21
2.5.1 SMAs in new constructions.....	21
2.5.1.1 Reinforcing bars in concrete structures	21
2.5.1.2 Bracing members.....	23
2.5.1.3 Joint connectors	24
2.5.1.4 Prestressed concrete.....	25

2.5.1.4.1 Pre-tensioning.....	25
2.5.1.4.2 Post-tensioning	26
2.5.2 SMA in retrofitting of existing structures.....	27
2.5.2.1 Bracing members.....	27
2.5.2.2 Prestressing.....	28
2.5.2.3 Dampers.....	29
2.6 LIMITATION OF USING SMAs.....	30
CHAPTER 3 : RESPONSE MODIFICATION FACTOR OF CONCRETE BUILDINGS REINFORCED WITH SHAPE MEMORY ALLOY (SMA) REBAR	31
3.1 GENERAL	31
3.2 RESPONSE MODIFICATION FACTOR	35
3.3 PROPERTIES OF SHAPE MEMORY ALLOYS AND ITS MODELLING.....	37
3.4 DESIGN OF FRAME STRUCTURES	38
3.5 ANALYTICAL MODEL	46
3.6 PUSHOVER ANALYSIS	47
3.7 DYNAMIC TIME-HISTORY ANALYSIS	52
3.8 RESULTS AND DISCUSSIONS	55
3.8.1 Response modification factor (R) supply	55
3.8.2 Response modification factor (R) demand	59
3.8.3 Ductility reduction factor (R_d) supply-demand ratio	61
3.9 SUMMARY	62
CHAPTER 4 : SEISMIC VULNERABILITY ASSESSMENT OF SHAPE MEMORY ALLOY REINFORCED CONCRETE FRAMES	63
4.1 GENERAL	63
4.2 DESIGN OF THE BUILDINGS AND ITS ANALYTICAL MODELING	66
4.2.1 Design of the building	66
4.2.2 Analytical modeling of the building.....	67
4.3 EIGEN VALUE ANALYSIS.....	67
4.4 SELECTION OF GROUND MOTION RECORDS AND ANALYSIS CHARACTERISTICS	68
4.5 RESULTS AND DISCUSSIONS	68
4.5.1 <i>IDA</i> curves for roof drift.....	70

4.5.2	IDA curves for maximum inter-storey drift	76
4.5.3	IDA curves for residual roof drift	81
4.5.4	IDA curves for maximum residual inter-storey drift	87
4.5.5	Inelastic distribution along height of the frame	92
4.6	SUMMARY	97
CHAPTER 5 : PERFORMANCE OF SHAPE MEMORY ALLOY REINFORCED CONCRETE		
	FRAME UNDER PROGRESSIVE COLLAPSE	98
5.1	GENERAL	98
5.2	PREVIOUS WORK	100
5.3	PROGRESSIVE COLLAPSE ANALYSIS METHOD	103
5.4	FRAME CHARACTERISTICS AND MODELLING	104
5.5	PROGRESSIVE COLLAPSE ANALYSES	106
5.5.1	Linear static analyses	108
5.5.2	Nonlinear static analyses	112
5.5.3	Linear dynamic analyses	115
5.5.4	Nonlinear dynamic analyses	118
5.5.4.1	Vertical displacement	121
5.5.4.2	Variation of axial forces	123
5.5.4.3	Variation of maximum shear forces	127
5.6	PERFORMANCE COMPARISON AMONG DIFFERENT ANALYSES TECHNIQUES	128
5.7	SUMMARY	131
CHAPTER 6 : CONCLUSIONS		
6.1	SUMMARY	132
6.2	LIMITATIONS OF THIS STUDY	132
6.3	CONCLUSIONS	133
6.4	RECOMMENDATIONS FOR FUTURE RESEARCH	139
BIBLIOGRAPHY		141

LIST OF TABLES

Table 2.1 Mechanical properties of Ni-Ti alloy (taken from Alam et al., 2007 with permission).....	16
Table 3.1 Material properties used in the finite element program.....	39
Table 3.2 Column size and reinforcement arrangements.	41
Table 3.3 Beam reinforcement details.....	42
Table 3.4 Fundamental period of the structure.....	45
Table 3.5 Seismic overstrength factor and ductility of different frames.	48
Table 3.6 Ensemble of ground motion records.....	54
Table 3.7 Elastic base shear V_e	55
Table 3.8 Response modification factor (R) supply.	56
Table 4.1 Fundamental Period and design spectral acceleration of the structure.....	67
Table 4.2 Summary of maximum roof drift at design level intensity.....	76
Table 4.3 Summary of maximum inter-storey drift at design level intensity	81
Table 4.4 Summary of maximum residual roof drift at design level intensity.	83
Table 4.5 Summary of residual maximum inter-storey drift at design level intensity	88
Table 5.1 Response Limit.....	107
Table 5.2 DCR values for corner column removal from linear static analyses.	109
Table 5.3 DCR values for exterior bay intermediate column removal for linear static analyses.	111
Table 5.4 Ductility and support rotation due to corner column removal from nonlinear static analyses..	112
Table 5.5 Ductility and support rotation due to exterior bay intermediate column removal from nonlinear static analyses.....	113
Table 5.6 DCR values for corner column removal from linear dynamic analyses.....	116
Table 5.7 DCR values for exterior bay intermediate column removal from linear dynamic analyses.	117
Table 5.8 Ductility and support rotation due to corner column removal from nonlinear dynamic analyses.	119
Table 5.9 Ductility and support rotation due to intermediate column removal from dynamic analyses...	119
Table 5.10 Ratio of the maximum axial force to its initial condition in column B1 due to corner column removal.	129
Table 5.11 Ratio of the maximum axial force to its initial condition in column B1 due to an exterior bay intermediate column removal.....	129
Table 5.12 Ratio of the beam maximum shear force to its initial condition due to corner column removal.	130

Table 5.13 Ratio of the beam maximum shear force to its initial condition due to an exterior bay intermediate column removal.....	130
--	-----

LIST OF FIGURES

Figure 1.1 Flow chart of analytical research	4
Figure 2.1 Stress-strain curve for SMA exhibiting the SME.....	11
Figure 2.2 Stress-strain hysteresis for superelastic SMA.	12
Figure 2.3 Typical stress-strain curve of superelastic SMA under cyclic (a) axial, (b) shear and (c) torsion forces (Adapted from Dolce and Cardone, 2001b; Vivet et al., 2001; Dolce and Cardone, 2001a).	14
Figure 2.4 Typical stress-strain curve of martensite SMA under cyclic (a) axial and (b) torsion forces (Adapted from Liu et al., 1999; Dolce and Cardone, 2001a).....	14
Figure 2.5 Typical stress-strain curve of SMA under tension/compression (Adapted from Alam et al., 2007).	17
Figure 2.6 Typical stress-strain curve of SMA under shear/torsion (Adapted from Alam et al, 2007).	18
Figure 2.7 1D-Superelastic model of SMA incorporated in FE Packages Seismostruct (2010).	20
Figure 3.1 The relationships between force reduction factors (R), overstrength (R_o), ductility reduction factor (R_d), and displacement ductility factor (μ). (Adapted from Mwafy and Elnashai, 2002).	36
Figure 3.2 Comparison between the ductility reduction factor (R_d) and the definition of R_d , supply (Adapted from Mwafy and Elnashai, 2002).....	37
Figure 3.3 Stress-strain behaviour of superelastic SMA and Steel.	38
Figure 3.4 Building geometry (a) plan, (b) elevation of 3-storey, (c) elevation of 6-storey and (d) elevation of 8-storey buildings.....	40
Figure 3.5 Typical longitudinal section of beam reinforcement.....	42
Figure 3.6 Moment curvature relationship for (a) B1 of 3-storey frame (b) Section 1-1 and 2-2 for beam B1 for both 6-and 8-storey frame, (c) Section 3-3 for beam B1 for both 6 and 8-storey frame and (d) beam B2 for both 6 and 8-storey frame.	44
Figure 3.7 Flexural strength versus reinforcement ratio of a singly reinforced concrete beam having cross-sections of (a) 300mm x 450mm and (b) 300mm x 500mm.....	45
Figure 3.8 Pushover curve for (a) 3-storey, (b) 6-storey and (c) 8-storey frame.....	49
Figure 3.9 Inter-storey drift distribution for (a) 3-storey, (b) 6-storey and (c) 8-storey frame.	50
Figure 3.10 Variation of spectral acceleration with period of structure.	53
Figure 3.11 Over-strength factor, R_o	57
Figure 3.12 Ductility reduction factor (R_d) supply.	58
Figure 3.13 Response modification factor (R) supply.	59

Figure 3.14 Ductility reduction factor (R_d) demand.	60
Figure 3.15 Response modification factor (R) demand.	61
Figure 3.16 Ductility reduction factor (R_d) supply-demand ratio.	61
Figure 4.1 <i>IDA</i> curves of “first mode” spectral acceleration, $S_a(T_1, 5\%)$, plotted against peak roof drift ratio θ_{roof} , for 3-storey (a) SMA RC, (b) Steel-SMA RC, (c) Steel RC frames; 6-storey (d) SMA RC, (e) Steel-SMA RC, (f) Steel RC frames; and 8-storey (g) SMA RC, (h) Steel-SMA RC, (i) Steel RC frames.	73
Figure 4.2 <i>IDA</i> curves of peak ground acceleration (<i>PGA</i>), plotted against peak roof drift ratio, θ_{roof} , for 3-storey (a) SMA RC, (b) Steel-SMA RC, (c) Steel RC frames; 6-storey (d) SMA RC, (e) Steel-SMA RC, (f) Steel RC frames; and 8-storey (g) SMA RC, (h) Steel-SMA RC, (i) Steel RC frames.	74
Figure 4.3 Summary of maximum roof-drift <i>IDA</i> curves into 16 th , 50 th , and 84 th fractile, for the 3-storey (a) SMA RC, (b) Steel-SMA RC, (c) Steel RC frames; 6-storey (d) SMA RC, (e) Steel-SMA RC, (f) Steel RC frames; and 8-storey (g) SMA RC, (h) Steel-SMA RC, (i) Steel RC frames.	75
Figure 4.4 <i>IDA</i> curves of “first mode” spectral acceleration, $S_a(T_1, 5\%)$, plotted against maximum inter-storey drift ratio, θ_{max} , for 3-storey (a) SMA RC, (b) Steel-SMA RC, (c) Steel RC frames; 6-storey (d) SMA RC, (e) Steel-SMA RC, (f) Steel RC frames; and 8-storey (g) SMA RC, (h) Steel-SMA RC, (i) Steel RC frames.	78
Figure 4.5 <i>IDA</i> curves of peak ground acceleration (<i>PGA</i>), plotted against maximum inter-storey drift ratio, θ_{max} , for 3-storey (a) SMA RC, (b) Steel-SMA RC, (c) Steel RC frames; 6-storey (d) SMA RC, (e) Steel-SMA RC, (f) Steel RC frames; and 8-storey (g) SMA RC, (h) Steel-SMA RC, (i) Steel RC frames.	79
Figure 4.6 Summary of maximum inter-storey drift <i>IDA</i> curves into 16 th , 50 th , and 84 th fractile for 3-storey (a) SMA RC, (b) Steel-SMA RC, (c) Steel RC frames; 6-storey (d) SMA RC, (e) Steel-SMA RC, (f) Steel RC frames; and 8-storey (g) SMA RC, (h) Steel-SMA RC, (i) Steel RC frames.	80
Figure 4.7 <i>IDA</i> curves of “first mode” spectral acceleration, $S_a(T_1, 5\%)$, plotted against residual roof drift ratio, θ_{rroof} for 3-storey (a) SMA RC, (b) Steel-SMA RC, (c) Steel RC frames; 6-storey (d) SMA RC, (e) Steel-SMA RC, (f) Steel RC frames; and 8-storey (g) SMA RC, (h) Steel-SMA RC, (i) Steel RC frames.	84
Figure 4.8 <i>IDA</i> curves of peak ground acceleration (<i>PGA</i>), plotted against residual roof drift ratio, for 3-storey (a) SMA RC, (b) Steel-SMA RC, (c) Steel RC frames; 6-storey (d) SMA RC, (e) Steel-	

SMA RC, (f) Steel RC frames; and 8-storey (g) SMA RC, (h) Steel-SMA RC, (i) Steel RC frames.....	85
Figure 4.9 Summary of residual roof drift <i>IDA</i> curves into 16 th , 50 th , and 84 th fractile 3-storey (a) SMA RC, (b) Steel-SMA RC, (c) Steel RC frames; 6-storey (d) SMA RC, (e) Steel-SMA RC, (f) Steel RC frames; and 8-storey (g) SMA RC, (h) Steel-SMA RC, (i) Steel RC frames.	86
Figure 4.10 <i>IDA</i> curves of “first mode” spectral acceleration, $S_a(T_1, 5\%)$, plotted against maximum residual inter-storey drift ratio, for 3-storey (a) SMA RC, (b) Steel-SMA RC, (c) Steel RC frames; 6-storey (d) SMA RC, (e) Steel-SMA RC, (f) Steel RC frames; and 8-storey (g) SMA RC, (h) Steel-SMA RC, (i) Steel RC frames.....	89
Figure 4.11 <i>IDA</i> curves of peak ground acceleration, (<i>PGA</i>), plotted against maximum residual inter-storey drift ratio for 3-storey (a) SMA RC, (b) Steel-SMA RC, (c) Steel RC frames; 6-storey (d) SMA RC, (e) Steel-SMA RC, (f) Steel RC frames; and 8-storey (g) SMA RC, (h) Steel-SMA RC, (i) Steel RC frames.....	90
Figure 4.12 Summary of maximum residual inter-storey drift <i>IDA</i> curves into 16 th , 50 th , and 84 th fractile for 3-storey (a) SMA RC, (b) Steel-SMA RC, (c) Steel RC frames; 6-storey (d) SMA RC, (e) Steel-SMA RC, (f) Steel RC frames; and 8-storey (g) SMA RC, (h) Steel-SMA RC, (i) Steel RC frames.	91
Figure 4.13 Peak inter-storey drift along the height of the 3-storey frames under selected ground motion records at different intensity levels, for SMA RC (a) $S_a = 0.7$ g, (b) $S_a = 1.4$ g, (c) $S_a = 2.1$ g; for Steel-SMA RC (d) $S_a = 0.71$ g, (e) $S_a = 1.42$ g, (f) $S_a = 2.13$ g and for Steel RC (g) $S_a = 0.72$ g, (h) $S_a = 1.44$ g, (i) $S_a = 2.16$ g.	93
Figure 4.14 Peak inter-storey drift along the height of the 6-storey frames under selected ground motion records at different intensity levels for SMA RC (a) $S_a = 0.47$ g, (b) $S_a = 0.94$ g, (c) $S_a = 1.41$ g; for Steel-SMA RC (d) $S_a = 0.49$ g, (e) $S_a = 0.98$ g, (f) $S_a = 1.47$ g; and for Steel RC (g) $S_a = 0.51$ g, (h) $S_a = 1.02$ g, (i) $S_a = 1.53$ g.	94
Figure 4.15 Peak inter-storey drift along the height of the 8-storey frames under selected ground motion records at different intensity levels, for SMA RC, (a) $S_a = 0.33$ g, (b) $S_a = 0.66$ g, (c) $S_a = 0.99$ g.; for Steel-SMA RC, (d) $S_a = 0.35$ g, (e) $S_a = 0.70$ g, (f) $S_a = 1.05$ g.; for Steel RC, (g) $S_a = 0.39$ g, (h) $S_a = 0.78$ g, (i) $S_a = 1.17$ g.	95
Figure 4.16 Median peak inter-storey drift ratios for all storey levels at different ground motion intensities, for 3-storey (a) SMA RC, (b) Steel-SMA RC, (c) Steel RC; for 6-storey (d) SMA RC, (e) Steel-SMA RC, (f) Steel RC; for 8-storey (g) SMA RC, (h) Steel-SMA RC, (i) Steel RC.	96
Figure 5.1 Definition of progressive collapse of a structure (Adapted from GSA 2003).....	103

Figure 5.2 Configuration of building geometry: (a) Plan, (b) Elevation of 3-storey, (c) Elevation of 6-storey and (d) Elevation of 8-storey building.	105
Figure 5.3 Typical column removal for 8-storey (a) exterior bay corner column and (b) exterior bay intermediate column.....	108
Figure 5.4 Comparison of <i>DCR</i> values due to (a) corner column removal and (b) exterior bay interior column removal from linear static analyses.....	111
Figure 5.5 Comparison of ductility from nonlinear static analyses due to (a) corner column removal, and (b) exterior bay intermediate column removal.....	114
Figure 5.6 Comparison of rotation due to (a) corner column removal, and (b) exterior bay intermediate column removal.	114
Figure 5.7 Time history loading (reaction at removed column) for linear and nonlinear dynamic analyses.	115
Figure 5.8 Comparison of <i>DCR</i> values from linear dynamic analyses due to (a) corner column removal, and (b) exterior bay intermediate column removal.....	118
Figure 5.9 Comparison of ductility due to (a) corner column removal, and (b) exterior bay intermediate column removal.	120
Figure 5.10 Comparison of rotation due to (a) corner column removal, and (b) exterior bay intermediate column removal.	120
Figure 5.11 Vertical displacement of the point at which the bottom storey column is removed from 3-storey frames due to: (a) corner column removal, and (b) exterior bay intermediate column removal.	122
Figure 5.12 Vertical displacement of the point at which the bottom storey column is removed from 6-storey frames due to: (a) corner column removal, and (b) exterior bay intermediate column removal.	122
Figure 5.13 Vertical displacement of the point at which the bottom storey column is removed from 8-storey frames due to: (a) corner column removal, and (b) exterior bay intermediate column removal.	123
Figure 5.14 Column axial force variation adjacent to the removed column (bottom storey B1) for 3-storey frames due to: (a) corner column removal, and (b) exterior bay intermediate column removal.	124
Figure 5.15 Column axial force variation adjacent to the removed column (bottom storey of B1) for 6-storey frames due to: (a) corner column removal, and (b) exterior bay intermediate column removal.	124

Figure 5.16 Column axial force variation adjacent to the removed column (bottom storey of B1) for 8-storey frame due to (a) corner column removal, and (b) exterior bay intermediate column removal.	125
Figure 5.17 Variation of axial forces in column B1 due to: (a) corner column removal from 3 storey, (b) intermediate column removal from 3-storey, (c) corner column removal from 6-storey, (d) intermediate column removal from 6-storey, (e) corner column removal from 8-storey, and (f) intermediate column removal from 8-storey frames.	126
Figure 5.18 Shear forces in beams for 3 storey frames due to: (a) corner column removal, and (b) exterior bay intermediate column removal.	127
Figure 5.19 Shear forces in beams for 6 storey frames due to: (a) corner column removal, and (b) exterior bay intermediate column removal.	127
Figure 5.20 Shear forces in beams for 8 storey frames due to: (a) corner column removal, and (b) exterior bay intermediate column removal.	128

LIST OF NOTATIONS

A_f	Austenite finishing temperature
A_s	Austenite starting temperature
DCR	Demand- capacity ratio
DP	Demand parameter
E_y	Young's modulus
f_y	Yield strength under tension or compression
f_{PI}	Maximum recovery stress
f_{P1}	Austenite-to-martensite finishing stress
f_{T1}	Martensite-to-austenite starting stress
f_{T2}	Martensite-to-austenite finishing stress
f_u	Ultimate strength
G_y	Shear modulus
IDA	Incremental dynamic analysis
IM	Intensity measures
PE	Superelasticity
PGA	Peak ground acceleration
PGV	Peak ground velocity
R	Seismic response modification factor
R_d	Ductility reduction factor
R_o	Over strength factor
S_a	Spectral acceleration
T	Temperature/ Fundamental period of the structure
V_d	Design base shear
V_e	Elastic base shear
V_y	Actual lateral strength
SME	Shape memory effects
σ	Stress
ε	Strain

μ	Ductility
ε_y	Elastic strain
ε_u	Elongation at failure
ε_{pl}	Recovered pseudo-elastic strain
τ_y	Yield strength under Shear
τ_u	Ultimate strength
τ_{pl}	Maximum recovery stress under shear
Δ_{max}	Maximum roof displacement
Δ_y	Yield roof displacement
Φ	Coefficient reflecting soil condition

ACKNOWLEDGEMENTS

The author wishes to convey his profound gratitude to the almighty Allah for allowing him to bring this effort to realization. The study was commencing under the supervision of Dr. M. Shahria Alam, Assistant Professor, School of Engineering, The University of British Columbia, Kelowna, BC, Canada. His systematic direction and continuous persuasion has greatly facilitated the author throughout this work. The author honestly acknowledges his heartiest appreciation and indebtedness to him for his advanced technical capability.

The author also pays his innermost homage to his parents, whom he deems to be key source of inspiration for all his achievement.

Dedicated To My Parents Musammat Selina Khatun and Sarder

Abul Hossain

CHAPTER 1: INTRODUCTION AND THESIS ORGANIZATION

1.1 GENERAL

Buildings are one of the most common and important civil engineering structures, which are usually made from reinforced concrete (RC), steel or wood. Every year buildings are subjected to extreme types of loads such as earthquakes, blast loads, accidental fires, terrorist attacks and accidental car loads. Therefore when a reinforced concrete (RC) structures are subjected to extreme loads, the energy is dissipated through yielding of reinforcement and inelastic deformation. Conventional structures are designed mainly for life safety. Although this will ensure the life safety, the structure may undergo excessive deformation inducing severe damages, which may result in collapse or make the structure unserviceable causing substantial economic losses.

In the present day mild steel is used as a reinforcing material for reinforced concrete structures. The main problem associated with mild steel is its post-elastic high residual strain under extreme loads and its high susceptibility to corrosion. In lieu of steel as reinforcement, another robust material considered in this present study is Shape Memory Alloy (SMA), which has the ability to come back to its original position after the removal of loads and also has high resistance to corrosion. The mechanical properties of its material play an important role when a structure is subjected to extreme loads. With the advanced knowledge of science and technology, and a better understanding of the microstructure as well as the thermo-mechanical treatment procedures to control the materials behaviour the field of material science has significantly improved in the past decades. Shape Memory Alloy (SMA) is a distinctive class of shape memory materials with the capability to recover the shape of the material when the temperature is raised. A rise in temperature can result in

shape recovery even under large applied loads therefore, resulting in high actuation energy densities (Kumar and Lagoudas, 2008). Under particular conditions, the SMAs can absorb and dissipate mechanical energy by undergoing a reversible hysteretic shape change when subjected to mechanical cyclic loading. These distinctive characteristics of SMAs attracted scientists, researchers and engineers. The applications of SMAs are spread widely over many industrial sectors, such as aerospace, automotive, biomedical, and oil exploration. Over the last few decades, numerous researchers have investigated the microstructural mechanisms, engineering effects, and applications of shape memory alloys. Jackson et al. (1972) have performed experimental work in order to find out the physical metallurgy, the properties and the applications of Nitinol SMAs. Duerig et al. (1990) have explored engineering aspects of the SMA, while Perkins (1975) has discussed the shape memory effect in alloys, and Funakubo (1987) and Otsuka and Wayman (1999) have also done research on SMAs.

The most basic design criteria of structures incorporate the safety of human lives and the serviceability of vital facilities. Recently, the seismic design of structures has evolved towards a performance-based approach (Ghobarah, 2001) where there is a need for new structural members and systems with enhanced deformation capacity and ductility, higher damage tolerance, and/or reduced permanent deformations (Alam et al., 2009). Currently owners and engineers do not want to sacrifice their structures during an extreme event. Research on the use of SMA as reinforcement in reinforced concrete structures exhibited that it can remarkably recover deformations after earthquakes (Saiidi and Wang, 2006). Therefore, SMA rebars might have huge potential to be used in RC structures against extreme load conditions. If such a RC structure can be constructed, this will allow

structural engineers to design with improved ductility, exhibiting little damage, and having reduced post earthquake repairs. This could substantially reduce the infrastructure management costs. It is hypothesized that this can be achieved by using SMAs as reinforcements in the beams of concrete buildings. This research will assess the suitability of this hypothesis by studying the performance of these new generation buildings under extreme load conditions.

1.2 OBJECTIVES OF THE STUDY

The key objectives of the current research include:

1. Evaluate the seismic response modification factor for SMA RC frame and a hybrid Steel-SMA RC frame and compare their performance with that of the Steel RC frame designed according to the current seismic standard (CSA A23.3-04).
2. Determine the seismic vulnerability of the SMA RC and Steel-SMA RC frames and compare their performance in terms of roof drift, maximum inter-storey drift, residual roof drift, and maximum residual inter-storey drift with those of the Steel RC frames designed according to current seismic standards (CSA A23.3-04).
3. Assess the performance of the SMA RC, Steel-SMA RC and Steel RC frames designed according to the current seismic standards (CSA A23.3-04) under progressive collapse.

1.3 SCOPE OF THE RESEARCH

In order to achieve the goals of the study, the properties and different techniques of using SMAs in civil engineering structures were obtained from the literature review. The study presents the state-of-the-art of possible applications of SMA for new construction, as

well as in retrofitting of existing civil engineering structures. The suitability of the use of SMA as reinforcing bars for ductile low-rise to mid-rise moment resisting frame is determined. The procedures to achieve the stated objectives of the study are shown in Figure 1.1.

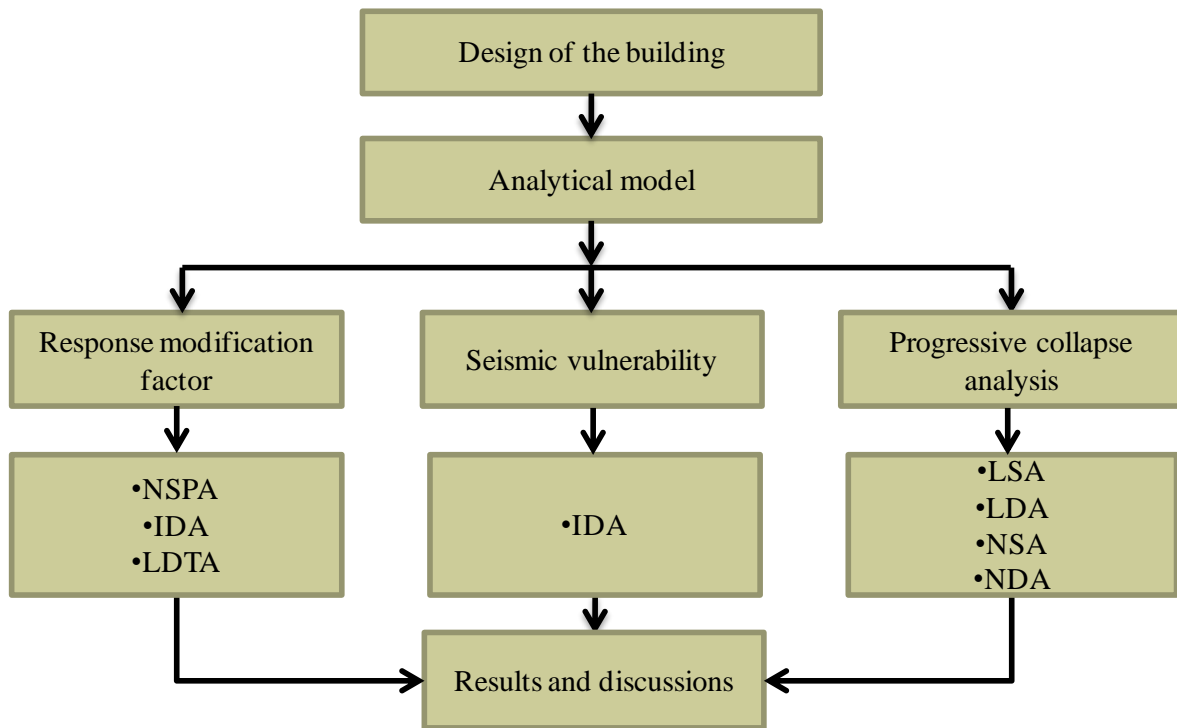


Figure 1.1 Flow chart of analytical research

1. Design of three (3, 6, and 8 storey) ductile moments-resisting reinforced concrete building was done as per NBCC-2005 and CSA A23.3-04 standard.
2. Analytical 2D models were generated by using software Seismostruct (2010) for SMA, Steel-SMA, and Steel RC frames. In the case of SMA RC frame SMA was used as longitudinal reinforcement in the beams, and steel in the other parts of the frames whereas in the case of Steel-SMA RC frame SMA was used only in the

plastic hinge region of the beam and regular steel in other parts of the structures and in the case of Steel RC frame only regular steel is used as reinforcement.

3. The seismic response modification factor (R) supply was computed by performing nonlinear static pushover analyses (NSPA), Incremental dynamic time history analyses (IDA), and linear dynamic time history analyses (LDTA). The response modification factor (R) demand was computed by using empirical equation, and the performance was evaluated in terms of base shear capacity and inter-storey drift capacity.
4. The seismic vulnerability of the SMA RC, Steel-SMA RC and Steel RC frames was evaluated by performing incremental dynamic time history analyses (IDA). Maximum roof drift, maximum inter-storey drift, residual roof drift, and maximum residual inter-storey drift have been considered as the performance indicators.
5. The progressive collapse performance of the seismically designed SMA RC, Steel-SMA RC and Steel RC frames were evaluated as per the General Services Administration (GSA 2003) standard.

1.4 THESIS ORGANIZATION

This thesis is arranged in six chapters. In the present chapter a short preface to the significance of SMAs as reinforcing bars was presented. The following five chapters describe the objectives of the study as per the sequence mentioned in Section 1.2.

In Chapter 2, a thorough literature review on shape memory alloys is presented. This chapter examines the special characteristics and constitutive material models of SMAs, as

well as the factors controlling their engineering properties and their role in civil engineering structures.

In chapter 3, the seismic response modification factor (R) supply and demand, and the performance of the considered buildings are described in terms of base shear capacity and inter-storey drift. The seismic response modification factor plays a significant role for designing any structure. The current NBCC (2005) allows the application of an equivalent static load procedure to calculate the seismic force for regular buildings. In this study, regular plan geometry and three different storeys are considered. To determine the seismic response modification factor supply linear dynamic analyses were performed, followed by the nonlinear incremental dynamic time history analyses. To calculate the seismic response modification factor demand for each frame type, an empirical formula provided by Miranda and Bertero (1994) was used. Finally, the seismic response modification factor (R) supply and demand was compared for SMA RC, Steel-SMA RC and Steel RC frames.

Chapter 4 demonstrates the seismic vulnerability evolution of SMA, Steel-SMA and Steel RC frames. In this study ten earthquake records have been considered to evaluate their seismic vulnerability of these frames. The seismic intensity measurements were expressed in terms of spectral acceleration, (S_a), peak ground acceleration (PGA) and peak ground velocity (PGV) and the demand parameters (DP) were expressed in terms of maximum inter-storey drift, maximum roof drift, maximum residual roof drift, and maximum residual inter-storey drift. Some important guidelines have been recommended in this chapter regarding the seismic vulnerability of SMA RC frames.

Chapter 5 discusses the performance of the SMA RC, Steel-SMA RC and Steel RC frames designed according to the NBCC (2005) and CSA A23.3-04 standard under progressive collapse. The performance indicators here are set as per the GSA (2003) standard. The performances have been evaluated by performing linear static and dynamic as well as non linear static and dynamic analyses techniques.

Finally, Chapter 6 presents the summary and conclusions attained from this research program. Few specific recommendations for future research have also been suggested.

CHAPTER 2: LITERATURE REVIEW

2.1 GENERAL

Reinforced concrete buildings constitute a significant portion of the national wealth in most countries. Under strong earthquakes or extreme loads like blast loads, reinforced concrete buildings may undergo large residual drift, causes permanent deformation and therefore the need for major rehabilitation works. Under these circumstances, building management can become an economic burden. However, if we can replace mild steel with a smart material, which has the ability to reduce the permanent deformation, this will significantly reduce the maintenance costs as well as the post disaster work (Ullakko, 1996). Researchers and scientists are introducing smart materials instead of mild steel as reinforcing bars in reinforced concrete structures, so that they behave like smart structures. Smart structures are those that can automatically adjust their structural characteristics in response to external disturbance and/or unexpected severe loads, to maintain their structural safety, and serviceability thus extending their lifetime (Otani et al., 2000; Alam et al., 2007). To produce such smart structures, the development and introduction of smart materials are mandatory (Song et al., 2006). Some examples of smart materials are shape memory alloys (SMAs), magneto-rheological (MR) fluids, piezoceramics, and electrorheological (ER) fluids (Song et al., 2006).

Shape Memory Alloys (SMAs) are smart materials that have the ability to undergo large deformation and can return to a predetermined shape upon unloading or by heating (Alam et al., 2007). Hardwicke (2003) and Alam et al. (2007) described the special and distinct properties of SMAs that make them smart materials, and explained that they have the

potential to be used in constructing smart structures that can automatically respond and adjust to external disturbance or unexpected severe loading.

Although SMA was first developed in the 1960s, the civil engineering application of SMA has been introduced in the last 15-20 years (DesRoches et al., 2004). SMAs have been used in the fields of medical equipment, aerospace, and different types of industry. In the biomedical industry arterial stents, medical guidewires, catheters, orthodontic braces, and orthopedic prostheses and other devices are made from shape memory alloys (Duerig et al., 1990). In the aerospace industry, to increase the efficiency and reduce the noise and vibration of aircraft wings and helicopter blades, shape memory alloys have been used (Beauchamp, 1992; Chandra, 2001). Besides space technology, SMAs have been used for instance as vibration dampers (Bauer et al., 1998). In addition to these uses, several commercial and consumer uses of shape memory alloys are also well known, such as in cellular telephone antennas, eye glass frames, golf clubs , and frames for brassiers, which all take benefit of the superelastic properties of SMAs (Asai and Suzuk, 2000; Hsu et al., 2000). Shape memory alloys are gradually gaining attraction and finding new applications in all engineering fields such as civil engineering (Norton, 1998; Shirmohamadi ,2005; Jung ,2006). There are several applications of SMAs in the civil engineering field, such applications have been discussed by Janke et al. (2005). The applications of SMAs, especially in the seismic field have been discussed by DesRoches and Smith (2004); Wilson and Wesolowsky (2005); and Song et al. (2006). Wilson and Wesolowsky (2005) and DesRoches and Smith (2004) provide a detailed information of experiments performed by different researchers on the mechanical properties of SMAs. Alam et al. (2007) provided

descriptive information about the mechanical properties of SMAs and their various uses in structural engineering applications.

This chapter covers the mechanical properties of SMAs, various applications of SMAs in the field of civil engineering including its advantages and disadvantages. A general description on the modelling feature of SMAs is also covered in this chapter.

2.2 SPECIAL PROPERTIES OF SMA

Different types of shape memory alloys have been developed in the past decades. The most commonly used SMA is equiatomic Ni-Ti alloy commonly known as Nitinol. Nitinol possesses superior thermo-mechanical and thermo-electrical properties compared to other SMAs (Duerig et al., 1990). In this study, SMAs used are Nitinol based unless otherwise stated. The two most important properties of SMAs are shape memory effects (*SME*) and superelasticity (*PE*). These two properties and performances of the SMAs under cyclic loading make them unique compared to other metals and alloys.

2.2.1 Shape memory effect (*SME*)

At low temperature the SMAs microstructures are in the martensite phase. This phase exits when the temperature is less than the austenite starting temperature, A_s . A residual strain is developed in the martensite SMA when it is deformed outside its elastic point. But if the temperature of the martensite SMA is raised beyond the austenite finishing temperature, A_f , this residual strain is recovered. This phenomenon is well known as the shape memory effect (*SME*), and it can be used to regain strains of up to 8% with minor residual deformation. The stress-strain curve of a SMA that experiences the shape memory effect is shown in Figure 2.1. If the *SME* strain regain is restrained, it is possible to generate

a recovery stress up to 800 MPa (Vokoun and Stalmans, 1999). Maji and Negret (1998) explained that due to the *SME* properties of SMA, this material can be used in prestressing of concrete structures. It can also be used in the deployment of arterial stents used in human arteries (Kuribayashi et al., 2006), and self deploying space structures (Todoroki et al., 2009).

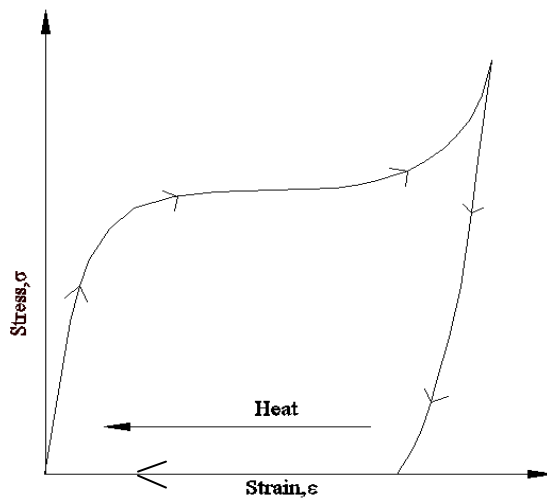


Figure 2.1 Stress-strain curve for SMA exhibiting the *SME*.

2.2.2 Superelasticity or pseudo elasticity (*PE*)

The other distinctive property of SMAs is called superelasticity or pseudo-elasticity (*PE*). This characteristic explains how SMAs at a temperature greater than the austenite finishing temperature (A_f) can be strained to its inelastic range (up to approximately 8%) and upon unloading (at constant temperature) can return to its original shape with no residual strain. Figure 2.2 shows the stress-strain hysteresis for superelastic SMA. The stress-induced transformation of SMAs is highly controlled by the unloading temperature. This unloading temperature also controls the residual martensite phase fraction. From Figure 2.2 it can be observed that the total strain for any phase consists of three

components; elastic strain, transformation strain and finally the plastic strain. When the alloy is either fully in the austenite phase or martensite phase the result is elastic strain. The elastic strain occurs at low strain (<1%) for the austenite phase but for the martensite phase the elastic strain occurs at high strain, which would be greater than 8%. The transformation strain is obtained when the alloy goes through the transformation process. The final stage is the plastic strain, which occurs due to the stress above the martensite yield limit.

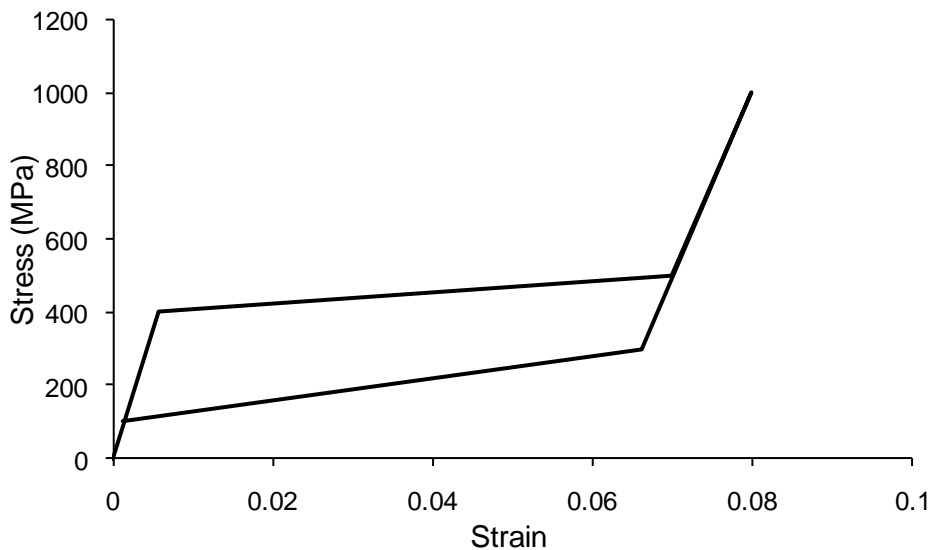


Figure 2.2 Stress-strain hysteresis for superelastic SMA.

2.2.3 Characteristics under repetitive or cyclic loading

The distinctive properties of SMA under cyclic load have made it ideal for different engineering applications. Many researchers have investigated the cyclic properties of SMA under different loading condition such as tension, compression, shear and torsion. The characteristics stress-strain behaviour of SMA under cyclic axial, shear and torsion forces are presented in Figures 2.3 (a), (b) and (c), respectively, for the austenite phase. The stress-strain behaviour of the martensite SMA under cyclic axial and torsion forces is shown in Figures 2.4 (a) and (b), respectively. If the austenite SMA is subjected to a repetitive load it

dissipates a certain amount of energy without permanent deformation. If a load is applied to the martensite SMA, it is yielded at a nearly constant stress after early elastic deformation and shows strain-hardening at larger strains. If the loaded martensite SMA is unloaded, there remains some residual strain even at a zero stress condition. From Figures 2.3 and 2.4 it is stated that the martensite SMA produces a full hysteresis loop around the origin. Since the martensite SMA shows a greater hysteresis loop compared to the austenite SMA, martensite SMA will dissipate higher amount of energy than austenite SMA. From Figure 2.4 it is observed that if the martensite SMA is subjected to cyclic tension and compression, the maximum stress will be achieved in compression at similar strain levels. This is the difference in cyclic hardening and softening process in tension and compression (Liu et al., 1999). Although martensite SMA dissipates a higher amount of energy compared to the superelastic SMA, its main disadvantage is that it is not self-balanced. The performance of the martensite-austenite co-existence phase is better than the individual phase under repeated loads (Ma and Song, 2005). From Figure 2.3 it is observed that under shear stress, the austenite SMA has some residual strain even after the complete removal of the load, which might be due to the existence of some partially stabilized martensite (Orgeas et al., 1997). The hysteresis behaviour of the austenite SMA under the cyclic torsion load depends on the frequency of the applied load, but the martensite SMA is independent of the frequency of the applied load. Under torsion, both austenite and martensite SMA shows highly stable hysteresis (Dolce and Cardone, 2001a).

Normally, under successive loading cycles, the hysteresis loop gradually decreases, and the residual strain increases for the superelastic SMA. As a result, the formation of stress-

induced martensite is facilitated. Miyazaki et al. (1986) mentioned that this behaviour will decrease and stabilize after a large number of cycles.

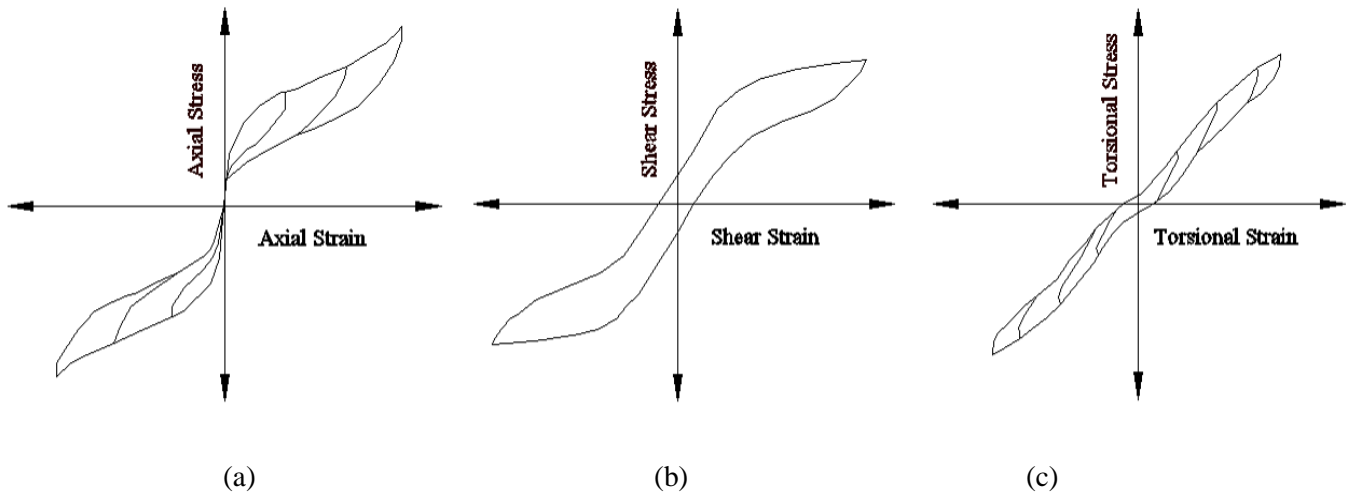


Figure 2.3 Typical stress-strain curve of superelastic SMA under cyclic (a) axial, (b) shear and (c) torsion forces (Adapted from Dolce and Cardone, 2001b; Vivet et al., 2001; Dolce and Cardone, 2001a).

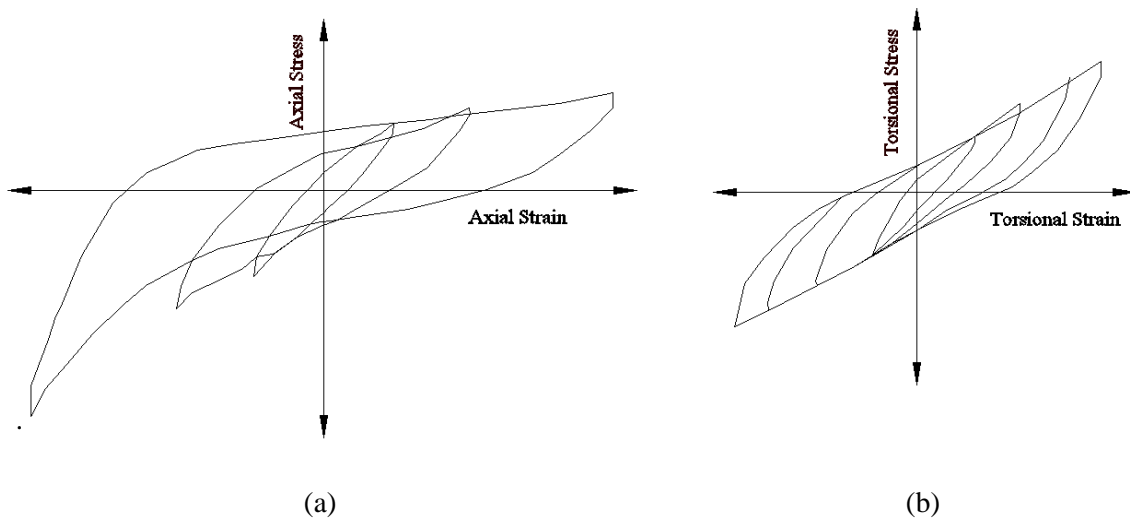


Figure 2.4 Typical stress-strain curve of martensite SMA under cyclic (a) axial and (b) torsion forces (Adapted from Liu et al., 1999; Dolce and Cardone, 2001a).

2.3 MECHANICAL PROPERTIES OF SMAs

SMAs have distinct mechanical properties compared to mild steel. To get the full benefits of such a unique material a better understanding of its mechanical properties is essential. There are different types of SMA and their mechanical properties differ considerably from each other. These properties of SMAs do not depend only on their chemical composition, but also on their atomic arrangement in the martensite and austenite phases. The atomic arrangement depends on the thermo-mechanical processing and heat treatment. At a relatively low temperature SMAs are in the martensite phase, and when heated they are transferred to the austenite phase. For an identical alloy, even a small change in the relative quantity of the constitutive metals may considerably affect the mechanical properties (Strnadel et al., 1995). Researchers have tested different types of SMAs in the form of wires and bars, with various diameters under different loading condition such as tension, compression, torsion and shear forces. Alam et al. (2007) summarized the findings of these test results. The various mechanical properties for the most widely used SMAs (Ni-Ti) summarized by Alam et al. (2007), are presented in Table 2.1.

2.3.1 Behavior under tension and compression

Properties of a material under tensile and compressive loads are important characteristics for any reinforcing material. A typical tensile and compressive stress-strain curve of SMAs is shown in Figure 2.5. This stress-strain curve consists of four different segments. First segment is linear elastic response, and it could be either the austenite or martensite phase. The modulus of elasticity in this phase is E_y and this is maintained until the stress reaches f_y . When the strain increases beyond ϵ_y , stage two begins.

Table 2.1 Mechanical properties of Ni-Ti alloy (taken from Alam et al., 2007 with permission).

Studies	Test types	Property	Phase	Unit	Range
Manach and Favier (1997)	Tension	Young's modulus, E_y	Austenite	GPa	30-98
			Martensite	GPa	21-52
Otsuka and Wayman (1999)		Yield strength, f_y	Austenite	MPa	100-800
			Martensite	MPa	50-300
Mazzolani and Mandara (2002)		Ultimate strength, f_u	Austenite	MPa	800-1900
			Martensite	MPa	800-2000
Rejzner et al. (2002)		Elengation at failure, ϵ_u	Austenite	%	5-50
Martensite			%	20-60	
Zak et al. (2003)		Recovered pseudoelastic strain, ϵ_{pI}	Austenite	%	≤ 8
DesRoches et al. (2004)		Maximum recovery stress, f_{pI}	Austenite	MPa	600-800
	Martensite		MPa	600-800	
Orgeas and Faiver (1995)	Yield strength, f_y	Austenite	GPa	56-69	
		Martensite	GPa	20-80	
Liu et al. (1998)	Ultimate strength, f_u	Austenite	MPa	550-800	
		Martensite	MPa	125-190	
Lim and Mcdowell (1999)	Elengation at failure, ϵ_u	Austenite	%	1500	
		Martensite	%	1800-2120	
Fukuta and Iiba (2002)	Recovered pseudoelastic strain, ϵ_{pI}	Austenite	%	-	
		Martensite	%	17-24	
	Maximum recovery stress, f_{pI}	Austenite	MPa	3-6	
		Martensite	MPa	650-820	
Manach and Favier (1997)	Shear modulus, G_y	Austenite	GPa	18-25	
		Martensite	GPa	25-40	
Liu and Favier (2000)	Yield strength, τ_y	Austenite	MPa	186	
		Martensite	MPa	42-100	
Delgadillo-Holtfort et al. (2004)	Ultimate strength, τ_u	Austenite	MPa	>515	
		Martensite	MPa	<515	
	Elengation at failure, ϵ_u	Austenite	%	≤ 40	
		Martensite	%	≤ 40	
	Recovered pseudoelastic strain, ϵ_{pI}	Austenite	%	3-6	
		Martensite	%	3-6	
	Maximum recovery stress, τ_{pI}	Austenite	MPa	300	
		Martensite	MPa	300	
Melton (1990)	Shear modulus, G_y	Austenite	GPa	6-28	
		Martensite	GPa	4-9	
Lim and Mcdowell (1999)	Yield strength, τ_y	Austenite	MPa	220-350	
		Martensite	MPa	88	
Dolce and Cardone (2001 a)	Ultimate strength, τ_u	Austenite	MPa	>500	
		Martensite	MPa	210-380	
McNaney et al. (2003)	Elengation at failure, ϵ_u	Austenite	%	10->24	
		Martensite	%	-	
	Recovered pseudoelastic strain, ϵ_{pI}	Austenite	%	1-6	
		Martensite	%	1-6	
	Maximum recovery stress, τ_{pI}	Austenite	MPa	270-500	

In this stage two the formation of stress-induced martensite occurs and the modulus of elasticity of the specimen is reduced to 10 to 15% of E_y . The modulus of elasticity for this stage is denoted by E_{P1} . When strain increases beyond ϵ_{P1} , a new stage will be initiated, called stage three. Stage three is the elastic deformation of martensite with indications of slip and dislocation motion. The modulus of elasticity for stage three is denoted as E_{P2} . This modulus of elasticity is 50% to 60% of E_y . The final stage indicates the plastic deformation of the martensite phase, (Ford and White, 1996; and Duerig et al., 1990). The final modulus of elasticity, E_u , is 3% to 8% of E_y and this modulus of elasticity will continue until failure. The length to diameter ratio is reduced in the case of specimens tested under compression, compared to those in tension, in order to avoid buckling. The value of the strains, stresses and young modulus for the Ni-Ti SMA are given in Table 2.1.

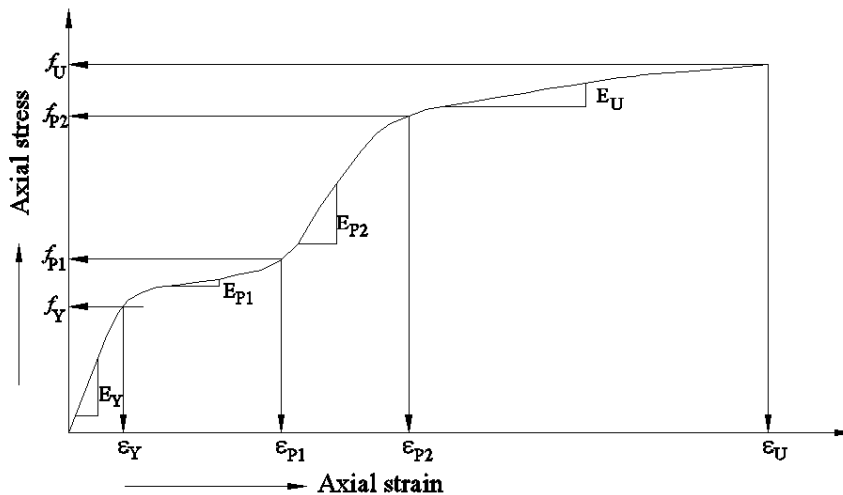


Figure 2.5 Typical stress-strain curve of SMA under tension/compression (Adapted from Alam et al., 2007).

2.3.2 Torsion and shear behaviour

The characteristic stress-strain curve of SMA under torsion and shear forces is shown in Figure 2.6. Similar to the tension/compression curve, it also has four segments. The pattern is also similar to the tension or compression curve. The characteristic parameters of shear stress (τ), shear strain (γ), and shear modulus (G) are denoted by: τ_y , τ_{P1} , τ_{P2} , τ_U , γ_y , γ_{P1} , γ_{P2} , γ_U , G_y , G_{P1} , G_{P2} and G_U . Typical values of these parameters are presented in Table 2.1.

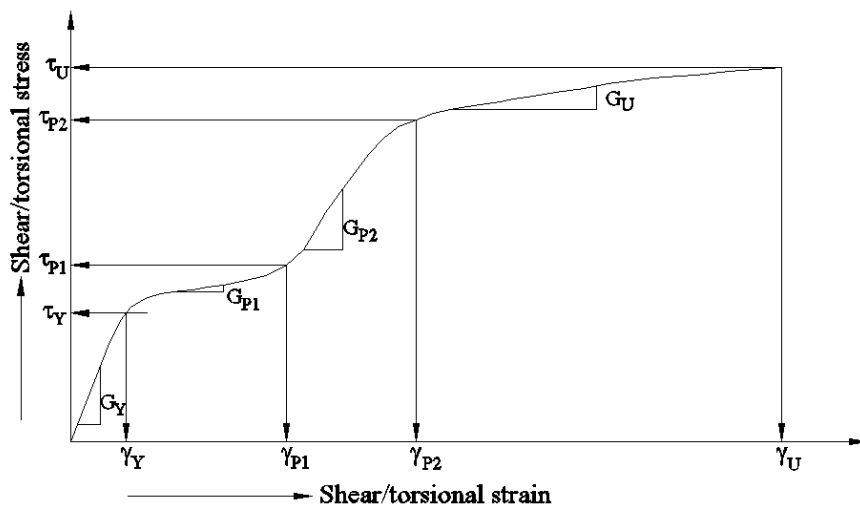


Figure 2.6 Typical stress-strain curve of SMA under shear/torsion (Adapted from Alam et al, 2007).

2.4 CONSTITUTIVE MATERIAL MODELLING OF SMAs

The development of exact and easily understandable constitutive models for SMAs is necessary. The irregular thermo-mechanical characteristics of SMA, with super elasticity and *SME*, have made SMA's constitutive modelling complex. Two very well-known approaches, known as phenomenological and thermodynamics models, are used to model SMA.

2.4.1 Phenomenological modelling

There are several phenomenological theories in the literature and these include: polynomial models, models based on plasticity, models with assumed phase transformation kinetics, and models with internal constraints. Falk (1980) proposes the polynomial model, and considers the temperature-induced first order phase transition combined with hysteresis. Muller and Xu (1991) stated that this model is one-dimensional model and they consider both the superelasticity and *SME* in a simple way. The three-dimensional model using the concepts of kinematics and isotropic hardening was proposed by Bertran (1982). Silva (1995), Souza et al. (1998), and Motta et al. (1999), proposed a model which is able to address the shape memory and pseudo-elastic effects. Auricchio and fellow workers also introduced models using the concepts of kinematics and isotropic hardening. Auricchio and Lubliner (1997) and Auricchio and Sacco (1997) proposed a one-dimensional model to incorporate the analysis in the set of three-dimensional media (Auricchio et al., 1997). Govindjee and Kasper (1997), Leclercq et al. (1995) and Govindjee and Hall (2000) also proposed a phenomenological model for SMA. Tanaka and Nagaki (1982) proposed the first model based on the transformation kinetics. Liang and Rogers (1990), Brinson (1993), Boyd and Lagoudas (1994), and Ivshin and Pence (1994) also proposed a model based on this theory. Possibly, these are the most accepted models to explain SMA behaviour.

Generally civil engineering applications of SMA are associated with the use of bars and wires, so one-dimensional phenomenological models are often considered suitable (Alam et al. 2007). Uniaxial phenomenological models have been proposed by several researchers like Tanaka and Nagaki (1982), Liang and Rogers (1990), Brinson (1993), Auricchio and Lubliner (1997). A number of finite element software, incorporated the superelastic

behaviour of SMA. Auricchio et al. (1997), Auricchio and Taylor (1996), and Auricchio and Sacco (1997) models are implemented in ANSYS 10.0 (ANSYS Inc. 2005), ABAQUS 6.4 (Hibbitt et al. 2003), and Seismostruct (2010), respectively.

The 1-D superelastic SMA model that considered by the software SeismoStruct (2010) are shown in Figure 2.7. Normally, seven model-calibrating parameters must be defined in order to fully describe the mechanical characteristics of the material in SeismoStruct (2010). The seven model-calibrating parameters are the Modulus of elasticity, E_a , austenite-to-martensite starting stress, f_y , austenite-to-martensite finishing stress, f_{P1} , martensite-to-austenite starting stress, f_{T1} , martensite-to-austenite finishing stress, f_{T2} , superelastic plateau strain length, ε_l , and specific weight.

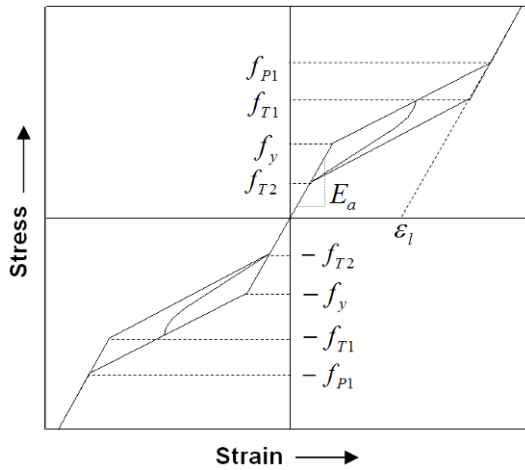


Figure 2.7 1D-Superelastic model of SMA incorporated in FE Packages Seismostruct (2010).

2.4.2 Thermodynamics-based modelling

Several Thermodynamic-based models have been developed by different researchers such as Sun and Hwang (1993), Patoor et al. (1994, 1996), Goo and Lexcellent (1997), and Huang and Brinson (1998) to explain one or more characteristics of SMA.

Phenomenological models are less complicated and less computationally demanding than thermodynamics-based models. But the thermodynamics-based models are more efficient techniques to develop exact three dimensional constitutive models as they are based on the exact examination of the physics of the materials (Brocca et al., 2002).

2.5 USES OF SMAs

The distinctive characteristics of SMAs have received much attention and have been used in many civil engineering structures. In this section, the use of shape memory alloys for newly build civil engineering structures and to rehabilitate the old structures are explored.

2.5.1 SMAs in new constructions

A considerable amount of research has been carried out by various researchers for the use of SMA in building new civil engineering structures. SMA has been used as reinforcing bars, bracings member, joint connectors, and prestressing strands. In the following section SMA for new constructions is discussed.

2.5.1.1 Reinforcing bars in concrete structures

Reinforced concrete buildings and bridges are the most common forms of structures. Under a strong ground motion, these structures are often subjected to a large lateral displacement, which may cause severe damages. It is not economically feasible to design and build such types of structures damage free during an earthquake. In seismic design, steel reinforcement in concrete is expected to yield in order to dissipate energy and thereby is subjected to permanent deformation during strong earthquakes. However when SMAs

are used as reinforcement they will have the ability to undergo large deformations and return to their original shape after an earthquake. Alam et al. (2008) performed an analytical study to compare the performance of SMA and steel reinforced concrete frames under earthquake loads. They considered two eight-storey concrete frames, one of which is reinforced with regular steel and the other with SMAs at the plastic hinge regions of beams and regular steel elsewhere. Their results illustrated that SMA RC frames are able to recover most of their post-yield deformation, even after a strong earthquake. Saiidi and Wang (2006) used SMA as reinforcement in the plastic hinge region of concrete columns, which was subjected to simulated earthquake loads on a shake table. The performance of SMA RC column was found better than that of regular Steel RC column to limit the column top residual drift.

Since SMA rebars or wires have self-restoration capacity, they could be effectively used in bridge decks and girders. To explore this idea, mortar beams reinforced with SMA wires were tested by Sakai et al. (2003). Sakai et al. (2003) performed single-point loading tests and compared the results with regular steel wire beams, by using the same loading conditions. Their study concluded that the beam reinforced with SMA wires could regain ten percent of its maximum deflection. Its deflection was seven times and its ductility was 25% higher than that of beams reinforced with steel wires. Czaderski et al. (2005) also performed tests on beams reinforced with SMA wires and compared their performance with regular steel reinforced beams. Janke et al. (2004) suggested that SMA rebars or wires can be used as prestressing tendons in new concrete structures. Since SMA tendons do not need an anchoring system, the use of SMA tendon can be the unique solution for extremely thin concrete members.

2.5.1.2 Bracing members

Shape memory alloys can be used as a bracing member for both steel and concrete buildings. They can be used either as passive or active bracing members. Active control can be achieved by applying heat to the austenite phase tendons by electrically resisting the structural motion. Passive control can be achieved without applying an electric current through the SMA tendons using superelasticity. Salichs et al. (2001) performed numerical study where on the use of SMA bracings to suppress the vibration of a building structure. They used SMA phenomenological models and applied harmonic load at a base of the one storey building. SMA bracings reduced the building peak displacement compared to that of steel bracing of similar stiffness. Shahin et al. (1997) utilized SMA tendons as bracing members in a building model and analytically evaluated its performance. The numerical results showed that the SMA tendons reduced the relative base displacement as well as the floor displacement. McCormick et al. (2007) performed a numerical study for 3- and 6-storey concentrically braced steel frames. They used SMA and steel bracing members and compared their results in terms of inter-storey drifts and residual drifts during an earthquake and suggested that SMA bracing performed better than steel bracing frames. DesRoches and McCormick (2007) performed a comparative study between conventional steel braced frames and SMA braced frames under cyclic loading, which proved the superiority of SMA braced frames over steel. Sun and Rajapakse (2003) used pre-strained SMA bracing elements in frame structures to improve its performance under harmonic loading. Liao and Mo (2006) used SMA bars as a bracing for one-storey RC frame and performed a shaking table test. They concluded that the use of SMA reduced the inter-storey drift and base shear demand. Tamai and Kitagawa (2002) used SMA bracing and

steel bracing and analytically compared their performance. They concluded that using SMA reduced the response of the frame and the level of damage compared with a steel braced frame. Since the damage can be reduced by using the SMA, consequently the repair cost will be significantly reduced.

2.5.1.3 Joint connectors

The performance of frame structures under cyclic loads can be increased by improving the performance of a beam-column joint and column-foundation joint (Alam et al., 2008). The weakest link in structures under an earthquake load is its connection between a beam-column and column-foundation. If SMA is used in the beam-column and the column-foundation, the connection will dissipate more energy and seismic vulnerability will be substantially reduced (Alam et al. 2008). Youssef et al. (2008) used SMA rebar at the beam-column joint and compared its performance with a regular steel reinforced beam-column joint. They compared the performances in terms of drifts, rotations, and the ability to dissipate energy and concluded that SMA RC beam-column joint is able to recover most of its post-yield deformation. They also concluded that if SMAs are used as reinforcement, it will require a minimum amount of repair even after a strong earthquake. Tamai et al. (2003) used SMA bolts to anchor a steel column connected with a steel base plate and performed pulsating loading tests. The same tests were also performed by using conventional mild steel bolts. The results indicated that the SMA anchoring system improves the restoring force characteristics, which will not require major repair even after a strong earthquake.

2.5.1.4 Prestressed concrete

SMA tendons or wires can be used as an alternative to traditional steel tendons or wires. The benefits of using SMA tendons or wires over conventional tendons or wires include: a) overcoming various prestress losses due to elastic shortening, friction loss, and anchorage loss, and b) no need for jacking and strand cutting. SMA tendons or wires can be used in case of pre-tensioning and post-tensioning of prestressed concrete structures.

2.5.1.4.1 Pre-tensioning

In case of conventional prestressing of concrete, the pretensioning force is applied to the tendon or wires before the casting of concrete where a jacking force is applied to the tendon or wires. Then the jacking force is released once concrete hardens. This release of jacking force may lead to the development of cracks or crushing of concrete at the end sections of the girders, but for the SMA wires or tendons there is no need to apply such anchoring forces, so there is no possibility of cracking or crushing. In case of SMA wires and tendons, the pretensioning force is applied in different techniques. First martensite state wires or tendons are embedded into the concrete and then these wires or tendons are heated by applying an electric current. As a result, it changes its phase from martensite to austenite and produces significant prestressing forces. There have been numerous investigations on prestressed concrete using shape memory alloys. Maji and Negret (1998) were the first researchers who tested a prestressing concrete beam by using SMA strands. In this study, the strands were first elongated beyond their plastic limit and then embedded in model concrete beams. Two SMA prestressed beams of rectangular shape having dimensions 305mm cm x 25 mm x 13 mm were considered in their study and they also used 0.64mm

SMA strands. The test results indicated that the amount of prestressing can be adjusted as required. Following Maji and Negret (1998), Deng et al. (2003, 2006) also tested prestressed concrete beams using SMA wires, which showed the effect of applying a variable initial pre-straining force using SMA wires. The modes of activating electrical current and the actuation times on the behaviour of prestressed beams were also investigated and the test results indicated that SMA improved the performance.

2.5.1.4.2 Post-tensioning

The conventional approach of post-tensioning is that prestressed force is applied against the hardened concrete by stretching the tendon. This procedure includes anchoring, jacking, and tendon cutting that create friction loss and anchorage losses. When SMA tendons or wires are used in post-tensioned prestressed concrete, the techniques of post-tensioning are completely different. In that case, pre-stretched SMA strands/tendons in the martensite phase are passed through post-tensioning ducts after maturing of concrete, and a post-tensioning force is applied by heating. In this system, anchoring is required, but there is no need to apply jacking forces. Therefore, there are no prestressing losses due to jacking and friction. Prestressing losses due to elastic shortening, creep, and shrinkage are also negligible, and prestressing with SMA bars can overcome those losses by heating when required. El-Tawil and Ortega-Rosales (2004), and Sawaguchi et al. (2006) observed different experimental aspects of the post-tensioning procedure and concluded that significant prestressing forces can be achieved through post-tensioning SMA bars. Moser et al. (2005) suggest that embedment of SMA fibres for thin walled and small tension stress is suitable. First, the SMA fibres were stretched and then embedded into the concrete mix at a

low temperature and finally heating the composite for tensioning. This procedure is known as activation prestressing.

2.5.2 SMA in retrofitting of existing structures

Retrofitting or strengthening of civil engineering structures is very common. The reasons behind retrofitting of civil engineering structures are a change of codes or standards, an increase of live loads, corrosion of steel, damage of concrete, inadequate design, faulty construction, time dependent deformation, etc. The most common materials used to retrofit civil engineering structures are fibre reinforced polymer (FRP) and steel. SMA is another promising material that can be used to retrofit a deficient structure. SMAs have several advantages over steel and FRP. SMA is less corrosive than steel, has less residual drift than steel, and has less permanent deformation than steel. FRP is brittle and less fire resistant than SMA. SMA can be used to retrofit a deficient structure in the form of bracing members, prestressing tendons or wires, dampers and connecting devices depending on the situation.

2.5.2.1 Bracing members

Some researchers have retrofitted existing reinforced concrete frame buildings with SMA bracing and have found better performance under cyclic loading. Dolce et al. (2004) retrofitted a 2-storey reinforced concrete frame with austenite Ni-Ti wire based bracings. The results showed that austenite SMA bracing increased the displacement control at the damage limit state and also increased the safety against the collapse of the reinforced concrete frame.

To reduce vibration of a one storey metal frame structure Ma et al. (2004) employed Ni-Ti shape memory alloy based braces. To guarantee the shape recovery of the martensite SMA braces, they maintained constant electrical current and periodically applied pulse current. A shake table test simulating the 1994 Northridge earthquake was performed to compare the performances of SMA braces and soft iron braces, which confirmed the superiority of SMA braces compared to that of steel braces.

2.5.2.2 Prestressing

Choi et al. (2009) mentioned in their study that cracks in prestressed concrete beams can be controlled by utilizing SMAs wires or cables as reinforcement. The prestressing of wires or cables controls the crack width during the loading phase and closes the crack at the unloading state. To control the bending cracks, horizontal SMA wires are used, and to control diagonal cracks, the diagonal wires are used. To confine the RC columns, prestrain SMA wires are also used. These confinements prevent the RC column from spalling off as well as provide the passive control of the column by allowing additional deformation. Choi et al. (2009) used the SMA wires for retrofitting RC columns and found that this increased the ductile behaviour of columns without significant strength degradation.

Indirli et al. (2001) retrofitted the historic Trignano S. Giorgio Church in Italy, which was severely damaged by a 4.8 Richter magnitude earthquake on October 15, 1996. The church was built in 1302, which consisted of masonry columns and bell towers. After the earthquake, this church was retrofitted by using four prestressing steel and four prestrained SMA wire based devices. Another 4.5 magnitude earthquake hit the retrofitted church and the structure survived the event without any form of damage.

2.5.2.3 Dampers

Passive protection devices are widely used to control the seismic vibration of new and existing deficient structures (Dolce, 1994). One of the most widely used passive protection devices is dampers. In current practice, several dampers are used such as rubber based dampers, metallic yield dampers, friction dampers, visco-elastic dampers, and viscous fluid dampers. These materials, that are used to develop passive protection devices, have several limitations. For rubber based dampers ageing and durability problems reduce the temperature based performance. For viscous fluid dampers, maintenance problems are critical. For friction type dampers, the main problems are associated with its reliability to run for a long time. For all types of dampers, a common problem is the geometric restoration after strong vibration. Dolce et al. (2000) suggested that all these shortcomings can be overcome by introducing shape memory alloys (SMAs). Several experimental and analytical studies were conducted by numerous researchers by using SMAs. With the increase of vibration magnitude or the magnitude of impact, the damping capacity of SMA increased and they were not dependent on the frequency (Humbeeck and Liu, 2000). Adachi et al. (2000) developed dampers by using shape memory alloys and performed a series of shake table tests. They concluded that damping devices that are made by using shape memory alloys were capable of absorbing the earthquake forces as well as reducing the forces by their pseudo yield effect. Clark et al. (1995) used SMAs in energy dissipation devices and performed both analytical and experimental studies. These devices showed stable hysteresis behaviour with little reduction of yield stress. Mao and Li (2004) developed an energy dissipation device by using the pseudo-elastic property of Ni-Ti SMA

wires. They performed shake table tests and the results showed that the SMA dampers are capable of reducing the seismic risk and reducing the inter-storey drift by up to 28%.

2.6 LIMITATION OF USING SMAs

Although there are many possibilities of utilizing SMAs in the civil engineering structures, there are still many obstacles that need to be overcome. One of the biggest obstacles in using SMA is its high cost. Although SMA is used widely in automotive engineering and medical devices, the structural engineering applications of SMAs require large volume of material due to their large magnitude of forces. As a result the size of initial investment will be substantially higher. Frick et al. (2004) mentioned in their paper the source of cost of high strength Ni-Ti SMA are fundamentally related to processing procedures of Ni-Ti materials. These processing procedures increase the cost two to three times more than the regular price. Although the cost of SMA has decreased about 10 times in the last 12 years, the current price is still much higher compared to other reinforcing materials. Without developing low-cost SMA, the large scale application in civil engineering structures is not possible. Material engineers and scientists are trying to introduce low-cost SMAs. Janke et al. (2005) stated that Fe-Mn-Si-Cr alloys can be used as low-cost SMA, which will be about one-tenth to one twelve-th of the cost of Ni-Ti SMA (Janke et al. 2005). Soroushian et al. (2001) successfully used a low-cost Fe-Mn-Si-Cr to retrofit a bridge. Bruno and Valente (2002) investigated the possibility of using SMA devices in full scale construction. They found that SMA devices for seismic protections turn out to be a better choice compared to conventional devices considering the life-cycle-benefit analysis.

CHAPTER 3: RESPONSE MODIFICATION FACTOR OF CONCRETE BUILDINGS REINFORCED WITH SHAPE MEMORY ALLOY (SMA) REBAR

3.1 GENERAL

Generally, current seismic design codes including the National Building Code of Canada (NBCC 2005) recommend a force-based design of structures. The technique is based on the postulation that well-detailed structures be able to sustain lateral forces in excess of their design strength and maintain large inelastic deformation without collapse (Kim and Choi 2005). The force-based approach generally considers a reduction in the elastic base shear so that the structure acquires considerable reserve strength (over-strength) and ductility. These two properties are included in the structural design through a response modification factor (R), which represents a ratio of the elastic base shear (V_e) of a structure under a specified ground motion to the design base shear (V_d). The role of the response modification factor is very important in designing the seismic load resisting structures. This factor was first introduced in 1984 by the Applied Technology Council (ATC 3-06), and there was no specific guideline about response modification factor. In 1995, ATC-19 and ATC-34 provided a detailed guideline in calculating the response modification factor of a structure by considering its overstrength, ductility reduction and redundancy factor. The present Canadian code NBCC (2005) accounts for ductility and overstrength to compute response modification factor. Besides NBCC (2005), US codes (FEMA 1997, UBC1997) also accounts for reserve strength and ductility for calculating response modification factors (ATC, 1995). Recent earthquakes in New Zealand (2010, 2011), Haiti (2010), Chile (2010) and China (2008) highlighted the vulnerability of such reinforced concrete structures due to

seismic related damages and their resulting impact on the economy. Conventional reinforced concrete (RC) structures are designed for safety against collapse, where the earthquake energy is dissipated through yielding of reinforcement and inelastic deformation. Though the life safety is ensured, however, the deformation of RC structures induces significant damage and often the structure needs to be demolished causing substantial economic losses. Although the present code of practice in North America for building design is force based, nowadays the earthquake design of structures is evolving towards a performance-based approach (Ghobarah 2001) where there are needs for robust structural elements and systems that exhibit enhanced deformation capacity and ductility, higher damage tolerance, and recovered and/or reduced permanent deformations (Alam *et al.* 2009). Nevertheless, conventional Steel RC structures experience high residual drifts during large earthquakes, which is often responsible for serviceability issues and structural collapse of a building.

Shape Memory Alloys (SMAs) are distinctive materials that have the ability to experience large deformation and return to its original position upon unloading or by heating. The use of the SMAs is gradually gaining appreciation in different engineering fields due to its unique properties (Alam *et al.* 2007). Recent experimental and analytical investigations have reported its potential uses in mitigating seismic induced damages of civil engineering structures (Dolce *et al.* 2004, and Wilde *et al.* 2000). Saiidi and Wang (2006) used SMA bars in the plastic hinge regions of RC columns to reduce its permanent deformation, and showed that the RC columns are capable of improving nearly all of their post-yield deformation. Saiidi *et al.* (2007) experimentally investigated the ability of NiTi-SMAs rebars for recovering deformation of a small scale concrete beam under half cycle-

loads. They used different reinforcement ratios ranging from 0.1% to 0.9%, and found that the residual deformation for SMA reinforced beam was only 20% to that of a steel reinforced beam. Youssef et al. (2007) and Alam et al. (2007, 2008) performed experimental and analytical study on SMA RC elements and found that SMA RC beam-column joints can exhibit better performance compared to that of Steel RC beam-column joints because of their capability of reducing permanent deformation after large inelastic displacements with adequate energy dissipation. Soroushian et al. (2001) used iron-based SMA bars to improve the shear strength of deficient bridge girders and concluded that the SMA bars are effective in improving the shear performance of bridge girders. Elbahy et al. (2009) conducted the stress block parameters for RC members reinforced with SMA rebar under flexure loads. Elbahy et al. (2010) determined the accuracy and reliability of different models for calculating the load-deflection behaviour of SMA RC beams. Although the existing literature provides a number of numerical and experimental studies on the use of SMAs in several components of RC frame structures, a little number of studies has been carried out on the use of SMAs as reinforcement in the entire RC frame structures. Alam et al. (2009) conducted a comparative study on the performance of two eight-storey RC frames where one was reinforced with SMA rebars in the plastic hinge region of the beams and steel in other regions, and the other was fully reinforced with steel. Static nonlinear pushover analyses were performed to investigate their different failure mechanisms, followed by a series of nonlinear dynamic time history analyses to determine the inter-storey residual drift and top-storey residual drift. The results showed that the SMA RC frames could recover most of their post-yield deformation. However, this study was only limited to eight storey frame structure and did not provide any information about its overstrength and ductility reduction factors. Due to the unique mechanical properties of

SMA compared to steel, its use as reinforcement in concrete frame structures of different stories might significantly change their seismic responses, and therefore, has a practical importance in their design (Alam et al., 2008).

The current version of NBCC (2005) recommends force-based seismic design methods and provides a list of overstrength and ductility factors for different types of RC frames, reinforced with mild steel (Mitchell et al. 2003). In NBCC (2005), there is no specific guideline for RC frames reinforced with SMAs. Since SMAs have lower modulus of elasticity compared to mild steel, it is postulated here that the overstrength factor (R_o) and ductility factor (R_d) will not be the same as provided in the NBCC (2005) for RC frames reinforced with regular mild steel.

In this chapter, the effect of SMA as a reinforcement in concrete frame structures is analytically investigated, where three different types of reinforced concrete (RC) buildings of different stories (3, 6, and 8) are considered. For each type of frame, three different reinforcement detailing are considered: i) only steel is used as reinforcing material (Steel RC); ii) Steel-SMA hybrid reinforcement where SMA is used particularly in the plastic hinge region of the beam and steel in other regions of the beam (Steel-SMA RC); and iii) only SMA is used as reinforcement in the beams (SMA RC). For each type of frame building, steel is used as the longitudinal and tie reinforcements in the columns. The current study provides a detailed view of the response modification factor (R) for SMA induced frame structures. Inelastic pushover analyses were performed to determine their overstrength factors and ductility. Linear dynamic and nonlinear incremental dynamic time history analyses were performed to determine the ductility reduction factor. Additionally, ductility reduction factor and response modification factor demand for the investigated

structures, were also computed by using empirical models. The ductility reduction factor and response modification factor supply-demand ratio were also discussed in this chapter.

3.2 RESPONSE MODIFICATION FACTOR

Elastic analysis of structures under seismic loads can create base shear, which is obviously greater than the actual response of the structures (Asgarian and Shokrgozar, 2009). Mazzolani and Piluso (1996) described a number of theoretical/analytical procedures to compute the response modification factor, such as the maximum plastic deformation, energy and low cycle fatigue approaches. The actual lateral base shear capacity, V_y is observed by performing pushover analyses. The overstrength factor (R_o) is defined as the ratio of the actual lateral strength (V_y) to the design lateral strength (V_d).

$$R_o = \frac{V_y}{V_d} \quad [3.1]$$

The ductility reduction factor (R_d) is defined as the ratio of the maximum base shear for an elastic system (V_e) to the maximum base shear (V_y) for an elastic perfectly plastic system.

$$R_d = \frac{V_e}{V_y} \quad [3.2]$$

Finally, the response modification factor (R) is obtained by dividing the elastic strength (V_e) to the design strength (V_d) or by multiplying the ductility reduction factor (R_d) to the overstrength factor (R_o).

$$R = \frac{V_e}{V_d} \quad [3.3]$$

Quantification of the actual overstrength is important as it can be employed to reduce the forces used in the design, hence leading to more economic structures (Uang 1991, Mitchell and Paulter 1994, Park 1996).

Figure 3.1 shows the actual nonlinear behaviour of a RC frame in terms of base shear versus roof top displacement, which is idealized by a bilinear elastic-perfectly plastic relationship. The idealized curve is developed as per FEMA 356. In the National Building Code of Canada (NBCC 2005), the base shear for earthquake load is calculated by the elastic strength demand divided by the strength reduction factor, known as the response modification factor (R), which accounts for the ductility and the over strength (Lee et al. 1999). Here, the ductility (μ) is defined as the ratio of displacement at actual capacity (Δ_{max}) to the displacement (Δ_y) corresponding to (V_y) on the idealized bilinear curve as shown in Figure 3.1.

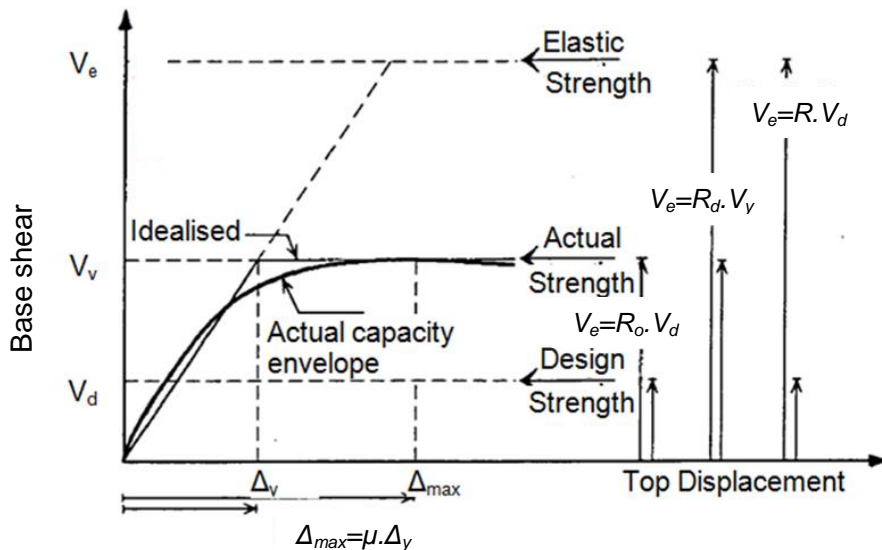


Figure 3.1 The relationships between force reduction factors (R), overstrength (R_o), ductility reduction factor (R_d), and displacement ductility factor (μ). (Adapted from Mwafy and Elnashai, 2002).

The way to compute the elastic base shear is shown graphically in Figure 3.2. The elastic base shear (V_e) is computed by performing nonlinear incremental dynamic time history analysis up to collapse and then performing the linear dynamic time history analyses by using the collapse earthquake ground motion history.

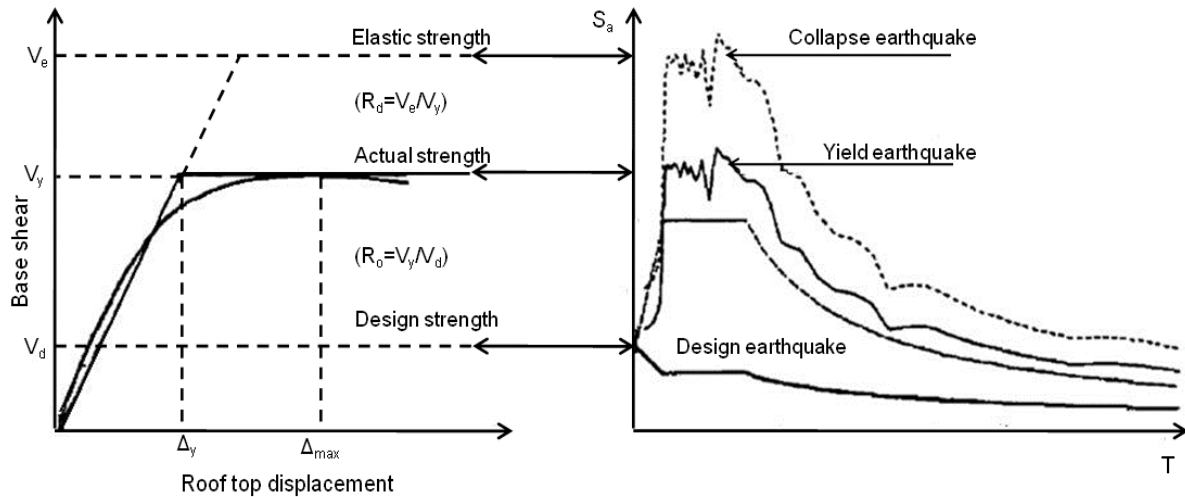


Figure 3.2 Comparison between the ductility reduction factor (R_d) and the definition of R_d , supply (Adapted from Mwafy and Elnashai, 2002).

3.3 PROPERTIES OF SHAPE MEMORY ALLOYS AND ITS MODELLING

A classic stress-strain curve of superelastic SMA and mild steel under cyclic axial force is shown in Figure 3.3. When an SMA is subjected to a cycle of axial deformation within its superelastic strain range, it dissipates a definite quantity of energy without permanent deformation. This has resulted due to the phase transformation between austenite and martensite during loading and unloading. Moreover, SMA has a benefit over steel material in the sense that it has a negligible residual strain as shown in Figure 3.3 because of its inherent property of superelasticity.

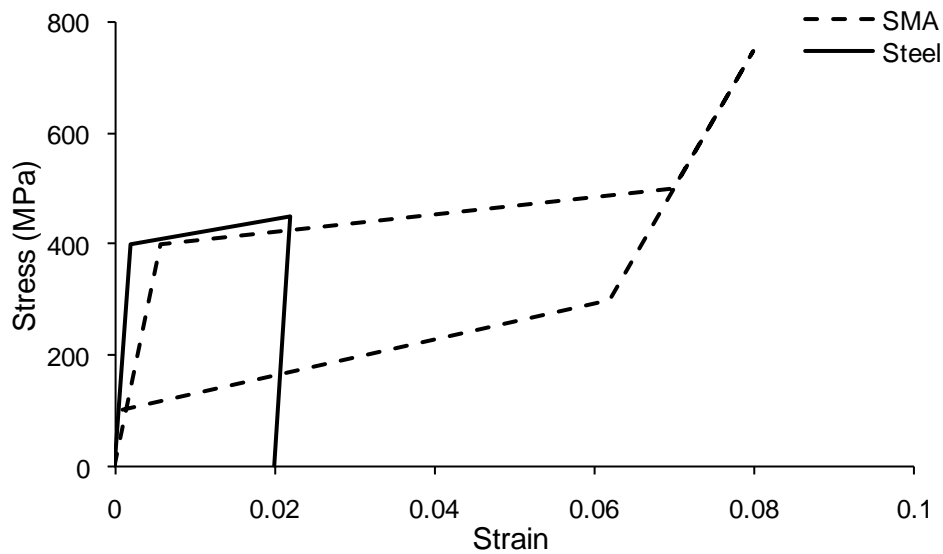


Figure 3.3 Stress-strain behaviour of superelastic SMA and Steel.

The modelling technique for SMA material in finite element software is discussed in section 2.4.1.

3.4 DESIGN OF FRAME STRUCTURES

In the present study 3, 6, and 8-storey frame buildings have been considered, where each building has three different types of rebar in its beams, i.e. Steel, Steel-SMA and SMA as described in Section 3.1. Each building has five bays in both directions with the same bay length of 5m each. These RC buildings have been analyzed as per NBCC (2005) and designed according to CSA A23.3-04 (2004) as ductile moment resisting frames. The buildings are considered to be located in the city of Vancouver, and the seismicity of Vancouver is obtained from NBCC (2005). Table 3.1 shows the material properties used for the design and analysis of the buildings.

Table 3.1 Material properties used in the finite element program.

Material	Mechanical Property	Value
Concrete	Compressive strength (MPa)	35
	Tensile strength (MPa)	3.5
	Strain at peak stress (%)	0.2
Steel	Modulus of elasticity (MPa)	200,000
	Yield strength (MPa)	400
	Strain hardening parameter	0.5
SMAs	Modulus of elasticity (MPa)	60,000
	Austenite to martensite starting stress (MPa)	400
	Austenite to martensite finishing stress (MPa)	500
	Martensite to Austenite starting stress (MPa)	300
	Martensite to Austenite finishing stress (MPa)	100
	Super elastic plateau strain length (%)	6

The plan of the investigated buildings is kept similar to each other and is shown in Figure 3.4(a), and the elevation of the 3, 6, and 8-storey building is shown in Figures 3.4 (b), (c) and (d), respectively, and the storey height was 3 m for all buildings. The reinforcement of the building has been detailed as per Canadian standards (CSA A23.3-04) and Tables 3.2 and 3.3 show the member sizes and the reinforcement detailing of the columns and the beams, respectively. The 20 columns located along the perimeter of the buildings are designated as C2, and the remaining interior 16 columns are designated as C1.

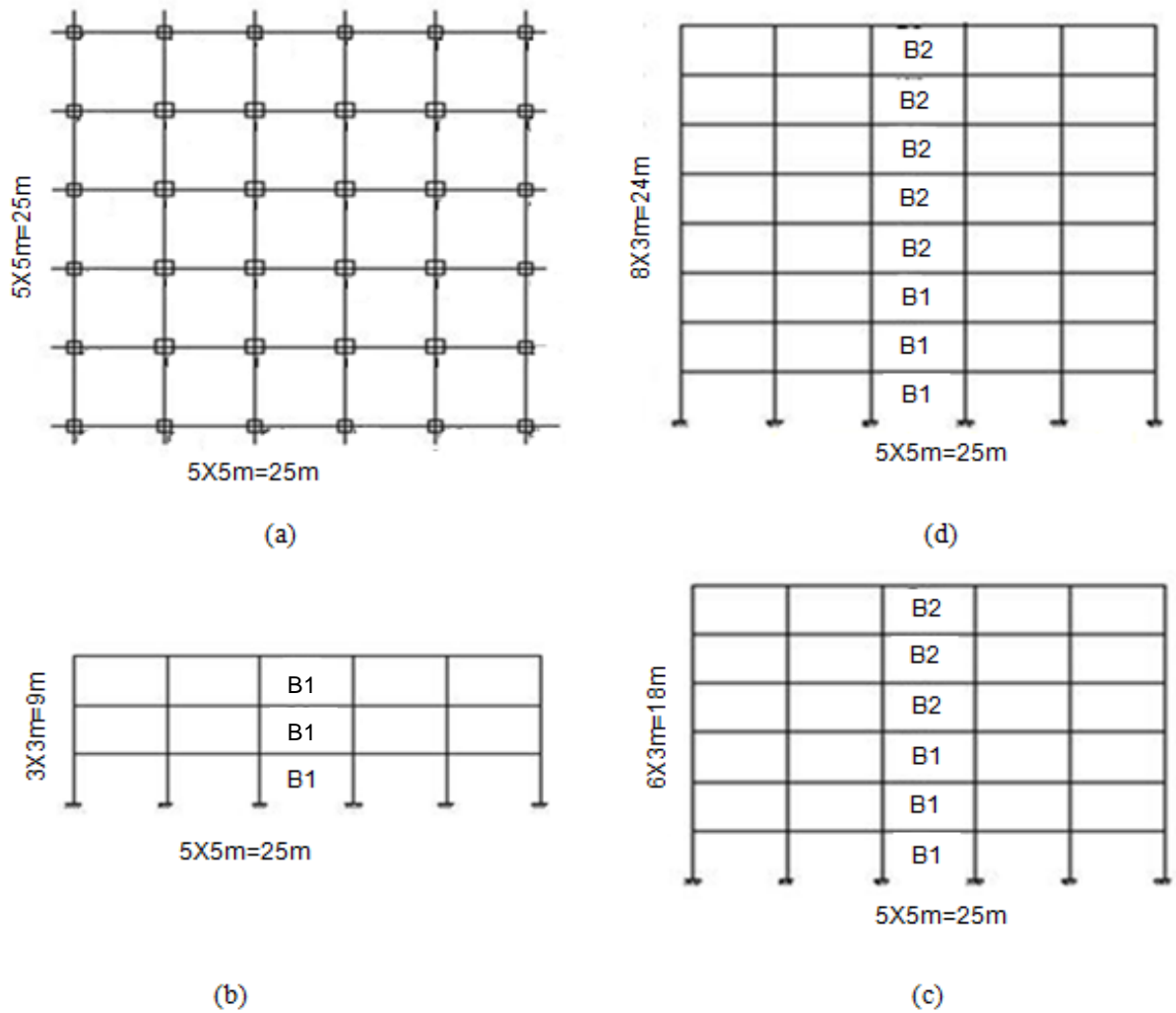


Figure 3.4 Building geometry (a) plan, (b) elevation of 3-storey, (c) elevation of 6-storey and (d) elevation of 8-storey buildings.

In the case of Steel-SMA building, SMA bars have been used in the plastic hinge regions of the beam, and steel reinforcements have been used in the remaining parts of the beam. The plastic hinge length of the beam was estimated using an analytical expression proposed by Paulay and Priestley (1992). In this study, it is assumed that the steel and the SMA rebar are coupled together using mechanical anchorages/couplers (Alam et al. 2010).

Table 3.2 Column size and reinforcement arrangements.

Building Id	Floor level	Description	Column ID	
			C1	C2
3-Storey building	Up to roof	Size (mm x mm)	375x375	300x300
		Main reinforcement	8-15M	4-20M
6 -Storey building	Up to 3rd floor	Size (mm x mm)	450x450	300x300
		Main reinforcement	8-25M	6-20M
	3rd floor to roof	Size (mm x mm)	450x450	300x300
		Main reinforcement	8-20M	4-20M
8-Storey building	Up to 3rd floor	Size (mm x mm)	500x500	300x300
		Main reinforcement	8-25M	6-25M
	3rd floor to roof	Size (mm x mm)	500x500	300x300
		Main reinforcement	6-25M	6-20M

Figure 3.5 shows the reinforcement detailing of a typical beam. For a 3-storey building, beam B1 is used in all the storeys, where the longitudinal reinforcements for all the beams are similar. For both the 6 and the 8-storey frames, beam B1 is used for the lower first three storeys and beam B2 for upper part of the frame.

Table 3.3 Beam reinforcement details.

Building Id.	Beam Id. (Figure 3.4)	Size (mm x mm)	Section Id. (Figure 3.5)					
			Section 1-1		Section 2-2		Section 3-3	
			Top	Bottom	Top	Bottom	Top	Bottom
3-storey	B1	300x450	3-20M	3-20M	3-20M	3-20M	3-20M	3-20M
6-storey	B1	300x500	3-25M	5-20M	3-25M	5-20M	3-25M+2-20M	3-20M
	B2	300x500	3-20m	3-20M	3-20M	3-20M	3-20M	3-20M
8-storey	B1	300x500	3-25M	5-20M	3-25M	5-20M	3-25M+2-20M	3-20M
	B2	300x500	3-20M	3-20M	3-20M	3-20M	3-20M	3-20M

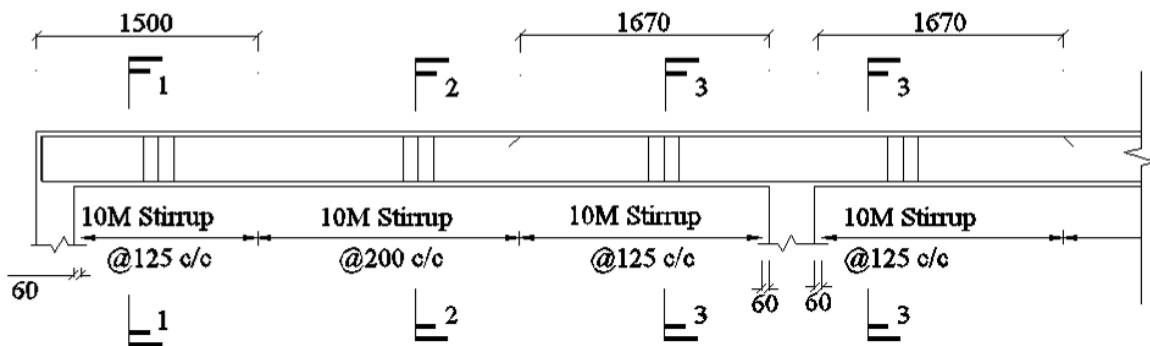


Figure 3.5 Typical longitudinal section of beam reinforcement.

From sectional analyses, moment curvature relationships have been developed for the considered beam sections to determine the effective stiffness for the SMA reinforced and the steel reinforced concrete sections. The effective stiffness is the slope of the straight line between the origin and the first yield point in the moment curvature relationship (Elwood and Eberhard 2006). The moment curvature relationships for SMA and steel reinforced sections are illustrated in Figure 3.6. The effective stiffness for Steel RC section is 2.19 to

2.77 times higher than that of the SMA RC section. The lower limit is obtained for section 3-3 of beam B1 for both the 6 and the 8-storey frames whereas the upper limit of 2.77 is obtained for the beam of the 3-storey frame. This effective stiffness value is then used to determine the fundamental period of the structures using SAP 2000 V14.0. Eigen value analyses were performed by considering the uncracked section and the effective stiffness method for all the frames to determine their fundamental periods (Table 3.4). The analyses results show that the use of the SMA as reinforcement in beams increased the fundamental period of the structure compared to mild steel, because of SMA's lower modulus of elasticity. As the stiffness decreases, the period of the structure increases. The fundamental period obtained by considering the effective stiffness was used to calculate the revised design base shear for different types of frames. The revised base shear is then used to determine the forces in different elements of different frames, followed by calculating the reinforcement of the beam and the column. From the analyses/design it is observed that although the design base shear for SMA RC frame is lower compared to Steel RC frame, it does not affect the number of bars used for the same beam of different framing systems. The comparison of moment capacity and the percentage of reinforcement for SMA RC and Steel RC beams are shown in Figure 3.7. From the figure it is observed that the balanced steel ratio for SMA reinforcement is 0.023, whereas for steel it is 0.042. In the case of all the different types of frames, the maximum allowable limit of reinforcement and the lower limit of reinforcement have been satisfied.

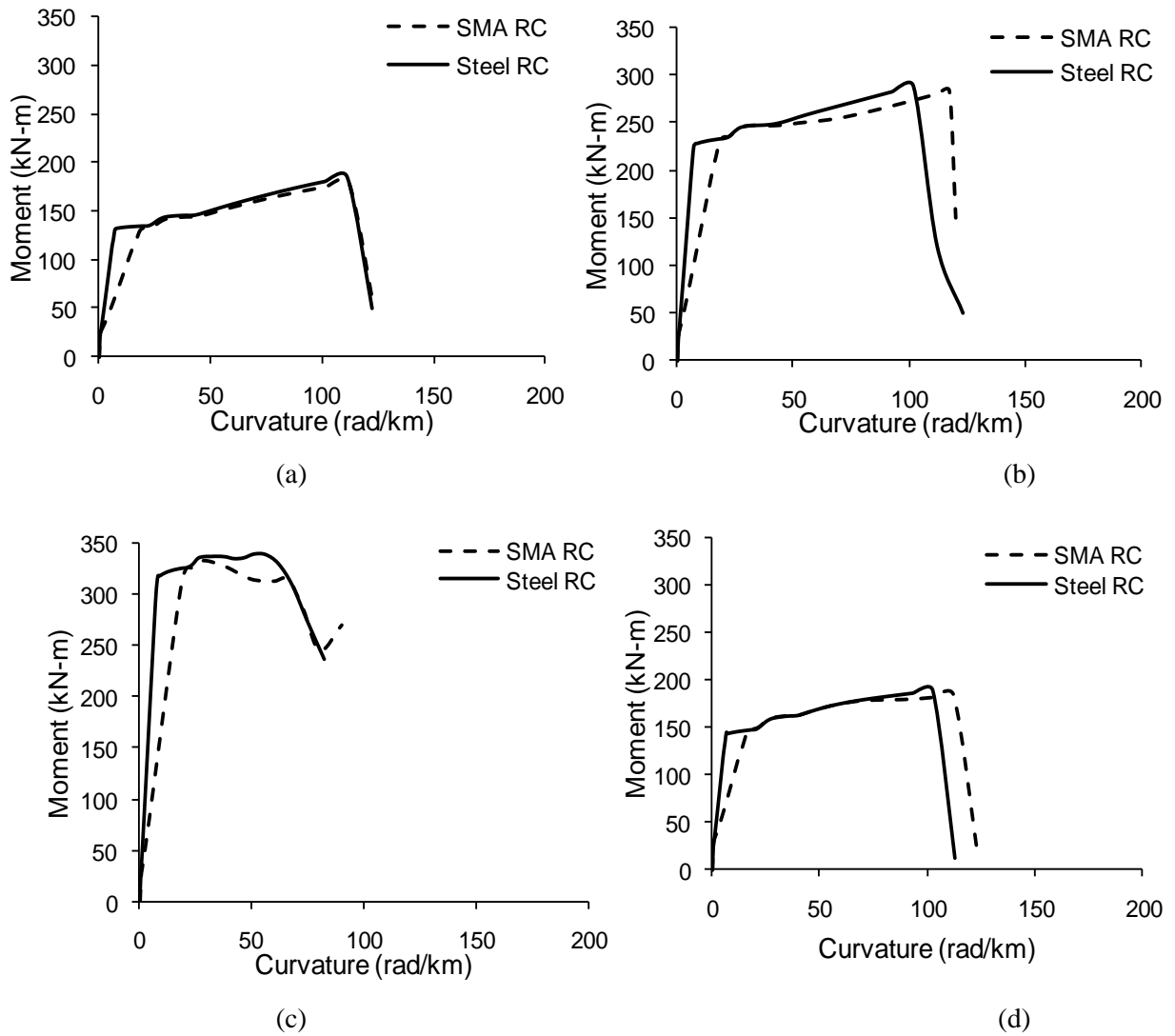


Figure 3.6 Moment curvature relationship for (a) B1 of 3-storey frame (b) Section 1-1 and 2-2 for beam B1 for both 6 and 8-storey frame, (c) Section 3-3 for beam B1 for both 6- and 8-storey frame and (d) beam B2 for both 6 and 8-storey frame.

Table 3.4 Fundamental period of the structure.

Building Id	Fundamental period, T_f (sec)						
	Code prediction	Uncracked section			Effective stiffness, K_{eff}		
		Steel	SMA	Steel-SMA	Steel	SMA	Steel-SMA
3	0.39	0.26	0.26	0.26	0.39	0.42	0.41
6	0.66	0.49	0.49	0.49	0.67	0.74	0.70
8	0.81	0.68	0.68	0.68	0.86	1.00	0.93

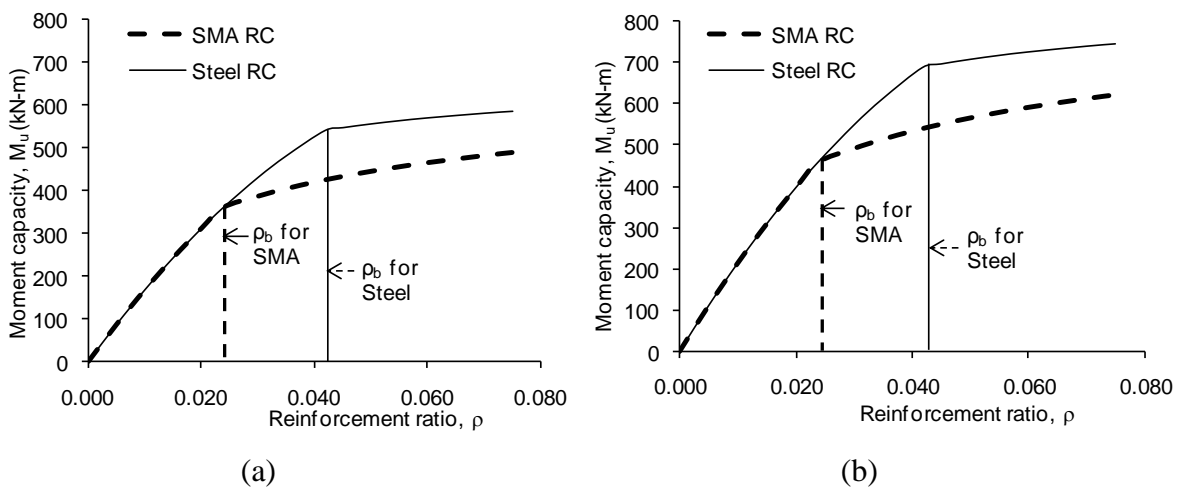


Figure 3.7 Flexural strength versus reinforcement ratio of a singly reinforced concrete beam having cross-sections of (a) 300mm x 450mm and (b) 300mm x 500mm.

Figure 3.7(a) and (b) are used to determine the reinforcement ratio required for the SMA and steel reinforced beams. It can be observed from the figure that if the required amount of reinforcement ratio is less than 0.023, the capacities for both the SMA and the steel reinforced beams are similar. However, if the reinforcement ratio exceeds this 0.023, the capacity will be different for SMA and steel. The serviceability limit states have also been checked against deflection, which has been found satisfactory for all SMA RC elements, as well as Steel-SMA RC frames as per CSA A23.3-04. For instance, the

maximum allowable deflection limit for the frame beams is 10.4 mm. From analyses it has been observed that the 8 storey SMA RC frame experienced the maximum deflection, which is only 6.4 mm, well below the 10.4 mm limit as per CSA standards.

3.5 ANALYTICAL MODEL

SeismoStruct (2010) software has been used to perform pushover analysis, linear and nonlinear dynamic time history analyses. Here, fibre modelling approach has been used to clearly represent the distribution of material nonlinearity along the length and cross-sectional area of the member. 3D beam-column elements have been used for modelling the beam and the column where the sectional stress-strain state of the elements is obtained through the integration of nonlinear uniaxial stress-strain response of the individual fibres in which the section has been subdivided. For nonlinear, pushover and incremental dynamic time-history analyses, inelastic displacement-based frame elements have been used for beams and columns whereas elastic frame elements have been used for linear dynamic analyses. Concrete has been represented using the constitutive relationship proposed by Mander et al. (1988) and the cyclic response by Martinez-Rueda and Elnashai (1997), and a bilinear kinematic strain hardening model is used for steel. SMA has been modelled according to the model of Auricchio and Sacco (1997), and the parameters used to define the material model were discussed in Section 3.4. The beam and column were divided longitudinally into 8 and 4 elements, respectively, where two of the beam elements represent the plastic hinge region of the beam at each beam-column joint region. Each beam and column element was divided transversely into 200 by 200 fibre elements.

3.6 PUSHOVER ANALYSIS

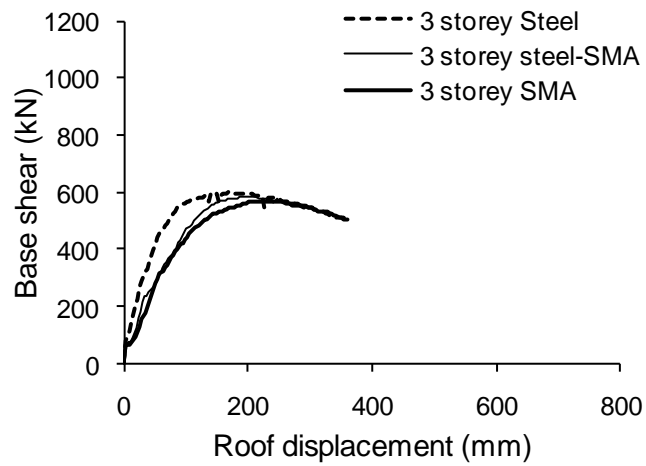
Nonlinear pushover analysis has been performed for each building using SeismoStruct (2010) considering a 2D interior frame. A triangular lateral load distribution has been considered to perform the analyses. The vertex of the triangular load is considered at the roof level, whereas the apex of the load is considered at the base of the building. The pushover response curves are shown in Figure 3.8 (a), (b) and (c) for the 3, 6, and 8-storey buildings, respectively. The design base shear values for different storey frames are presented in Table 3.5. In the case of the pushover response curves for the 3-storey frames (Figure 3.8 a), the actual lateral capacities, (V_y) for Steel, Steel-SMA and SMA RC frames are 1.45, 1.45 and 1.42 times the design base shear (V_d), which reached the capacity at a roof drift of 1.9% (169 mm), 2.3% (205 mm) and 2.6% (230 mm), respectively. Here, the roof drift corresponds to the global drift of the entire structure. For the 6-storey frames (Figure 3.8 b), the capacities (V_y) for Steel, Steel-SMA and SMA RC frames are 1.52, 1.53 and 1.59 times the design base shear (V_d) where the corresponding roof drifts are 1.2% (207 mm), 1.7% (297 mm) and 2.0% (351 mm), respectively. For the 8-storey frames (Figure 3.8 c) the lateral capacities are 1.55, 1.61 and 1.68 times the V_d where the corresponding roof drifts are 1.6% (383 mm), 2.2% (538 mm) and 2.4% (586 mm) for Steel, Steel-SMA and SMA RC frames, respectively. For each storey height, the initial stiffness of the Steel, Steel-SMA and SMA RC frames were similar. Once the concrete cracks in beams, the SMA rebars become effective in resisting tensile forces, which resulted in reduced stiffness for Steel-SMA and SMA RC frames, compared to that of Steel RC frames. Similar results were obtained in the experimental investigations of Youssef et al. (2008) and in the

numerical investigations of Alam et al. (2007, 2008). This is the same reason why the post-cracked stiffness of SMA RC frame is lower compared to that of Steel- SMA RC frames.

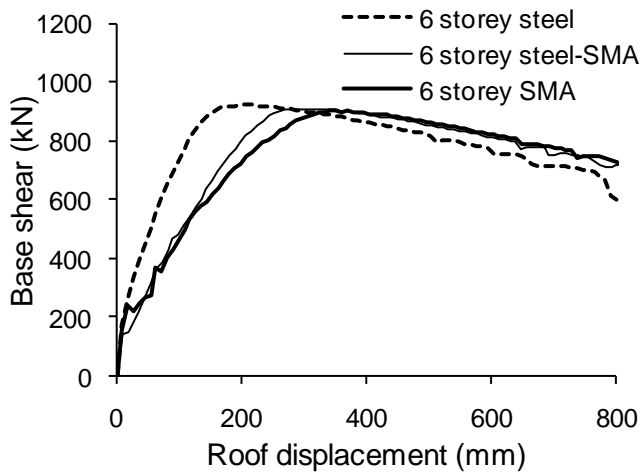
Figure 3.9(a), (b), and (c) show the distribution of inter-storey drift at collapse observed from the pushover analyses over the different floor levels for the 3, 6, and 8-storey frames, respectively. The inter-storey drift of the investigated frame is calculated when the base shear of the frame reaches its maximum capacity. Here, the inter-storey drift capacity is considered as the maximum inter-storey drift at collapse, which is the state when the beams and the columns of different storeys have failed and the frame is not capable of taking any further load, i.e. the point of maximum load. As expected, all SMA RC frames experienced higher inter-storey drift compared to Steel-SMA and Steel RC frames. In all cases, Steel RC frames exhibited the highest stiffness and lowest inter-storey drift. The maximum inter-storey drift was observed as 3.1, 3.9 and 4.2 percent for the Steel, Steel-SMA and SMA RC frames, respectively (for 8-storey frames, Figure 3.9(c)).

Table 3.5 Seismic overstrength factor and ductility of different frames.

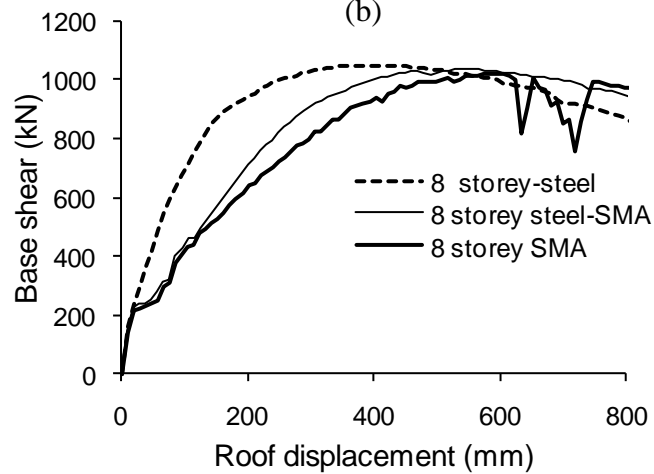
	3 storey			6 storey			8 storey		
	Steel	Steel-SMA	SMA	Steel	Steel-SMA	SMA	Steel	Steel-SMA	SMA
Design base shear, V_d (kN)	414	402	402	605	593	568	678	642	605
Base shear capacity, V_y (kN)	600	582	569	922	910	903	1050	1038	1019
Overstrength factor, R_o	1.45	1.45	1.42	1.52	1.53	1.59	1.55	1.61	1.68
Maximum displacement, Δ_{max} (mm)	169	205	230	207	297	351	393	538	586
Global Yield displacement, Δ_y (mm)	77	107	123	112	185	225	185	275	336
Ductility, μ	2.34	1.92	1.79	1.85	1.61	1.56	2.12	1.96	1.74



(a)



(b)



(c)

Figure 3.8 Pushover curve for (a) 3-storey, (b) 6-storey and (c) 8-storey frame.

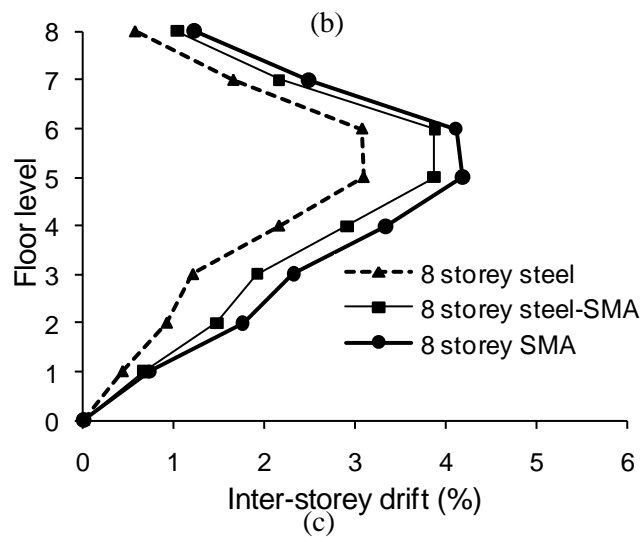
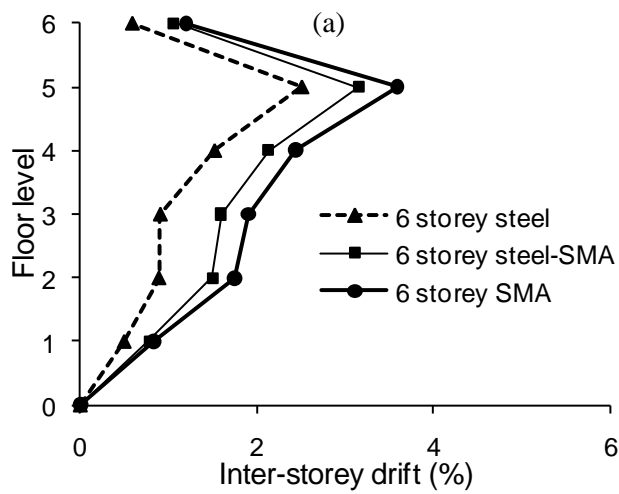
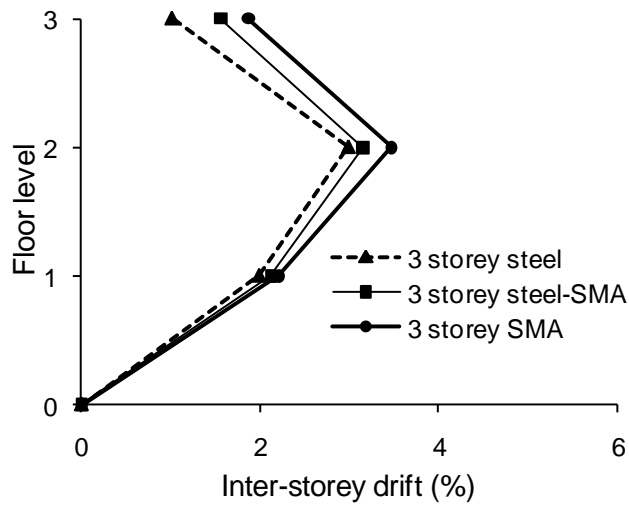


Figure 3.9 Inter-storey drift distribution for (a) 3-storey, (b) 6-storey and (c) 8-storey frame.

Table 3.5 summarizes the base shear capacity of Steel, Steel-SMA and SMA RC frames. It can be observed that the Steel RC frames reached their capacity at a relatively smaller roof drift compared to Steel-SMA and SMA RC frames. First, local yield was observed in the beams for all the frames where the corresponding base shear for each storey frame was higher for Steel compared to that of the Steel-SMA and SMA RC frame. The design base shear is also presented for all the frame types in Table 3.5, which is used to determine the overstrength factors for different storeys of SMA, Steel-SMA and Steel RC frames, with the ratio of V_y/V_d . The results show that SMA RC frames possess slightly lower overstrength compared to those of the Steel RC frames (Table 3.5). Since SMA has a lower modulus of elasticity, the SMA reinforced frames experienced higher flexibility and reduced stiffness, which caused delay in achieving the capacity. This also caused a more reduced capacity of the SMA frames than that of Steel and Steel-SMA frames, as the column resistance gets diminished at higher storey drift. The displacements corresponding to the peak base shear have also been presented in Table 3.5 as Δ_{max} . This Δ_{max} gradually increases with the increasing storey numbers, where SMA RC frames experience 36%, 69% and 49% higher roof displacements at peak base shear for the 3, 6, and 8 storey frames, respectively, compared to those of the Steel RC frames. The Steel-SMA RC frame experienced 21%, 43% and 36% higher roof displacements at peak base shear for 3, 6, and 8-storey frames, respectively, compared to those of Steel RC frames. From the force-displacement curve, a bilinear elastic perfectly plastic model has been used to obtain the yield displacement value. In order to determine the equivalent bilinear curve from the pushover results, the area under the curve was calculated, then a horizontal line is drawn intersecting the peak base shear. Then an inclined line is drawn through the origin to connect the horizontal line in such a way that the area under the two lines is equal to the

area under the original curve up to Δ_{max} . Then the yield displacement is defined as the point of intersection between the two lines, as shown in Figure 3.1. Yield displacements (Δ_y) for SMA frames are 1.6, 2.1 and 1.8 times higher than those of the 3, 6, and 8-storey Steel RC frames, respectively. The Steel-SMA frames' yield displacements are 1.4, 1.65 and 1.5 times higher than those of the 3, 6, and 8-storey Steel RC frames. Ductility is also calculated and presented in Table 3.5, which is a ratio of Δ_{max}/Δ_y . All the SMA RC frames exhibit lesser ductility compared to those of Steel RC frames by 30%, 20% and 21% for the 3, 6, and 8-storey frames, compared to Steel-SMA frames by 22% 15% and 8% for, respectively. Although SMA RC frames experienced much higher displacement compared to the Steel RC frames, the overall ductility of the Steel RC frames was higher because of the SMA frames' higher yield displacement values resulting from their lower stiffness.

3.7 DYNAMIC TIME-HISTORY ANALYSIS

Incremental nonlinear dynamic time history analyses were performed for each frame using nine real earthquake data and an artificial earthquake ground motion data developed by Atkinson (2009) for the city of Vancouver. These accelerograms were chosen such that they represent the seismic characteristics of the site of the structure. The ratio between the peak ground acceleration (*PGA*) and peak ground velocity (*PGV*) is an indicator of the frequency content of seismic motion. The characteristic seismic motions for the western part of Canada have a *PGA/PGV* ratio around 1.0 (Naumoski et al. 1988). The selected ensemble of earthquake records is presented in Table 3.6 where the *PGA/PGV* ratio varies between 0.8 and 1.2. A summary of the ground motion data is presented in Table 3.6. In order to scale the earthquake records presented in Table 3.6, a 5% damping spectral

acceleration spectrum of each of the 10 ensemble of records are generated and plotted with respect to the NBCC (2005) spectral acceleration of Vancouver (Figure 3.10).

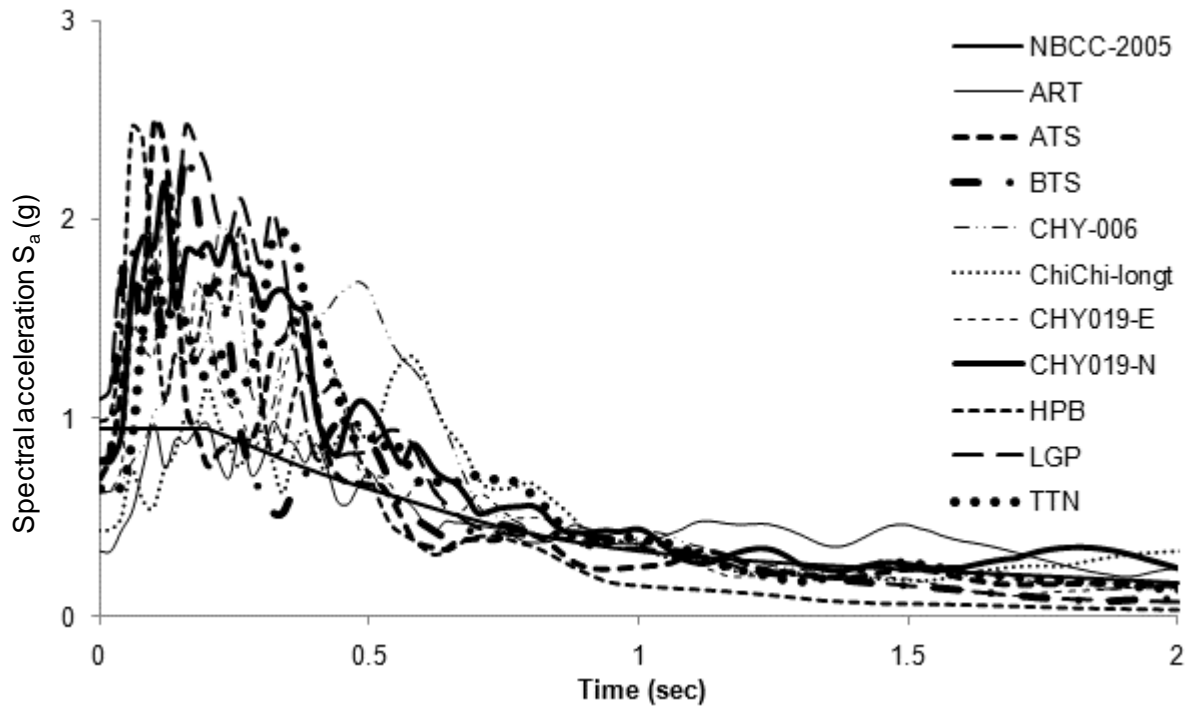


Figure 3.10 Variation of spectral acceleration with period of structure.

Table 3.6 Ensemble of ground motion records.

Records No.	Earthquake	Station	Magnitude	PGA (g)	$\frac{PGA}{PGV}$ (sec ⁻¹)	Data Source
1	Artificial (ART)	-	6.5	0.35		Atkinson (2009)
2	ATS, Kocaeli, 199/08/17	ATS-UP,150	7.8	0.67	0.93	http://peer.berkeley.edu (PEER strong ground motion database 2007)
3	BTS, Kocaeli, Turkey 1999/08/17	Botas	7.8	.62	1.0	http://peer.berkeley.edu (PEER strong ground motion database 2007)
4	Chi-Chi,Taiwan. 1999/09/20	CHY-006	7.6	0.63	0.81	http://peer.berkeley.edu (PEER strong ground motion database 2007)
5	ChiChi-longt,Taiwan. 1999/09/21	unknown	7.6	0.43	1.13	http://peer.berkeley.edu (PEER strong ground motion database 2007)
6	Chi-Chi,Taiwan. 1999/09/20	CHY019-E	7.6	0.63	0.83	http://peer.berkeley.edu (PEER strong ground motion database 2007)
7	Chi-Chi,Taiwan. 1999/09/20	CHY019-N	7.6	0.7	1.0	http://peer.berkeley.edu (PEER strong ground motion database 2007)
8	Victoria, Mexico 6/9/1980 3:02	VICT/H PB000	6.4	0.95	0.86	http://peer.berkeley.edu (PEER strong ground motion database 2007)
9	Loma Prieta 1989/10/18 00:05	16 LGPC	6.9	1.11	-	http://peer.berkeley.edu (PEER strong ground motion database 2007)
10	Chi-Chi,Taiwan. 1999/09/20	TTN042-N	7.6	0.65	1.0	http://peer.berkeley.edu (PEER strong ground motion database 2007)

3.8 RESULTS AND DISCUSSIONS

In this study the supply and the demand of response modification factor (R) has been computed for the different reinforced concrete frames.

3.8.1 Response modification factor (R) supply

Table 3.7 shows the elastic base shear (V_e) for the considered frames. The arithmetic average of the ten elastic base shear is used to compute the ductility reduction factor and the response modification factor. From Table 3.7 it can be concluded that the elastic base shear completely depends on the characteristic of the earthquake records.

Table 3.7 Elastic base shear V_e .

Types of RC Frames	ART	ATS	BTS	ChiChi-longt	Chy-006	Chy-019E	Chy-019N	HBP	LGP	TTN	Average
3 SMA	3619	5328	8624	2332	6255	3013	3896	10104	28834	3822	7583
3 steel-SMA	3619	2420	4617	2332	7216	4645	7216	3932	20710	1433	5814
3 steel	3800	5808	8315	2332	6735	3658	6762	9782	17799	2866	6786
6 SMA	4102	10074	21222	2275	14980	4732	4690	9044	19045	8649	9881
6 steel-SMA	5127	11230	20915	2225	10943	11603	10577	16137	25208	7842	12181
6 steel	6896	13112	18640	2543	10943	11853	10577	6926	18467	7842	10780
8 SMA	12402	17517	13740	2596	25546	17064	10636	9670	32167	7696	14904
8 steel-SMA	9286	10789	17114	2714	6016	5958	7305	34712	43246	17927	15507
8 steel	11956	11071	14514	2784	23278	11153	15277	24518	36995	15780	16733

The elastic base shear observed for the earthquake record LGP is much higher than the average value whereas that for the ChiChi-longt earthquake is much lower compared to the average. Mwafy and Elnashai (2002) mentioned in their studies that the ductility reduction

factor (R_d) and the response modification factor (R) obtained in this way is called the ductility reduction factor (R_d) supply, and the response modification factor (R) supply. The summary for the response modification factor (R) supply is presented in Table 3.8.

Table 3.8 Response modification factor (R) supply.

Parameters	3 storey			6 storey			8 storey		
	Steel	Steel-SMA	SMA	Steel	Steel-SMA	SMA	Steel	Steel-SMA	SMA
Overstrength factor, R_o	1.45	1.45	1.42	1.52	1.53	1.59	1.55	1.61	1.68
Ductility, μ	2.34	1.92	1.79	1.85	1.61	1.56	2.12	1.96	1.74
Ductility reduction factor, R_d	11.3	10.0	13.3	11.7	13.4	10.9	15.9	14.9	14.6
Response modification factor, R	16.4	14.5	18.9	17.8	20.5	17.4	24.7	24.1	24.6

Figure 3.11 shows the comparison of the overstrength factor (R_o) for the different types of frames considered in this study. Although NBCC-2005 specifies (R_o) as 1.7 for ductile reinforced concrete buildings, the result of this study shows that the framing system offers a lower overstrength factor in all cases. This might be due to neglecting the slab action during the analysis. From Figure 3.11 it can be observed that although SMAs have lower modulus of elasticity compared to regular steel, SMA RC frames offer almost a similar overstrength factor (R_o). The overstrength factors of the 6 and the 8-storey SMA RC frames are slightly higher than those of the Steel and Steel-SMA RC frames, but in the case of the 3-storey frame these values are slightly lower for SMA RC frames.

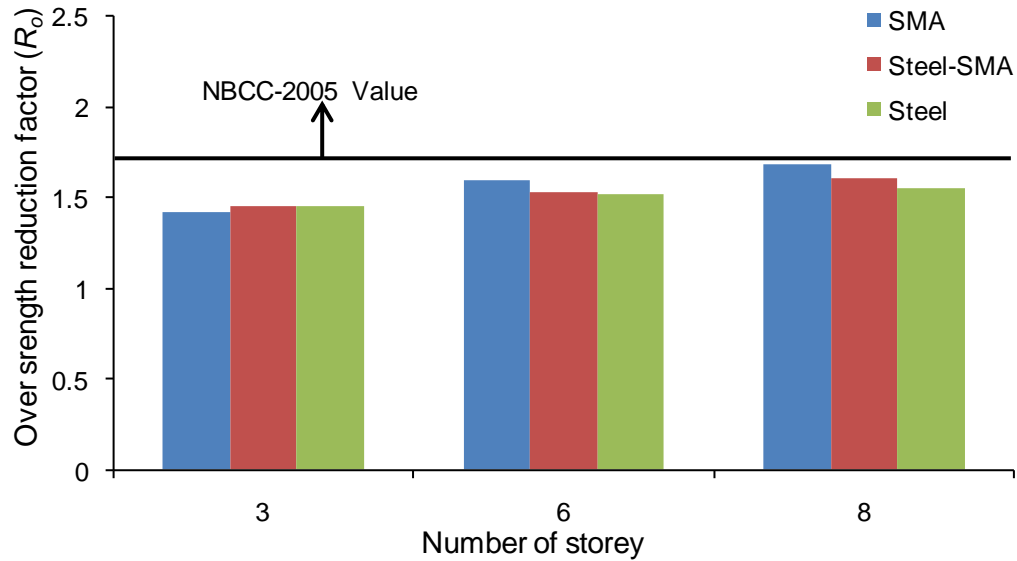


Figure 3.11 Over-strength factor, R_o .

The ductility reduction factor (R_d) supply obtained in this study is given in Figure 3.12. NBCC (2005) proposes a ductility reduction factor (R_d) of 4.0 for ductile reinforced concrete buildings, but in this study the minimum ductility reduction factor obtained was 10.0 for the 3-storey Steel-SMA RC frame. The ductility reduction factor (R_d) supply obtained from this study is inconsistent in pattern. In the case of the 3-storey frames, the SMA RC frame offers more ductility reduction factor compared to Steel-SMA and Steel RC frames. While in the case of the 6 and the 8-storey the Steel-SMA and the Steel RC frames a higher ductility reduction factor (R_d) was computed compared to SMA RC frames.

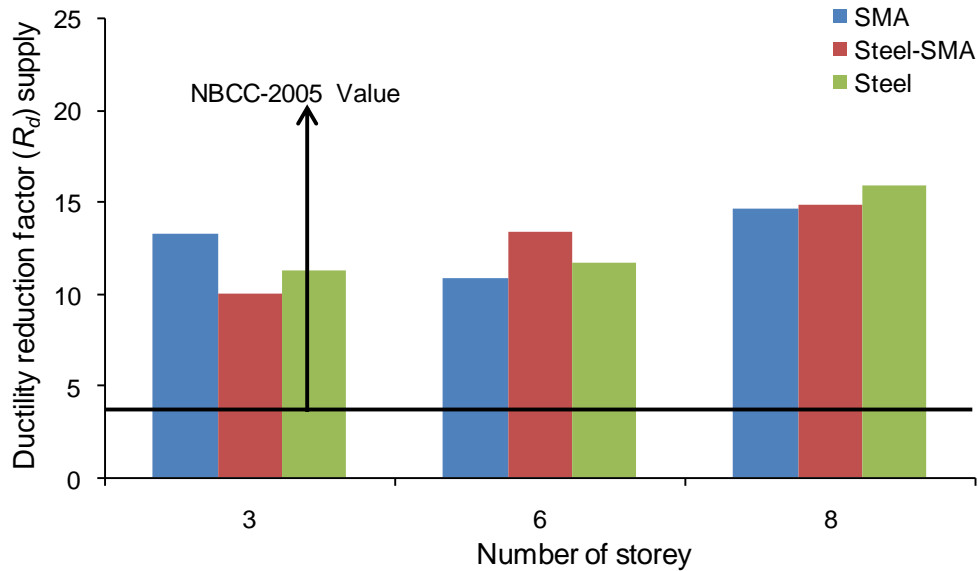


Figure 3.12 Ductility reduction factor (R_d) supply.

The Response modification factor (R) supply obtained in this study is illustrated in Figure 3.13. NBCC-2005 proposes a response modification factor of 6.8 for ductile moment-resisting reinforced concrete buildings, but in this study the minimum response modification factor (R) supply obtained was 14.5 for the 3-storey Steel-SMA RC frame. There is no particular pattern in the response modification factor (R) supply obtained from this study. The highest response modification supply is offered by the 8-storey Steel RC frame. For 3-stories the SMA RC frame offers a higher response modification factor compared to the Steel-SMA and the Steel RC frames. In the case of the 6-storey Steel-SMA and the 8-storey Steel RC frames, they supply a greater response modification factor compared to other frames respectively. The response modification factor (R) supply depends on the elastic base shear obtained from the dynamic time history analyses. Since the elastic base shear depends on the characteristics of the considered ground motion records the R values also depend on it. Some of the considered earthquake records

produced more elastic base shear that's why the R supply obtained in this study is higher compared to the code specified values.

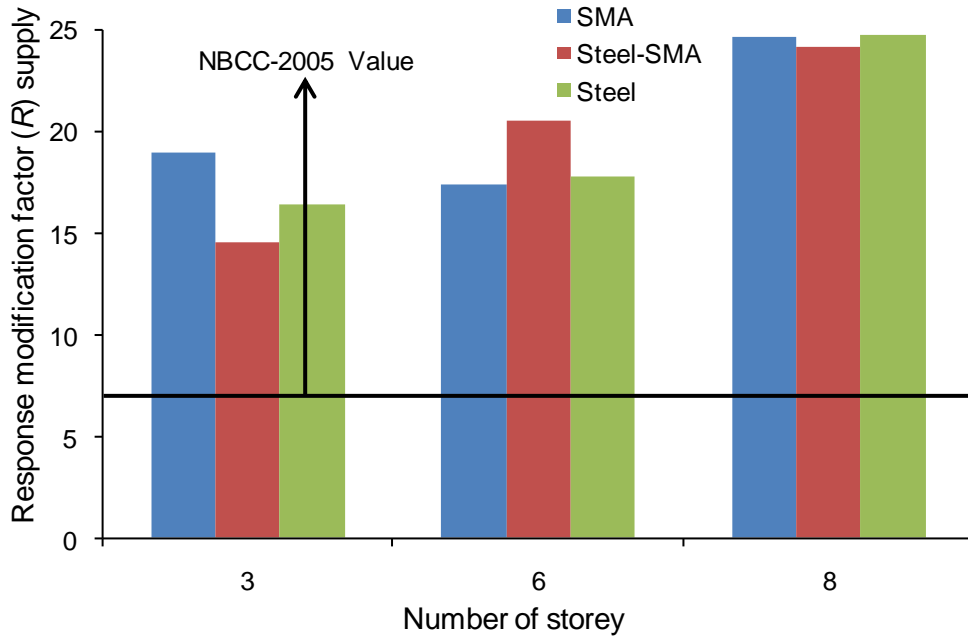


Figure 3.13 Response modification factor (R) supply.

3.8.2 Response modification factor (R) demand

The ductility factor (R_d) demand is calculated by using the system ductility factor (μ) as described by Miranda and Bertero (1994) and presented in Eq. 3.4 and 3.5 to calculate the ductility reduction factor. They used 124 ground motion data to develop this equation and they showed that the ductility factors depend on the fundamental period of the structures, system ductility and soil condition.

$$R_d = \frac{\mu - 1}{\phi} + 1 \quad [3.4]$$

$$\phi = 1 + \frac{1}{10T - \mu T} - \frac{1}{2T} e^{-1.5(\ln(T) - 0.6)^2} \quad [3.5]$$

Where T is the fundamental period of a structure, μ is the system ductility and Φ is a coefficient reflecting the soil condition. The system ductility is obtained by dividing the maximum roof displacement and the system yield displacement (Mwafy and Elnashai 2002). The ductility reduction factor and the response modification factor are calculated by using Equations 3.4 and 3.5 as demand, which are presented in Figure 3.15 and 3.15. The results show that the ductility reduction factor demand increases with the increase of number of stories. Although NBCC (2005) specifies ductility reduction factor at 4.0 for ductile moment-resisting reinforced concrete buildings, the maximum demand obtained from this study is 2.24 for the 8-storey Steel RC frame. The ductility reduction factor demand is lower for SMA RC frames, compared to the Steel-SMA and Steel RC frames for the 3, 6, and 8-stories.

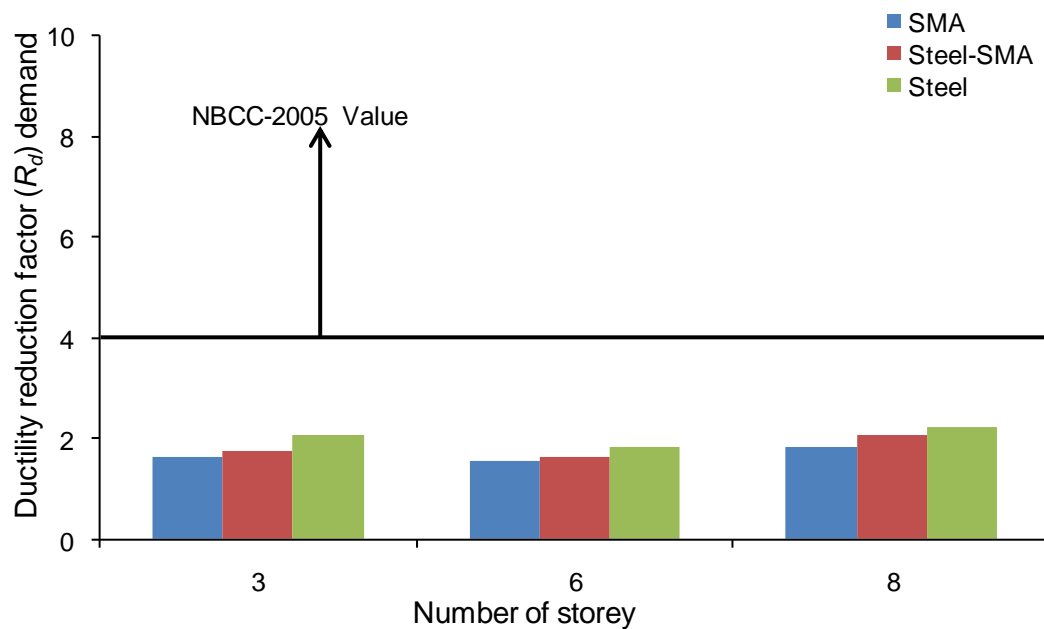


Figure 3.14 Ductility reduction factor (R_d) demand.

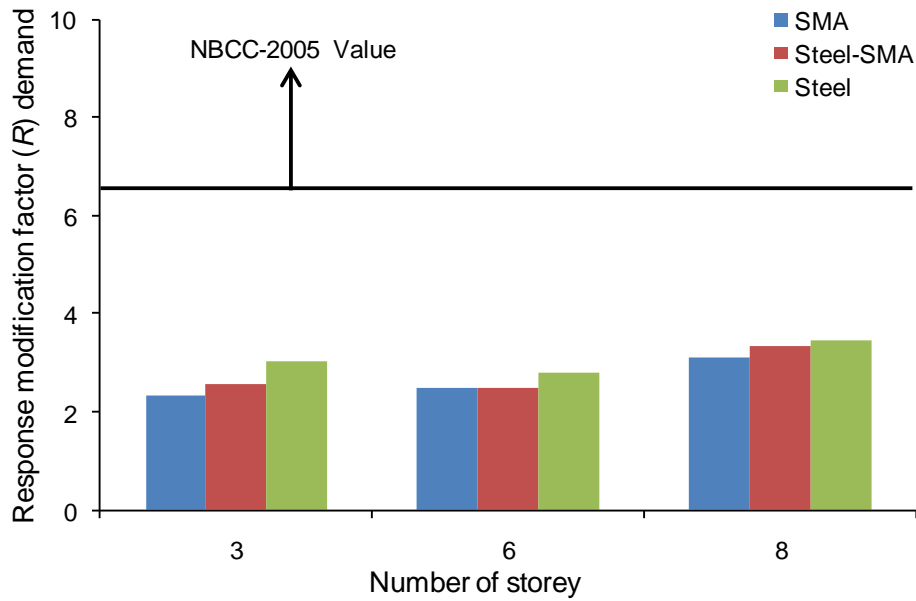


Figure 3.15 Response modification factor (R) demand.

3.8.3 Ductility reduction factor (R_d) supply-demand ratio

The ductility reduction factor supply-demand ratio is presented in Figure 3.16. The ductility reduction supply demand ratio for SMA RC frames is higher compared to the Steel RC frames of different stories.

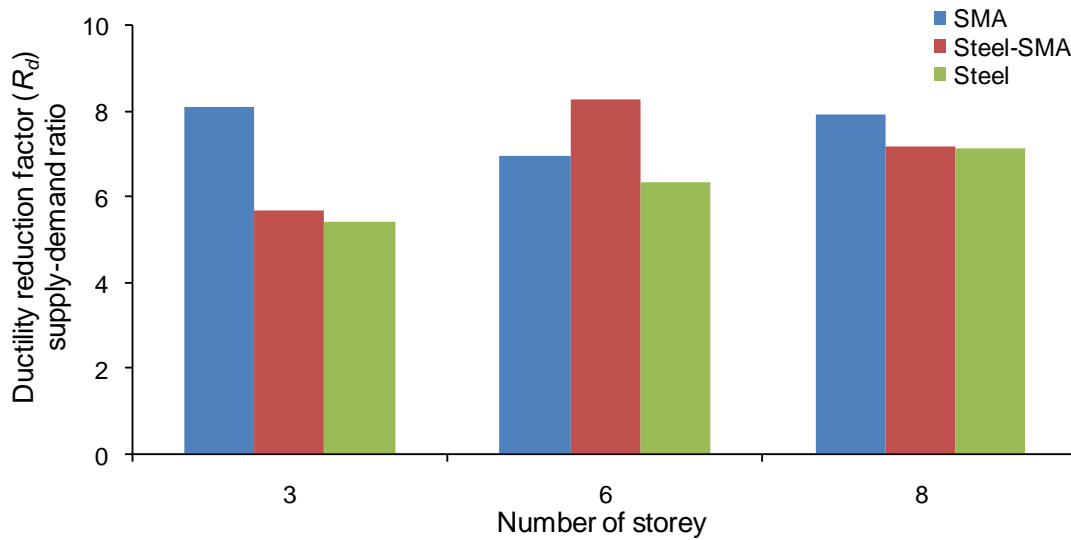


Figure 3.16 Ductility reduction factor (R_d) supply-demand ratio.

3.9 SUMMARY

The results obtained from this chapter indicated that although SMAs have low modulus of elasticity, it provided similar seismic overstrength factor, ductility reduction factor supply and response modification factor supply. The response modification factor demand was calculated for different frame types, which showed that the values obtained for SMA RC frames were less than those of Steel RC frames.

CHAPTER 4: SEISMIC VULNERABILITY ASSESSMENT OF SHAPE MEMORY ALLOY REINFORCED CONCRETE FRAMES

4.1 GENERAL

Earthquake is now the most common type of natural disaster, which is being felt in different parts of the world. An earthquake can cause substantial damage to civil infrastructure and devastation to a society. Many civil engineering structures like buildings, bridges, and roads may collapse or get damaged severely during an earthquake as observed in the 2011 Christchurch Earthquake in New Zealand. The most recent high magnitude earthquake in the northeastern coast of *Japan* on March 11th, 2011 triggered a tsunami and washed away many houses and damaged the nuclear power plant buildings at Fukushima. The magnitude of damages largely depends on numerous factors like the geometry of the building, the dynamic characteristics of the building, and finally the characteristics of the earthquake (Anan et al. 2009). For particular ground motion parameters, the seismic vulnerability indicates the possibility of multiple damages to the building through graphical representation (Jian and Ping, 2009). In the past, different researchers proposed various vulnerability relationships such as earthquake intensity in terms of Peak Ground Acceleration (*PGA*), Spectral Acceleration (S_a), Peak Ground Velocity (*PGV*) versus damages in terms of roof drift, inter-storey drift or base shear for reinforced concrete (RC) buildings, which were completely based on analytically simulated building damage statistics (Rossetto and Elnashai, 2005). There is no unique approach for the derivation of these relationships since different analysis techniques, structural idealizations, seismic hazard, and damage models are being used.

Several researchers evaluated the seismic vulnerability for different structures using different methods. Erduran and Yakut (2007) performed both analytical and experimental investigation to assess the vulnerability of reinforced concrete moment resisting frame buildings with masonry infill wall. They considered the member damage functions in terms of inter-storey drift ratios and developed member functions for the primary components like beams, columns, and infill walls. Rossetto and Elnashai (2005) proposed a new analytical procedure to assess the vulnerability of reinforced concrete structures. They developed displacement based vulnerability curves for populations of RC structures. El Howary and Mehanny (2010) evaluated the seismic vulnerability of reinforced concrete frame buildings located in moderate seismic zones by performing incremental dynamic analyses. Annan et al. (2009) assessed the seismic vulnerability of modular steel buildings by performing nonlinear incremental dynamic analyses in terms of maximum inter-storey drift and peak global roof drift. It is vital to simulate these reasons as close to reality as possible in order to appropriately forecast seismic performance or vulnerability of a given structural system by experimental and/or analytical procedures. When the response is predominantly inelastic, uncertainties and randomness in many of these cases pose a severe challenge in the analysis technique (Annan et al. 2009). Vulnerability of a structure under seismic loading largely depends on its inelastic behaviour, such as energy dissipation and strength degradation. For instance, building systems with high energy dissipation capacity are likely to undergo excessively large inelastic deformations than those systems with comparatively low energy dissipation capacity. According to modern building codes like the National Building Code of Canada (NBCC 2005), it is expected that under a severe earthquake, the building system will undergo large inelastic deformation and dissipate substantial amount of energy, and will be able to sustain load.

The forces resulting from an idealized elastic response spectrum, representing site seismicity, are reduced by a force modification factor or response behaviour factor, R . This factor is also used to intensify the calculated elastic drift, which provides an estimate of the potential seismic damages. Generally, the building codes impose drift limits based on their storey heights. Each building code prescribes different R values for different structural frame systems, which represent the capability of a particular type of structure to dissipate energy through inelastic behaviour. The R factor is partially attributed to system's ductility and to the increase in strength beyond the design strength as a result of strain hardening of steel, larger dimensions than standard, higher yield strength than specified values, design assumptions, and redistribution of internal forces in the inelastic range of response and failure mechanism (Mitchell et al. 2003). In the National Building Code of Canada (NBCC 2005), the R factor is the result of the ductility-related force modification factor, R_d , and the overstrength-related force modification factor, R_o . Therefore, it is essential to determine appropriate R values for designing new types of structures to estimate their seismic design base shear and assess their structural drift demands.

Since SMAs have lower modulus of elasticity compared to mild steel, it is postulated here that the overstrength factor R_o , ductility factor, R_d , and structural drift demand will not be the same as presented in NBCC (2005) for regular Steel RC frame structures. The overstrength factor R_o and ductility factor R_d are discussed in Chapter 3. In the current chapter, roof drift demand and maximum inter-storey drift demand, residual roof drift demand and maximum residual inter-storey drift demand is computed for shape memory alloy reinforced concrete frames. The effect of SMA as reinforcement in concrete frame structures has been analytically investigated where three different types of reinforced

concrete (RC) buildings of different stories (3, 6 and 8) were considered. For each type of building, three different reinforcement detailings are considered, i) only steel is used as longitudinal reinforcement (Steel RC), ii) Steel-SMA hybrid reinforcement where SMA is used particularly in the plastic hinge region of the beams as longitudinal reinforcement and steel in other regions (Steel-SMA RC), and iii) SMA is used as longitudinal reinforcement in beams (SMA RC). For each type of considered frame structures steel is used as longitudinal reinforcement in columns and tie reinforcement in each element.

The current study focuses on computing seismic inelastic demands and capacities for 3, 6, and 8-storey SMA RC, Steel-SMA RC and Steel RC frames located in western Canada and designed for ductile moment resisting frames according to NBCC (2005) and Canadian standards CSA A-23.3-04. The performance and response of these structures were evaluated by developing nonlinear analytical models of the frames to an ensemble of 10 earthquake ground motions scaled to different intensity levels. The spectral acceleration at the structure's fundamental mode period was used to scale each record, thus allowing a reduction in record-to-record variability. The corresponding peak ground acceleration (*PGA*) was also used as a seismic hazard representation for comparison in order to determine the more consistent intensity measure for the SMA RC frame system.

4.2 DESIGN OF THE BUILDINGS AND ITS ANALYTICAL MODELING

4.2.1 Design of the building

The details in the design procedure for these buildings have been described in Section 3.4.

4.2.2 Analytical modeling of the building

The details about the analytical model for these buildings have been described in Section 3.5.

4.3 EIGEN VALUE ANALYSIS

Eigen value analyses were performed using SAP 2000 V14.0 considering effective stiffness method for all the frames to determine their fundamental period (T_1) of vibration. Depending on this fundamental period, design spectral acceleration for the considered frames has been calculated. The fundamental period and design spectral acceleration values are given in Table 4.1. From this table it was observed that the use of SMA as reinforcement in beam increases the fundamental period of the structure compared to steel because of SMA's lower modulus of elasticity compared to steel. As the stiffness decreases, the period of the structure increases. As the fundamental period of the structure increased for SMA RC frames, the design spectral acceleration values decreased.

Table 4.1 Fundamental Period and design spectral acceleration of the structure.

RC Frame Types	Fundamental period, T_1 (sec) and Spectral Acceleration, S_a					
	Effective stiffness, K_{eff}					
	3-Storey		6-Storey		8-Storey	
	T_1	S_a	T_1	S_a	T_1	S_a
SMA	0.42	0.7	0.74	0.47	1	0.33
Steel-SMA	0.41	0.71	0.7	0.49	0.93	0.35
Steel	0.39	0.72	0.67	0.51	0.86	0.39

4.4 SELECTION OF GROUND MOTION RECORDS AND ANALYSIS CHARACTERISTICS

The selection of ground motion records has been described elaborately in Chapter 3 under section 3.7.

4.5 RESULTS AND DISCUSSIONS

Nonlinear incremental dynamic time history analyses have been performed to determine the seismic vulnerability of the SMA, the Steel-SMA and the Steel RC frames. Almost all the current seismic design codes and recommendations specify seismic hazard in terms of a single intensity measure, such as the peak ground acceleration (*PGA*), or a spectral ordinate at a given period (S_a). In the current version of NBCC (2005), the seismic hazard is defined by spectral acceleration values at periods of 0.2, 0.5, 1.0, and 2.0 s. Spectral acceleration (S_a) is an assessment of ground motion that takes into consideration the sustained shaking energy at a specific period. For a selected site of a chosen reinforced concrete buildings, the 2% in 50-year intensity of ground motion (expressed as spectral accelerations, $S_a(T)$ that correspond to the fundamental period of the building frame), were evaluated as 0.72g, 0.51g, and 0.39g for the 3, 6, and 8-story Steel RC frames, respectively. For the Steel-SMA RC frames the spectral acceleration values are 0.71g, 0.49g and 0.35g for 3, 6 and 8storey frames, and in the case of 3, 6 and 8 storey SMA RC frames the spectral acceleration values are 0.7g, 0.47g and 0.33g, respectively (Table 4.1).

It is well-recognized that dissimilar ground motion records scaled to the same *PGA* do not persuade the same level of response, and do not cause the same quantity of damage to a given structure. This is due to differences in other seismic hazard parameters, such as the frequency content, the event duration, and the effective number of loading cycles. Hence,

the response found using one ground motion record may not grant sufficient assurance that the structure will yield a similar response if subjected to another ground motion record which has the same *PGA*. Shome and Cornell (1999) proved that sufficient precision can be earned in the estimation of seismic demands of mid-rise buildings if 10–20 ground motion records are considered. The Federal emergency management agency (FEMA2000a) suggests selecting a suite of 10–20 accelerograms to represent the site and the hazard level to attain the collapse prevention level.

The seismic inelastic demands of the chosen building systems were determined by using the incremental dynamic analysis (*IDA*) procedure. *IDA* was introduced by Luco and Cornell (1998) and has been explained in detail in Vamvatsikos and Cornell (2002) and Yun et al. (2002). This analysis procedure has also been included in a modern seismic design recommendation (FEMA, 2000a). Determining the seismic demand with an adequate accuracy requires the selection of competent analysis characteristics. Shome et al. (1998) showed that by scaling ground motion records to the target spectral acceleration at the fundamental-mode period of a structure, the seismic demands at this intensity can be efficiently determined. The spectral acceleration at 5% damping, $S_a(T_1, 5\%)$, was principally used as an intensity measure (*IM*) in this study.

Seismic performance can be calculated using fracture life, energy dissipation capacity, maximum inter-storey drift, maximum roof drift, and ductility capacity. Maximum inter-story drift is frequently used as a prime damage intensity factor in the vulnerability assessment of moment resisting frames (Sabelli, 2001; Uriz and Mahin, 2004). The maximum peak inter-story drift ratio (θ_{max}), and peak roof drift ratio (θ_{roof}) were selected as global Demand Parameters (*DP*) to study the structural response of the selected frames

during the ground motion's duration. The inter-story drift ratio is calculated as the difference in displacements of the adjacent stories divided by the inter-story height, and the peak roof drift ratio is computed from the ratio of the peak roof drift to the overall height of the structural frame. The *IDA* curves are then obtained for each record from a plot of the demand parameters against their corresponding intensity measure parameters.

To evaluate the seismic vulnerability of the considered frames using inelastic dynamic analyses, an assessment of their dynamic response characteristics is necessary. Incremental nonlinear dynamic time history analyses have been performed for each frame using nine real earthquake data and an artificial earthquake ground motion data developed by Atkinson (2009) for the city of Vancouver (see Section 3.7).

4.5.1 *IDA* curves for roof drift

Results of nonlinear incremental dynamic time history analyses, performed on the 9 nonlinear numerical models of the SMA RC, Steel-SMA RC and Steel RC frame for the selected ten ground motion records, were plotted as *IDA* curves in terms of roof drift and are shown in Figure 4.1 and Figure 4.2. To develop the *IDA* curves, a structural Demand Parameter (*DP*) like roof drift resulting from a scaled ground motion record for a known Intensity Measure (*IM*) is set on the horizontal axis and the corresponding intensity measure is set on the vertical axis. The different *IM* values for a particular ground motion record produce different *DP* values. The spline connecting all the points for a particular ground motion record produces a fit line. Each *IDA* curve contains ten fit lines.

In Figure 4.1 the earthquake record's *IM* was the 5% damped spectral acceleration of the scaled earthquake records at the fundamental mode period of the structure, $S_a(T_1, 5\%)$.

Figure 4.1 shows the variation of the engineering DP , and the roof drift, θ_{roof} with respect to the demand spectral acceleration. Figure 4.2 was constructed by keeping those DP on the horizontal axis and their corresponding PGA of the damped spectral acceleration on the vertical axis. The diversity and scattering of the results obtained for different ground motions and different frames, as shown by these curves, is large. All curves, however, display an individual linear elastic behaviour before the first sign of a considerable nonlinearity has occurred. Comparing Figure 4.1 against Figure 4.2, which has been constructed for roof drift demand, it is observed that the $S_d(T_1, 5\%)$ is a more regular intensity measure than the PGA . It can be observed from the IDA curves that the intensity measure (IM) is high for the 8-storey compared to that of the 3 and 6-storey frames. From the IDA curves it is concluded that the demand parameter not only depends on the magnitude of the intensity measure (IM) but it also depends on the pattern and timing of the records. In some cases, a higher intensity measure produced a lower demand parameter.

Although each of the IDA curves is a distinct deterministic unit, the natural random variability within the earthquake records requires a statistical assessment for demand. The IDA curves developed for the considered ground motion records need to be summarized by defining the 16%, 50% and 84% IDA curves (Vamvatsikos and Cornell, 2002, 2004). This summary produces more reliable data to use and analyse. Normally, engineering design is based on the median, mean or 84%. The fractile curves were developed by calculating the 16%, 50% and 84% fractile values of the demand parameters for a specific ground motion intensity measure. Figure 4.3 shows the 16%, 50% and 84% fractile IDA curves for the 3, 6 and 8-storey frames in terms of roof drift. The fractile IDA curves can also signify the seismic demand curves of the frames and may be used to evaluate their performance by

comparing them with the permissible drift demand at any specified intensity and probability level. For example, given the design level ground motion intensity of $S_a(T_I, 5\%) = 0.72g, 0.71g$ and $0.70g$ for the 3-storey Steel RC, Steel-SMA RC and SMA RC frame at the 2.0% in a 50-year probability level the 16% fractile of the records would produce $\theta_{roof} \leq 0.33\%, 0.54\%, 0.36\%$; the 50% fractile would produce $\theta_{roof} \leq 0.88\%, 0.96\%$ and 0.72% ; and the 84% fractile of the records would produce $\theta_{roof} \leq 1.55\%, 1.84\%$ and 1.4% for Steel, Steel-SMA and SMA RC frames, respectively. For the 6-storey SMA RC, Steel-SMA RC and Steel RC frame at its design level intensity, 16% of the records would produce $\theta_{roof} \leq 0.52\%, 0.45\%, 0.52\%$; the 50% of the records would produce $\theta_{roof} \leq 1.09\%, 1.22\%$ and 0.96% ; and 84% of the records would yield $\theta_{roof} \leq 2.19\%, 2.23\%$ and 1.78% , respectively.

For the 8-storey SMA RC, Steel-SMA RC and Steel RC frame at its design level intensity, the 16% of the records would produce $\theta_{roof} \leq 0.87\%, 0.79\%$, and 0.38% ; the 50% of the records would produce $\theta_{roof} \leq 1.57\%, 1.46\%$ and 0.87% ; and the 84% of the records would yield $\theta_{roof} \leq 3.03\%, 2.88\%$ and 1.62% , respectively. From this probabilistic analysis, it can be concluded that the SMA RC and Steel-SMA RC frames exceed the limiting value of 2.5% for the 8-storey frame for a high intensity earthquake. However at the median level, the SMA RC and Steel-SMA RC frame are safe. From the fractile *IDA* curves in terms of roof drift, it is also concluded that with the increase of the height of the frame the demand parameter increases. The summary of the *IDA* curves in terms of roof drift at the design level intensity is given in Table 4.2.

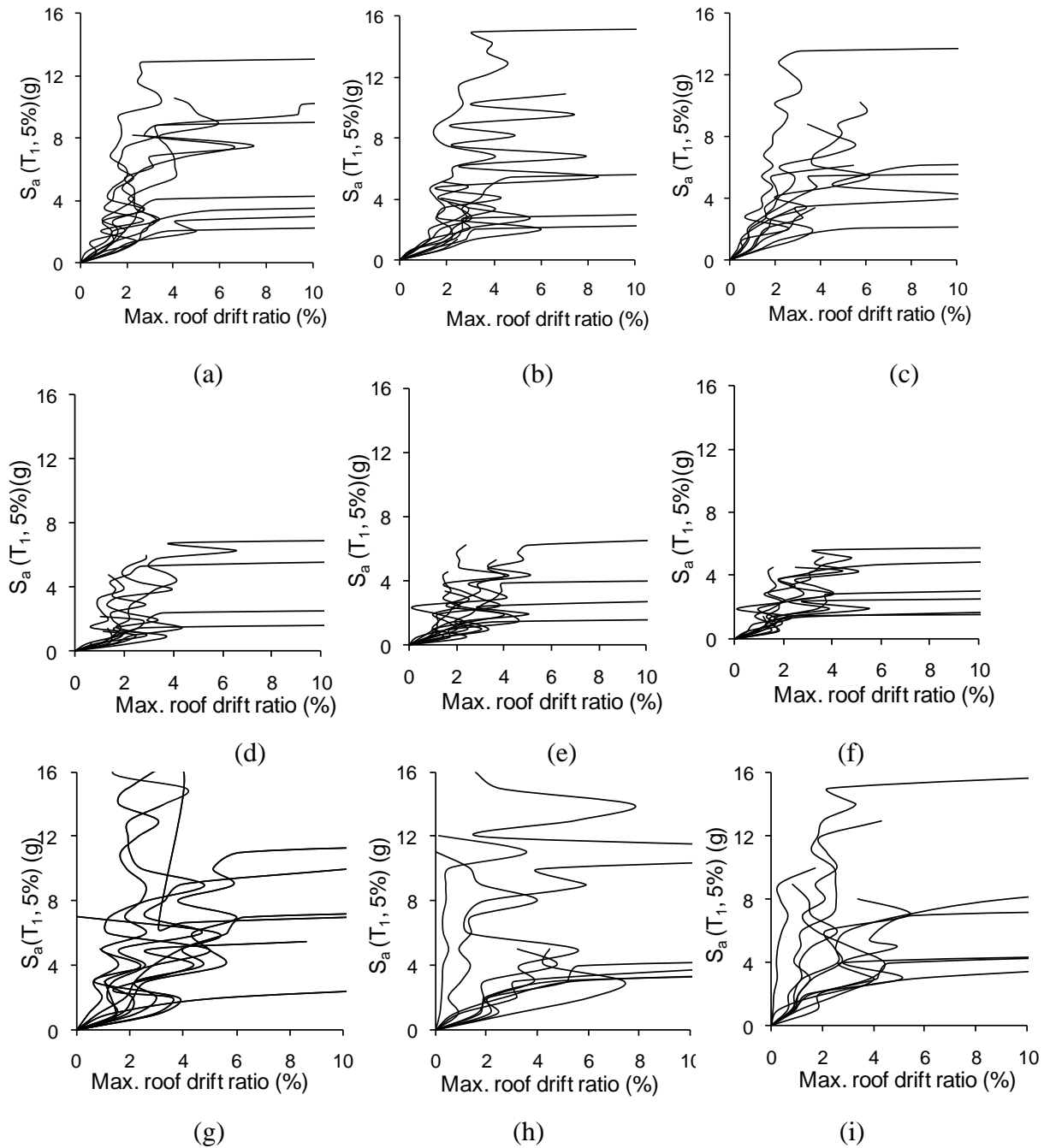


Figure 4.1 IDA curves of “first mode” spectral acceleration, $S_a(T_1, 5\%)$, plotted against peak roof drift ratio θ_{roof} , for 3-storey (a) SMA RC, (b) Steel-SMA RC, (c) Steel RC frames; 6-storey (d) SMA RC, (e) Steel-SMA RC, (f) Steel RC frames; and 8-storey (g) SMA RC, (h) Steel-SMA RC, (i) Steel RC frames.

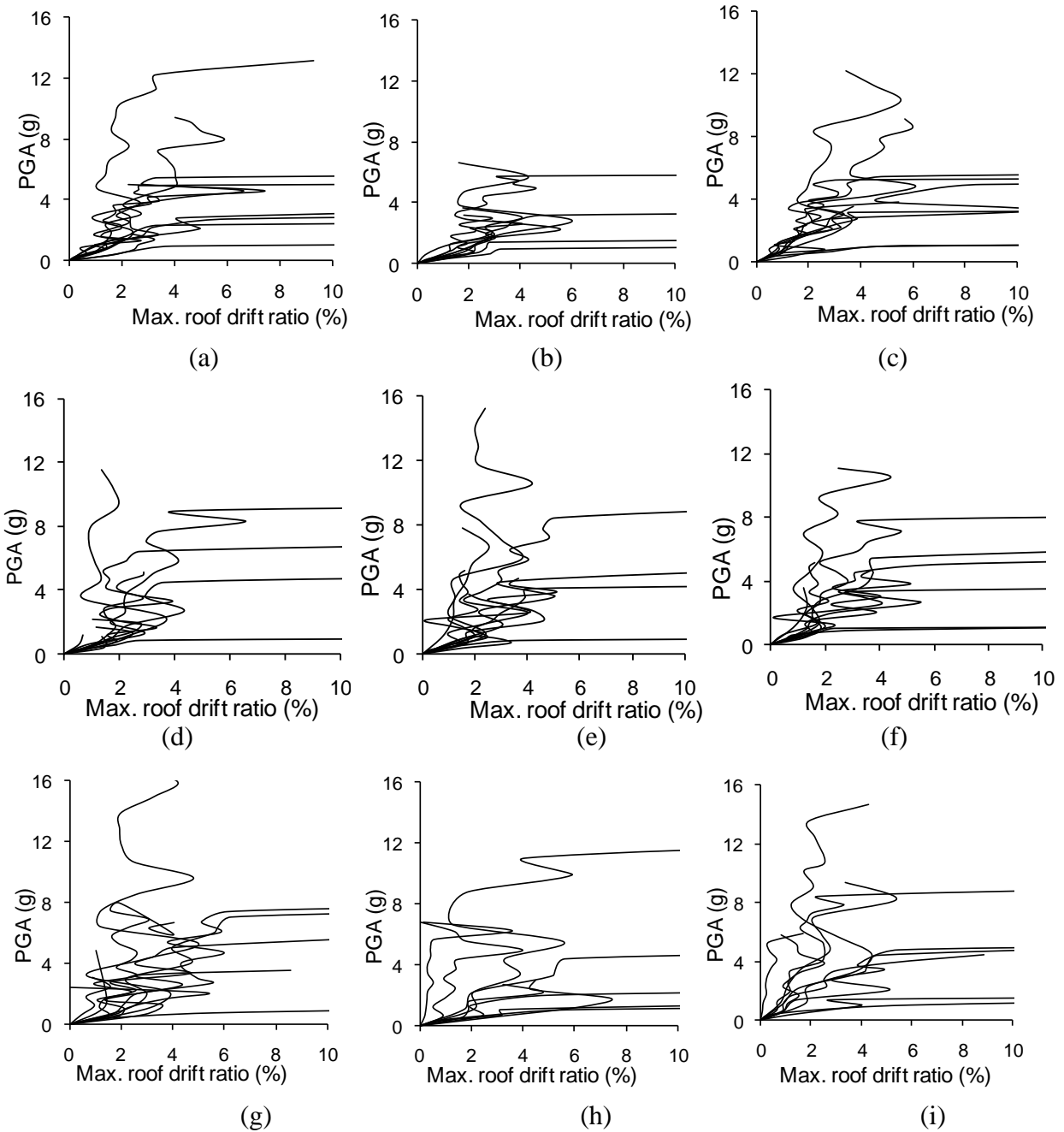


Figure 4.2 *IDA* curves of peak ground acceleration (*PGA*), plotted against peak roof drift ratio, θ_{roof} , for 3-storey (a) SMA RC, (b) Steel-SMA RC, (c) Steel RC frames; 6-storey (d) SMA RC, (e) Steel-SMA RC, (f) Steel RC frames; and 8-storey (g) SMA RC, (h) Steel-SMA RC, (i) Steel RC frames.

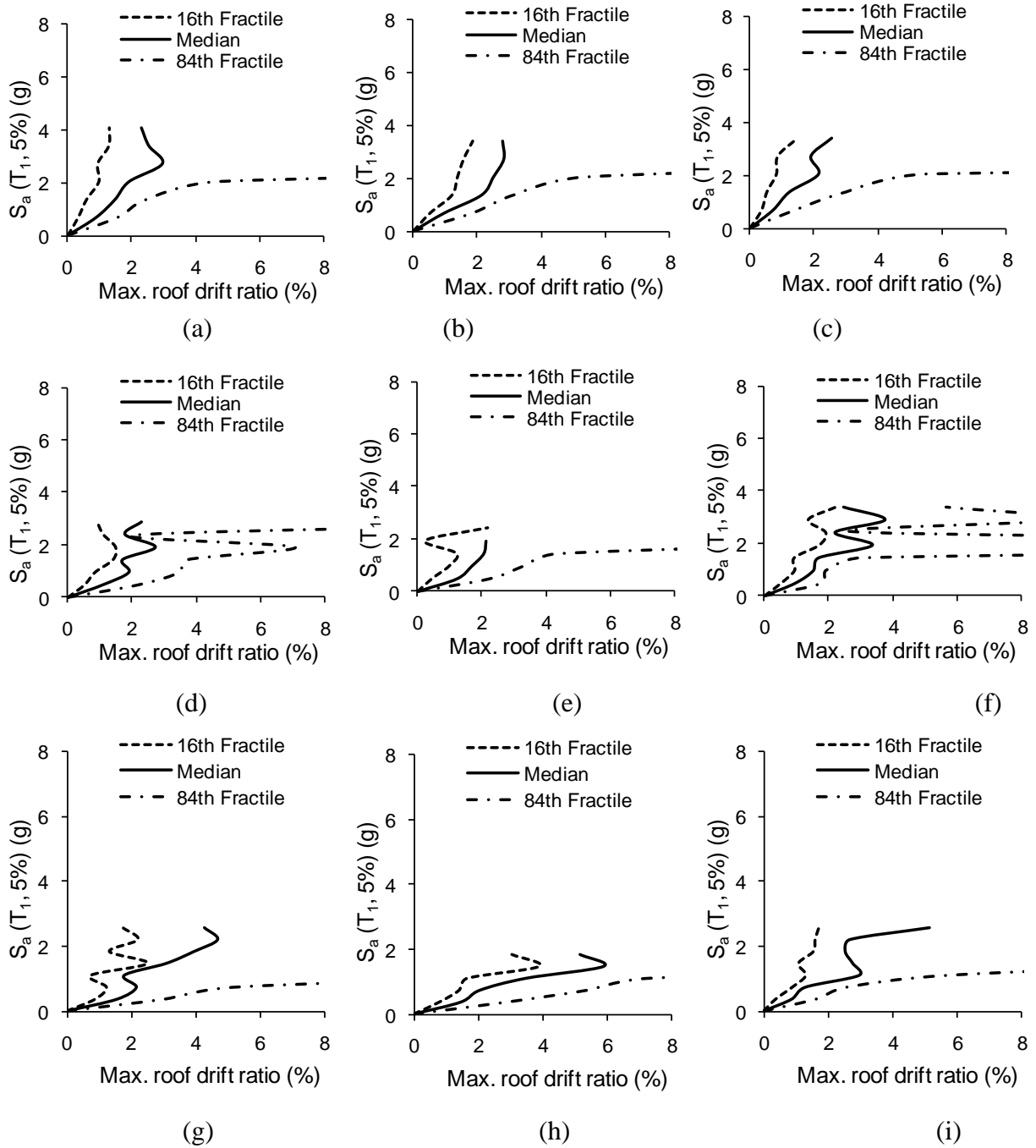


Figure 4.3 Summary of maximum roof-drift *IDA* curves into 16th, 50th, and 84th fractile, for the 3-storey (a) SMA RC, (b) Steel-SMA RC, (c) Steel RC frames; 6-storey (d) SMA RC, (e) Steel-SMA RC, (f) Steel RC frames; and 8-storey (g) SMA RC, (h) Steel-SMA RC, (i) Steel RC frames.

Table 4.2 Summary of maximum roof drift at design level intensity

RC Frame Types	Building ID								
	3-Storey			6-storey			8-storey		
	16 th Fractile	Median	84 th Fractile	16 th Fractile	Median	84 th Fractile	16 th Fractile	Median	84 th Fractile
SMA	0.33	0.88	1.55	0.52	1.09	2.19	0.87	1.57	3.03
Steel-SMA	0.54	0.96	1.84	0.45	1.22	2.23	0.79	1.46	2.88
Steel	0.36	0.72	1.40	1.40	1.84	1.55	0.38	0.87	1.62

4.5.2 IDA curves for maximum inter-storey drift

Besides the maximum roof drift, the maximum inter-storey drift is also considered an important parameter for building structures in order to evaluate the vulnerability. In this study from the nonlinear incremental time history analyses, the *IDA* curves are plotted in terms of the maximum inter-storey drift and are shown in Figures 4.4 and 4.5. In Figure 4.4 the earthquake record's *IM* was the 5% damped spectral acceleration of the scaled earthquake records at the fundamental mode period of the structure, $S_a(T_1, 5\%)$. Figure 4.4 shows the variation of the engineering *DP*, and the maximum inter-storey drift θ_{max} with respect to *IM*, spectral acceleration. Figure 4.5 is constructed by keeping those *DP* on the horizontal axis and the corresponding *PGA* of the damped spectral acceleration on the vertical.

A statistical assessment is also performed for demand calculation. This statistical assessment produces more reliable data to use and understand the application of vulnerability assessment. Figure 4.6 shows the 16%, 50% and 84% fractile *IDA* curves for the 3, 6, and 8-storey frames in terms of maximum inter-storey drift.

The fractile *IDA* curves can also signify seismic demand curves of the frames and may be used to evaluate their performance by comparing with permissible drift demands at any specified intensity and probability level. For example, given the design level ground motion intensity at the 2.0% in a 50-year probability level for the 3-storey SMA RC, Steel-SMA RC and Steel RC frame, the 16% of the records would produce $\theta_{max} \leq 0.42\%$, 0.17%, 0.49%; the 50% would produce $\theta_{max} \leq 1.08\%$, 1.19 % and 0.96%; and the 84% of the records would yield $\theta_{max} \leq 2.02\%$, 2.51% and 2.20%, respectively. Figure 4.6 (d), (e) , and (f) shows the fractile *IDA* curve for the 6-storey SMA RC, Steel-SMA RC and Steel RC frame, respectively and from these figures it is concluded, that at its design level intensity, the 16% of the records would produce $\theta_{max} \leq 0.85\%$, 0.68%, 0.72%; the 50% would produce $\theta_{max} \leq 1.8\%$, 2.03 % and 1.91%; and the 84% of the records would yield $\theta_{max} \leq 5.18\%$, 5.75% and 3.58%, respectively. For the 8-storey SMA RC, Steel-SMA RC and Steel RC frame, Figure 4.6 (g), (h), and (i) presents the fractile *IDA* curve, respectively and from these figures it is observed that at its design level intensity the 16% of the records would produce $\theta_{max} \leq 1.35\%$, 0.8%, 1.05%; the 50% would produce $\theta_{max} \leq 2.65\%$, 2.27 % and 1.64%; and the 84% of the records would generate $\theta_{max} \leq 5.18\%$, 3.84% and 3.34% for SMA, Steel-SMA and Steel RC frames, respectively. In the NBCC (2005), drift limits are based on the median 2% in a 50-year seismic hazard level and are given as 1% for post-disaster buildings, 2% for school and other important buildings, and 2.5% for other buildings types.

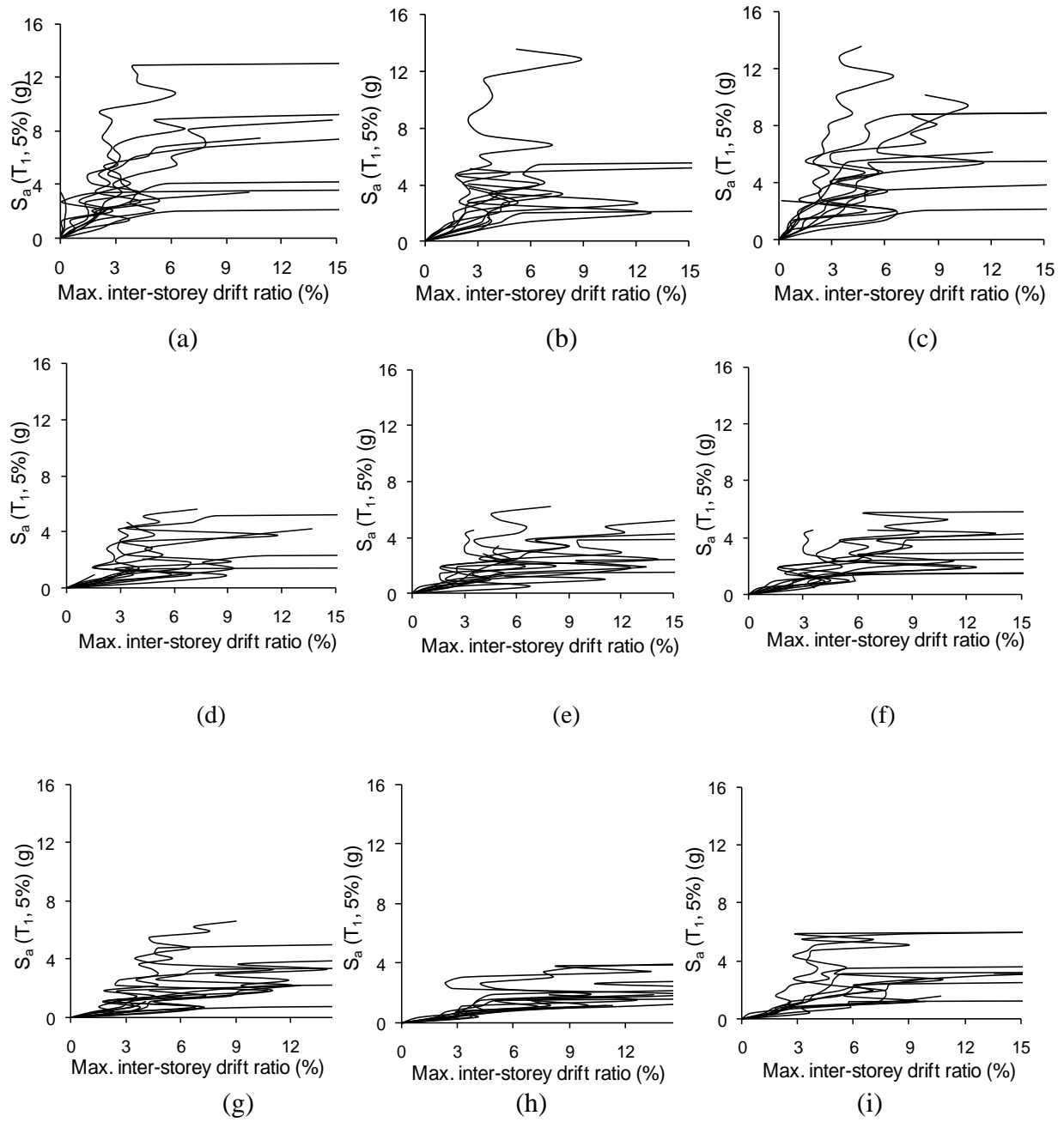


Figure 4.4 IDA curves of “first mode” spectral acceleration, $S_a(T_1, 5\%)$, plotted against maximum inter-storey drift ratio, θ_{max} , for 3-storey (a) SMA RC, (b) Steel-SMA RC, (c) Steel RC frames; 6-storey (d) SMA RC, (e) Steel-SMA RC, (f) Steel RC frames; and 8-storey (g) SMA RC, (h) Steel-SMA RC, (i) Steel RC frames.

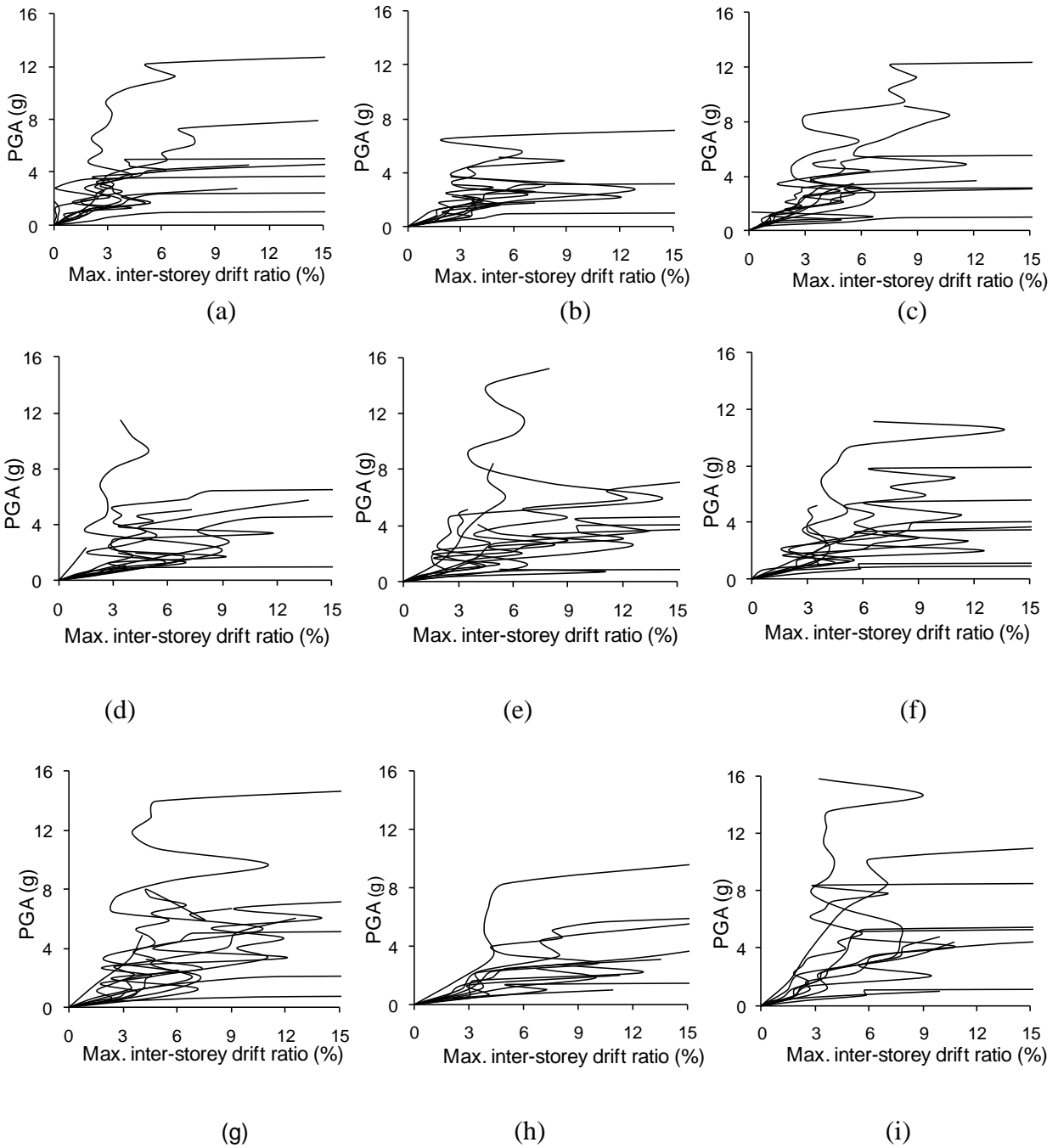


Figure 4.5 IDA curves of peak ground acceleration (PGA), plotted against maximum inter-storey drift ratio, θ_{max} , for 3-storey (a) SMA RC, (b) Steel-SMA RC, (c) Steel RC frames; 6-storey (d) SMA RC, (e) Steel-SMA RC, (f) Steel RC frames; and 8-storey (g) SMA RC, (h) Steel-SMA RC, (i) Steel RC frames.

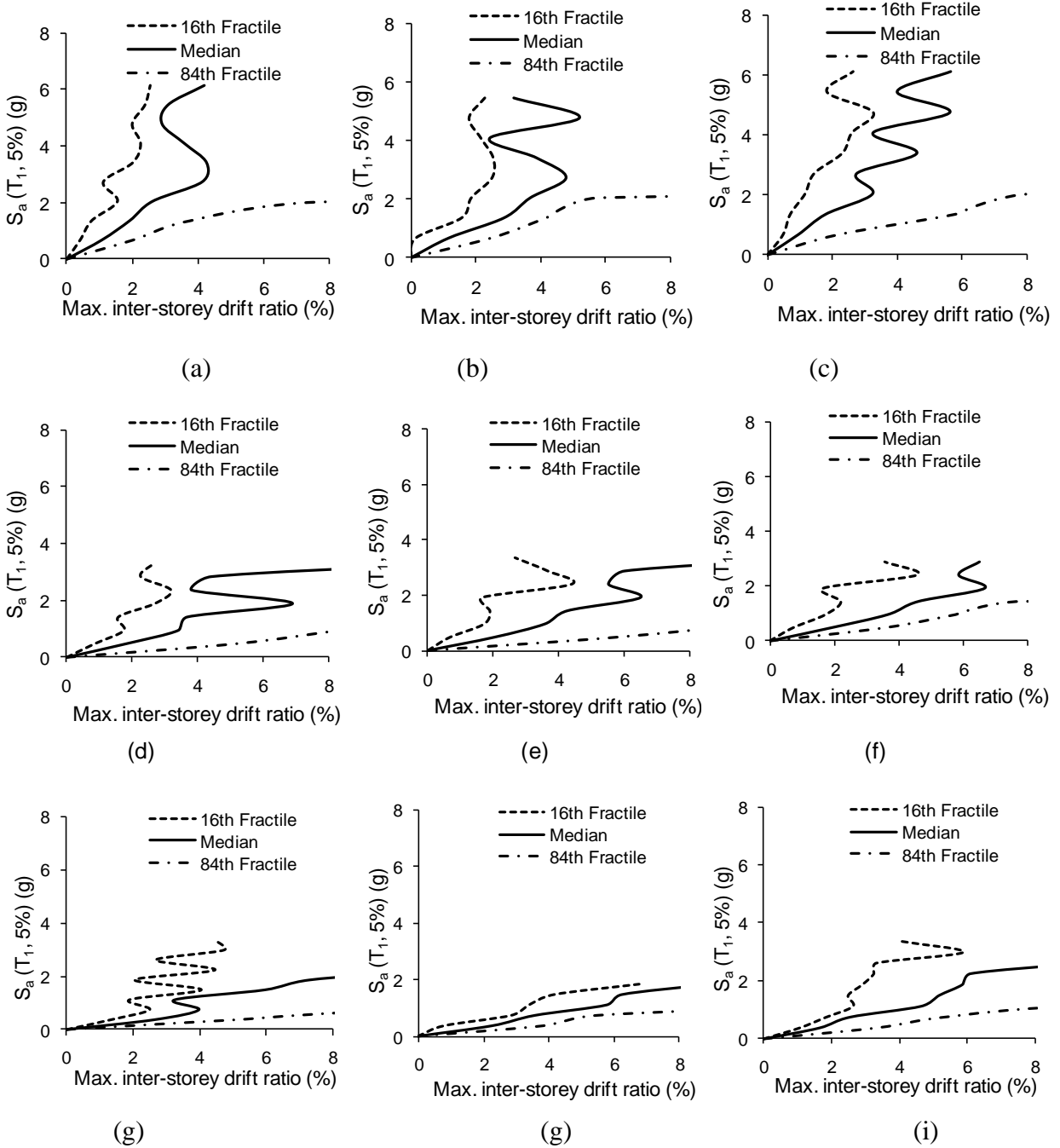


Figure 4.6 Summary of maximum inter-storey drift *IDA* curves into 16th, 50th, and 84th fractile for 3-storey (a) SMA RC, (b) Steel-SMA RC, (c) Steel RC frames; 6-storey (d) SMA RC, (e) Steel-SMA RC, (f) Steel RC frames; and 8-storey (g) SMA RC, (h) Steel-SMA RC, (i) Steel RC frames.

From these probabilistic analyses it can be observed that the SMA RC frame exceeds the limiting value of 2.5% for 8-storey frames. Therefore the SMA can be used for low rise buildings up to 6-storey safely and the Steel-SMA RC frames perform safely up to 8-storey. From the fractile *IDA* curves it can also be concluded that, with the increase of the height of the frame, the demand parameter increases for the SMA RC frames significantly. However for the Steel RC and Steel-SMA RC frames, the demand for the 8-storey frame is less compared to the 6-storey frame. The summary of the *IDA* curves in terms of inter-storey drift at the design level intensity is given in Table 4.3.

Table 4.3 Summary of maximum inter-storey drift at design level intensity

RC Frame Types	Building ID								
	3-Storey			6-storey			8-storey		
	16 th Fractile	Median	84 th Fractile	16 th Fractile	Median	84 th Fractile	16 th Fractile	Median	84 th Fractile
SMA	0.42	1.08	2.02	0.85	1.80	5.18	0.87	1.57	3.03
Steel-SMA	0.17	1.19	2.51	0.68	2.03	5.75	0.79	1.46	2.88
Steel	0.49	0.96	2.20	0.72	1.91	3.58	0.38	0.87	1.62

4.5.3 *IDA* curves for residual roof drift

One of the main reasons of excessive repair costs for reinforced concrete structures after a high intensity earthquake is its high residual deformation. The *IDA* curves plotted in terms of residual roof drift are shown in Figure 4.7 and Figure 4.8. An *IDA* curve, for residual roof drift is developed by keeping residual roof drift on a horizontal axis, and the corresponding spectral acceleration values on the vertical axis. The different *IM* values for a particular ground motion record produce different *DP* values. Figure 4.7 shows the variation of engineering *DP* (residual roof drift) with respect to *IM* (spectral acceleration). Figure 4.8 is constructed by keeping those *DP* on the horizontal axis and the corresponding

PGA of the damped spectral acceleration on the vertical axis. A large scatter in the results obtained for different ground motions and different frames is observed as shown by these curves. However, all the *IDA* curves displayed an individual linear elastic behaviour before the first sign of a considerable nonlinearity occur.

Comparing Figures 4.7 and 4.8 which have been constructed for residual roof drift demand it can be observed that the $Sa(T_1, 5\%)$ is a more regular intensity measure than the *PGA*. From the *IDA* curves it can be concluded that the intensity measure (*IM*) is high for the 3-storey and comparatively lower for the 6 and 8-storey frames. Therefore, with the increase in height of the building the intensity measures decrease. It is also concluded from the *IDA* curves that the demand parameter not only depends on the magnitude of the intensity measure (*IM*) but it also depends on the frequency and duration of the records.

The fractile *IDA* curves can also imply seismic residual demand curves of the frames and can be used to compare the performance among the framing systems. For example, given the design level ground motion intensity at 2.0% in a 50-year probability level for the 3-storey SMA RC, Steel-SMA RC and Steel RC frame, the 16% of the records would produce $\theta_{roof} \leq 0.03\%$, 0.03%, 0.004%; the 50% would produce $\theta_{roof} \leq 0.05\%$, 0.04 % and 0.03%; and the 84% of the records would generate $\theta_{roof} \leq 0.12\%$, 0.09% and 0.16%, respectively (Figure 4.9). From the fractile curves (Figure 4.9) of a 6-storey frame it is observed that the SMA RC, Steel-SMA RC and Steel RC frame, at its design level intensity the 16% of the records would create $\theta_{roof} \leq 0.01\%$, 0.002%, and 0.01%; the 50% would produce $\theta_{roof} \leq 0.04\%$, 0.03 % and 0.03%; and the 84% of the records would generate $\theta_{roof} \leq 0.11\%$, 0.03% and 0.30%, respectively. Figure 4.9 also shows the fractile curve for 8-storey SMA RC, Steel-SMA RC and Steel RC frame. From this figure it is observed that at

its design level intensity the 16% of the records would produce $\theta_{rroof} \leq 0.01\%$, 0.002% , 0.01% ; the 50% would generate $\theta_{rroof} \leq 0.05\%$, 0.02% and 0.12% ; and the 84% of the records would produce $\theta_{rroof} \leq 0.23\%$, 0.15% and 0.23% . For all frames the residual drift percentage for the case of 50% is less for Steel-SMA frame. The amount of residual roof drift increased for steel RC frame with increase of number of storey. The summary of the *IDA* curves in terms of residual roof drift at the design level intensity is given in Table 4.4.

Table 4.4 Summary of maximum residual roof drift at design level intensity.

RC Frame Types	Building ID								
	3-Storey			6-storey			8-storey		
	16 th Fractile	Median	84 th Fractile	16 th Fractile	Median	84 th Fractile	16 th Fractile	Median	84 th Fractile
SMA	0.03	0.05	0.12	0.01	0.04	0.11	0.01	0.05	0.23
Steel-SMA	0.03	0.04	0.09	0.00	0.03	0.08	0.00	0.02	0.15
Steel	0.00	0.03	0.16	0.01	0.03	0.30	0.01	0.12	0.22

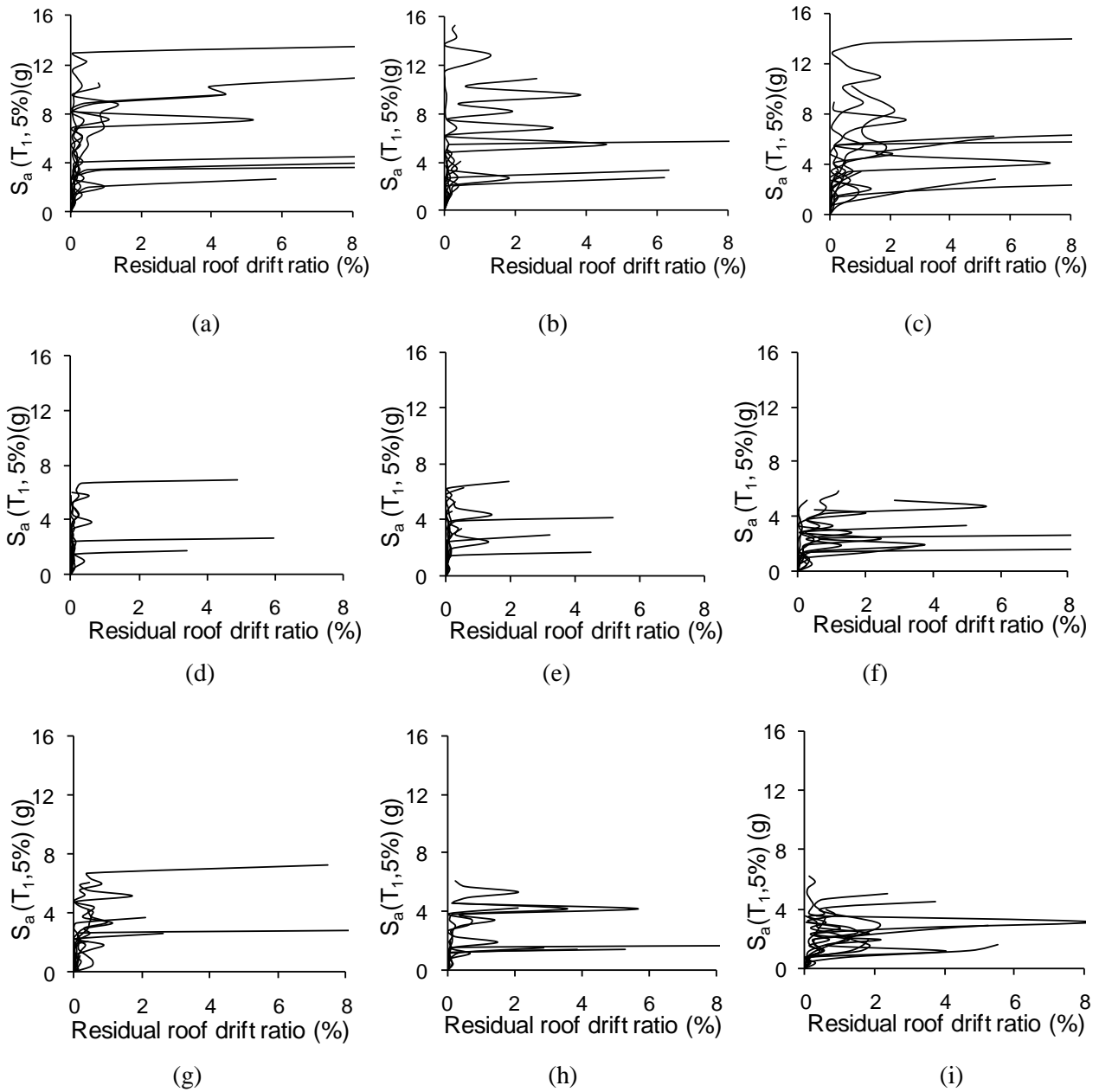


Figure 4.7 IDA curves of “first mode” spectral acceleration, $S_a(T_1, 5\%)$, plotted against residual roof drift ratio, θ_{roof} , for 3-storey (a) SMA RC, (b) Steel-SMA RC, (c) Steel RC frames; 6-storey (d) SMA RC, (e) Steel-SMA RC, (f) Steel RC frames; and 8-storey (g) SMA RC, (h) Steel-SMA RC, (i) Steel RC frames.

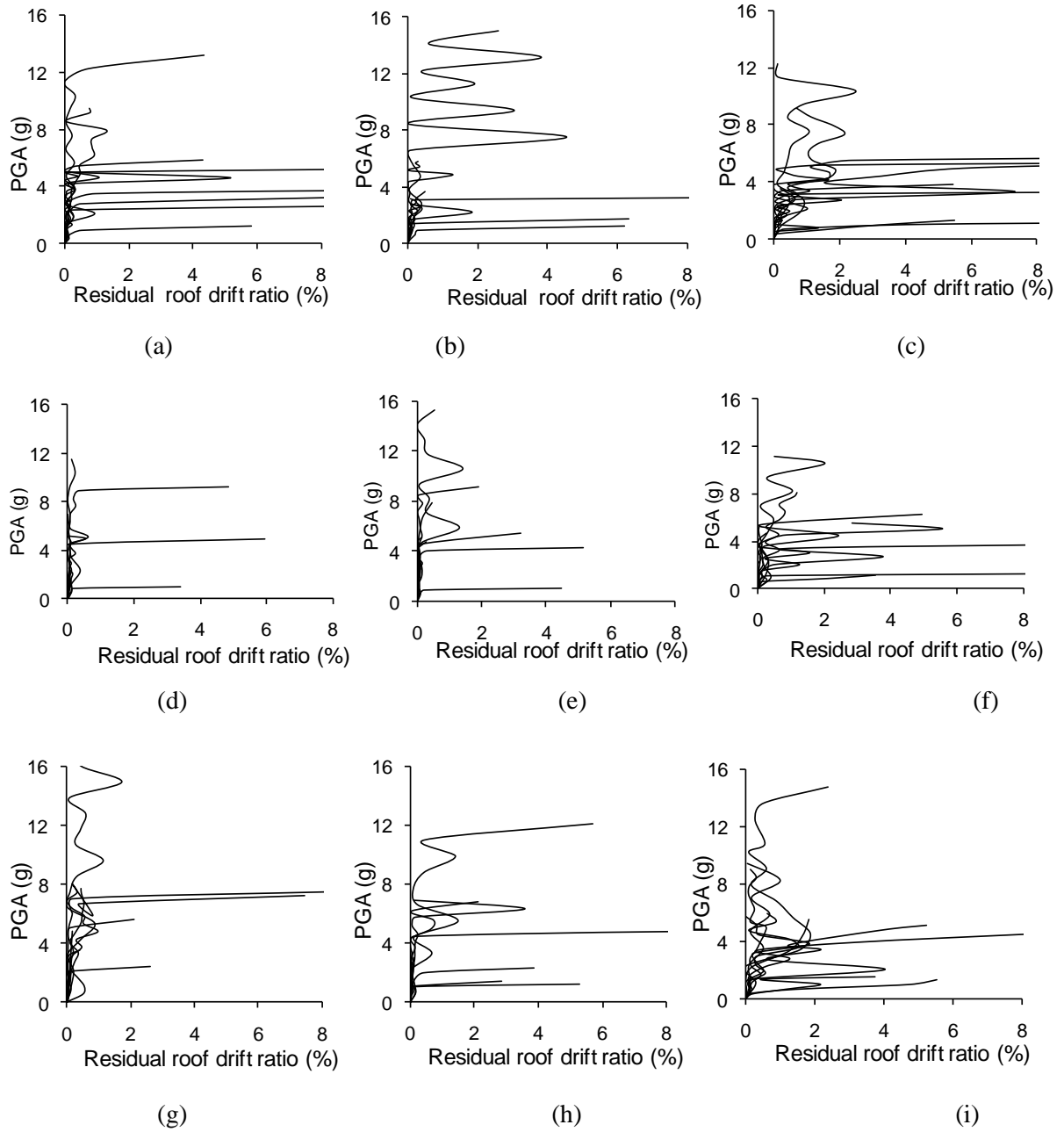


Figure 4.8 IDA curves of peak ground acceleration (PGA), plotted against residual roof drift ratio, for 3-storey (a) SMA RC, (b) Steel-SMA RC, (c) Steel RC frames; 6-storey (d) SMA RC, (e) Steel-SMA RC, (f) Steel RC frames; and 8-storey (g) SMA RC, (h) Steel-SMA RC, (i) Steel RC frames.

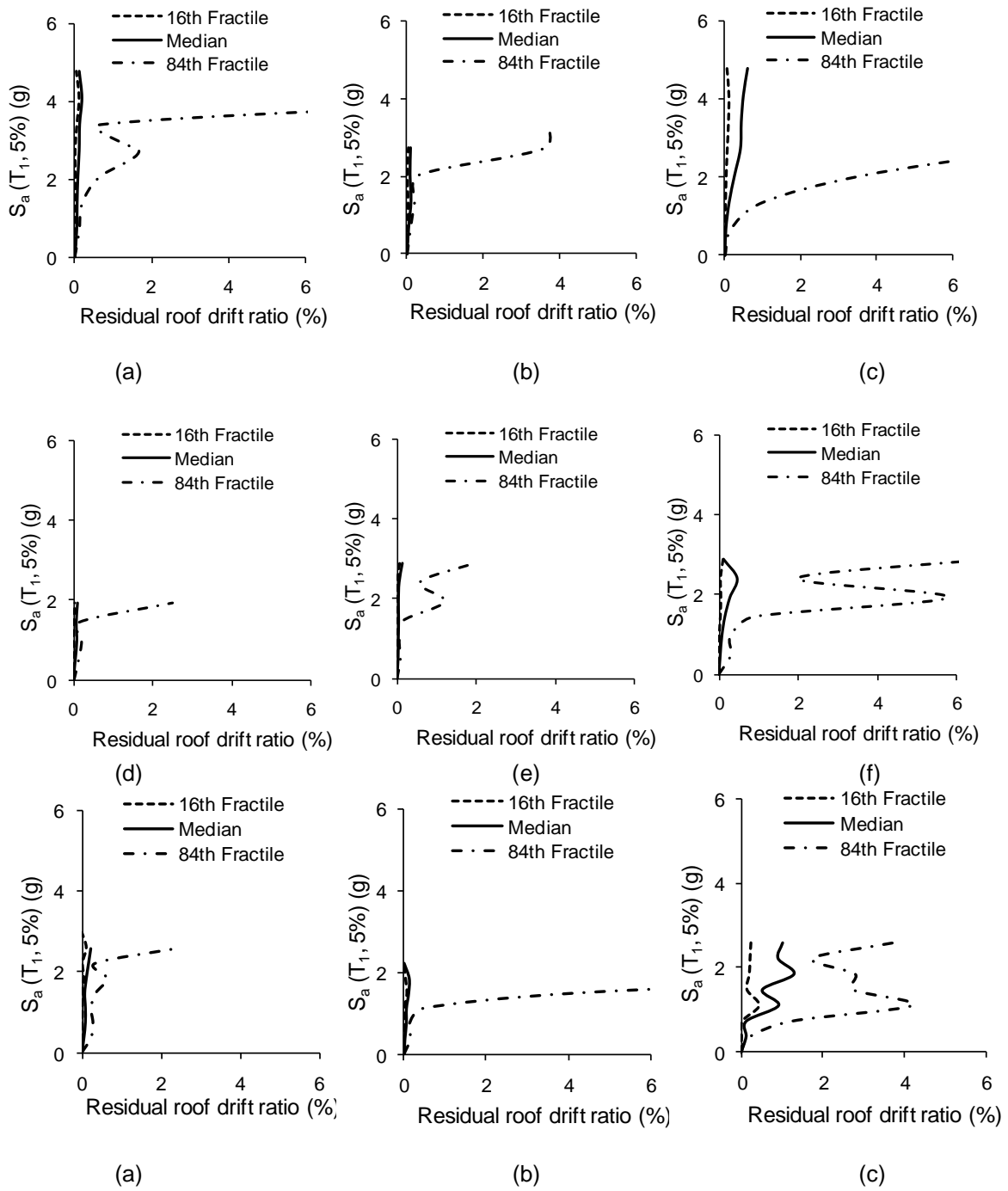


Figure 4.9 Summary of residual roof drift *IDA* curves into 16th, 50th, and 84th fractile 3-storey (a) SMA RC, (b) Steel-SMA RC, (c) Steel RC frames; 6-storey (d) SMA RC, (e) Steel-SMA RC, (f) Steel RC frames; and 8-storey (g) SMA RC, (h) Steel-SMA RC, (i) Steel RC frames.

4.5.4 *IDA* curves for maximum residual inter-storey drift

The *IDA* curves plotted in terms of the maximum residual inter-storey drift are shown in Figure 4.10 and Figure 4.11. To develop an *IDA* curve, the maximum residual inter-storey drift, θ_{max} is obtained from a scaled ground motion record is set on the horizontal axis and the corresponding intensity measure is set on the vertical axis. For a particular ground motion record, the different *IM* values produced different *DP* values. A fit line of an *IDA* curve connecting all the points that are observed for a particular ground motion record and each *IDA* curve contained ten fit lines.

Figure 4.10 shows the variation of the engineering *DP* maximum residual inter-storey drift with respect to demand spectral acceleration. Figure 4.11 is constructed by keeping this *DP* on the horizontal axis and the corresponding *PGA* of the damped spectral acceleration on the vertical axis. It is observed from the *IDA* curves that the intensity measure (*IM*) is high for the 3-storey and comparatively lower for the 6 and 8-storey buildings. With the increase in height of the buildings, the intensity measure decreases. From the *IDA* curves it is observed that the demand parameter not only depends on the magnitude of the earthquake but also on the pattern and the duration of the records. Like the previous demand parameters, it is also observed that a higher intensity measure produces a lower demand parameter.

In order to compare the performance of the framing systems in terms of maximum residual inter-storey demand, a fractile *IDA* curve can be used. The fractile *IDA* curve is presented in Figures 4.12 (a), (b) and (c) for the 3-storey SMA RC, Steel-SMA RC and Steel RC frame. From this figure it can be observed that at the design level intensity the

16% of the records would produce $\theta_{rmax} \leq 0.15\%$, 0.08% , and 0.05% ; the 50% would create $\theta_{rmax} \leq 0.17\%$, 0.15% and 0.1% ; and the 84% of the records would yield $\theta_{rmax} \leq 0.26\%$, 0.49% and 0.51% , respectively. From the fractile curve, for the 6-storey SMA RC, Steel-SMA RC and Steel RC frame, at its design level intensity the 16% of the records would produce $\theta_{rmax} \leq 0.08\%$, 0.06% , and 0.07% ; the 50% would produce $\theta_{rmax} \leq 0.14\%$, 0.12% and 0.31% ; and the 84% of the records would yield $\theta_{rmax} \leq 0.33\%$, 0.35% and 0.78% , respectively. However for the 8-storey SMA RC, Steel-SMA RC and Steel RC frame, at its design level intensity the 16% of the records would be $\theta_{rmax} \leq 0.09\%$, 0.05% , and 0.27% ; the 50% would be $\theta_{rmax} \leq 0.18\%$, 0.15% and 0.41% ; and the 84% of the records would be $\theta_{rmax} \leq 0.31\%$, 0.38% and 0.67% , respectively. The summary of the *IDA* curves in terms of residual inter-storey drift at the design level intensity is given in Table 4.5.

Table 4.5 Summary of residual maximum inter-storey drift at design level intensity

RC Frame Types	Building ID								
	3-Storey			6-storey			8-storey		
	16 th Fractile	Median	84 th Fractile	16 th Fractile	Median	84 th Fractile	16 th Fractile	Median	84 th Fractile
SMA	0.15	0.17	0.26	0.08	0.14	0.33	0.09	0.18	0.31
Steel-SMA	0.08	0.15	0.49	0.06	0.12	0.35	0.05	0.15	0.38
Steel	0.05	0.10	0.51	0.07	0.31	0.78	0.27	0.41	0.67

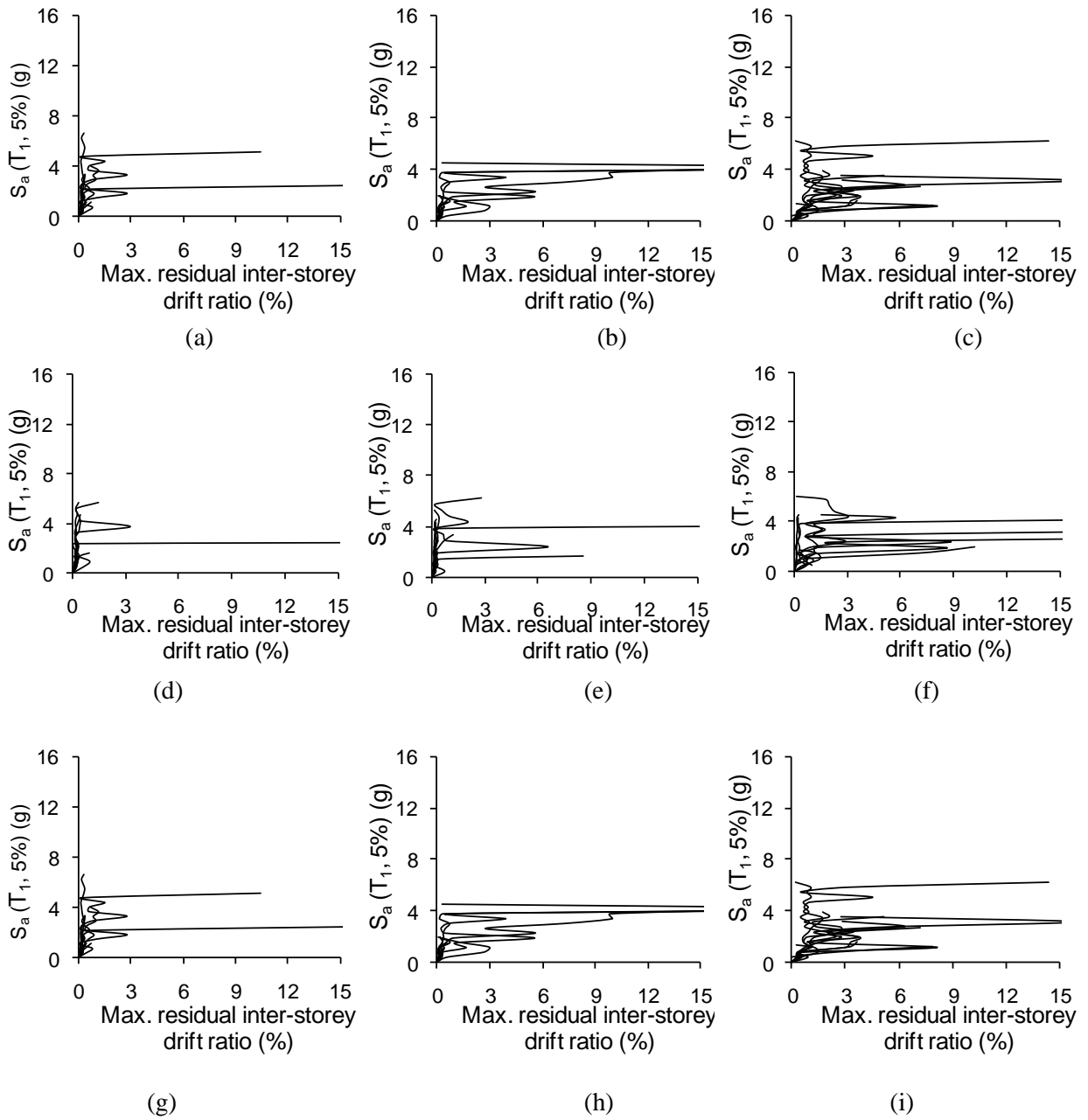


Figure 4.10 IDA curves of “first mode” spectral acceleration, $S_a(T_1, 5\%)$, plotted against maximum residual inter-storey drift ratio, for 3-storey (a) SMA RC, (b) Steel-SMA RC, (c) Steel RC frames; 6-storey (d) SMA RC, (e) Steel-SMA RC, (f) Steel RC frames; and 8-storey (g) SMA RC, (h) Steel-SMA RC, (i) Steel RC frames.

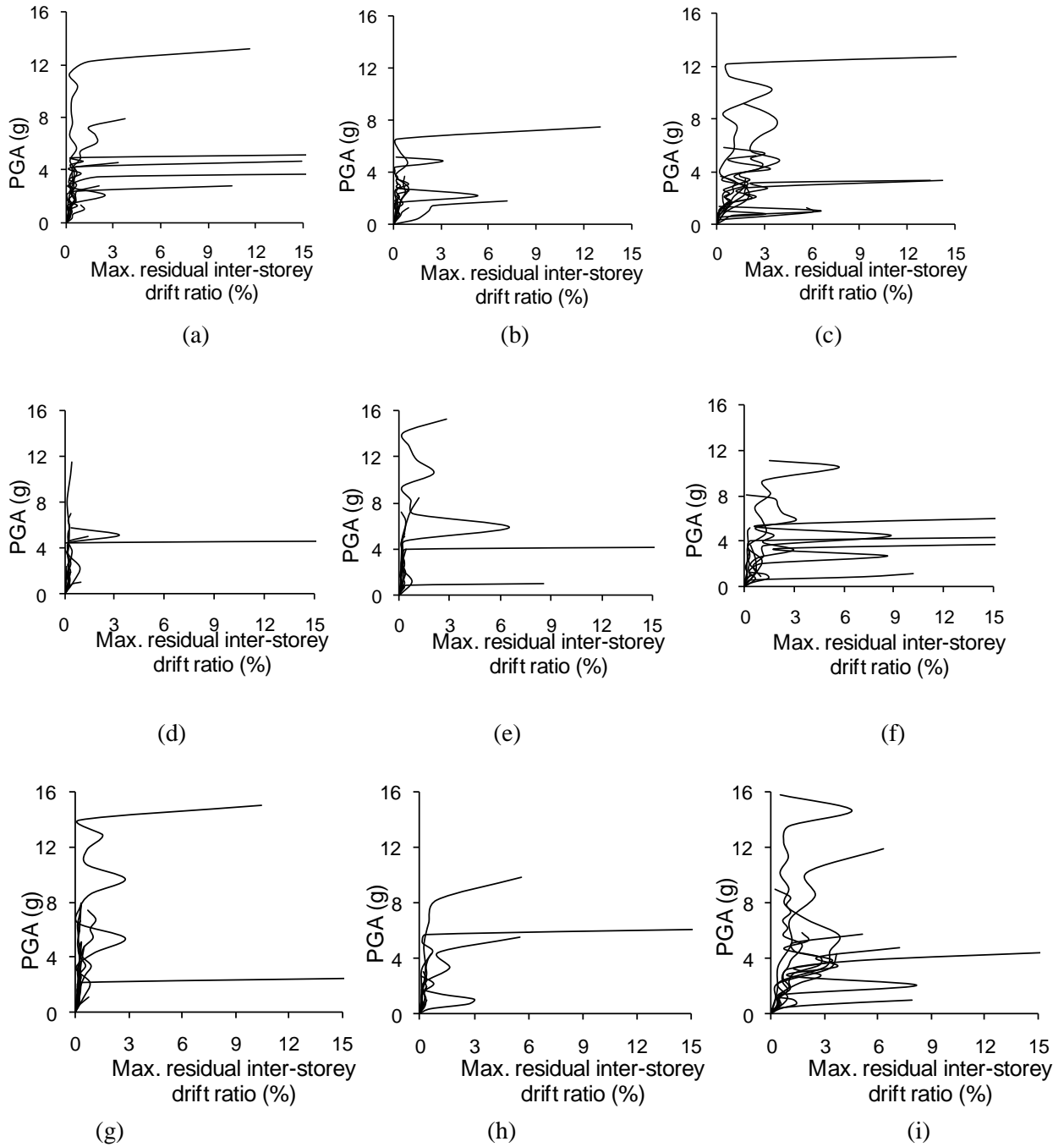


Figure 4.11 IDA curves of peak ground acceleration, (PGA), plotted against maximum residual inter-storey drift ratio for 3-storey (a) SMA RC, (b) Steel-SMA RC, (c) Steel RC frames; 6-storey (d) SMA RC, (e) Steel-SMA RC, (f) Steel RC frames; and 8-storey (g) SMA RC, (h) Steel-SMA RC, (i) Steel RC frames.

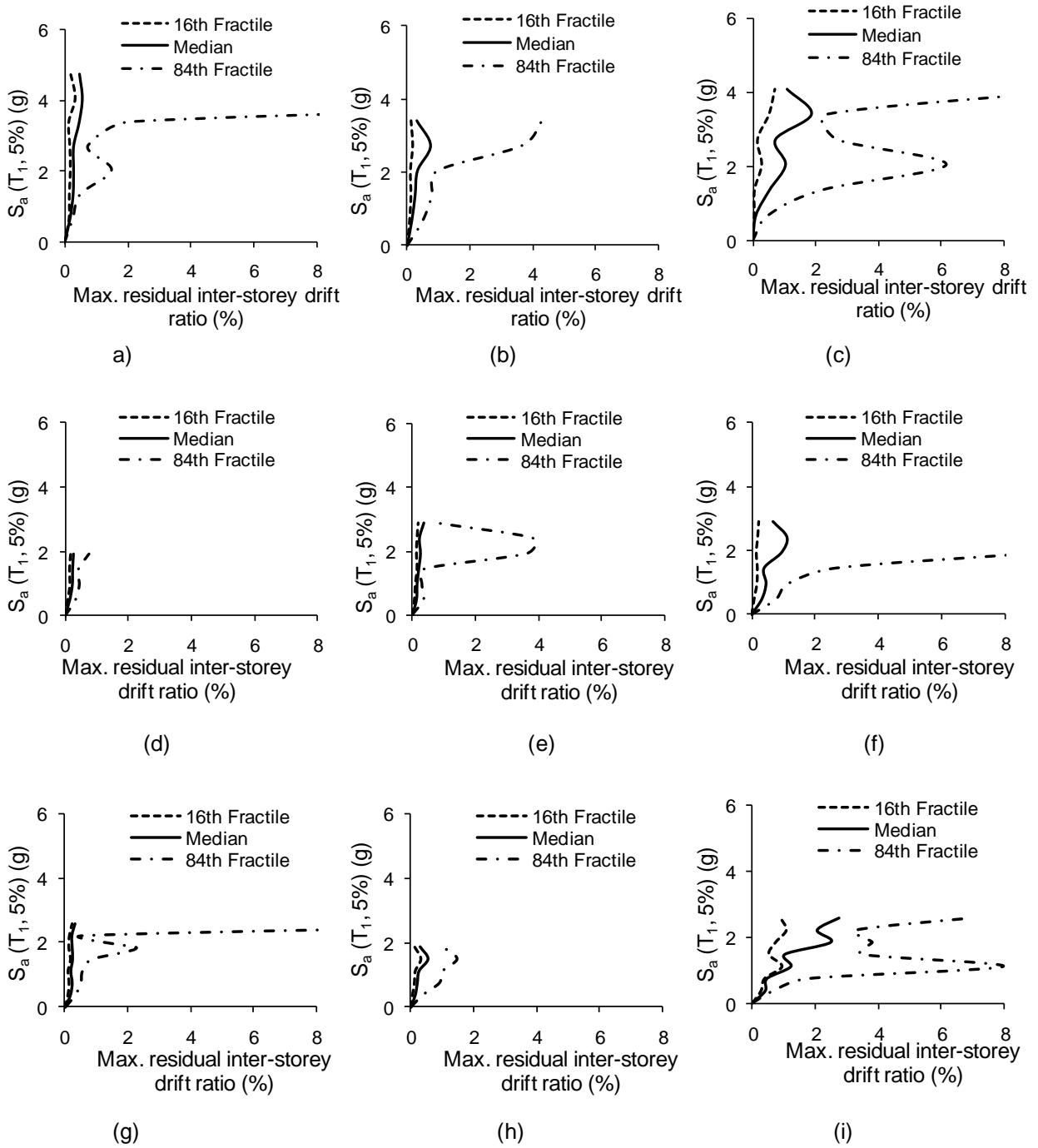


Figure 4.12 Summary of maximum residual inter-storey drift *IDA* curves into 16th, 50th, and 84th fractile for 3-storey (a) SMA RC, (b) Steel-SMA RC, (c) Steel RC frames; 6-storey (d) SMA RC, (e) Steel-SMA RC, (f) Steel RC frames; and 8-storey (g) SMA RC, (h) Steel-SMA RC, (i) Steel RC frames.

4.5.5 Inelastic distribution along height of the frame

Figure 4.13 shows a storey-to-storey profile of the peak inter-storey drift ratios at different intensity levels, for the selected ground motion records, for the 3 storey SMA, Steel-SMA and Steel RC frames respectively.

For the 6-storey SMA, Steel-SMA, and Steel RC frames, a storey to storey profile of the peak inter-storey drift ratios at different intensity level is shown in Figure 4.14. Figure 4.15 displays a storey-to-storey profile of the peak inter-storey drift ratios at different intensity, $S_a(T_l, 5\%)$, levels for the selected ground motion records for the 8-storey frames. Figure 4.16 (a), (b) and (c) shows the median peak inter-story drift ratios of the selected ground motion records at some selected ground motion intensities for the 3-storey SMA RC, Steel-SMA RC and Steel RC frames and it is observed that for all the types of frames the maximum storey drift occur in the 1st storey level. The median peak inter-storey drift ratios over the selected ground motion records at some selected ground motion intensities for the 6-storey frames are shown in Figure 4.16 (d), (e) and (f) and it is observed that for all the types of frames, inter-storey drift distribution is non uniform in nature. For the 6-storey SMA RC and Steel-SMA RC frames it is observed that the highest demand is at floor level 4 whereas the demand is high at floor level 5 for the Steel RC frame. Figure 4.16 (g), (h) and (i) shows the median peak inter-storey drift ratios of the selected ground motion records at some selected ground motion intensities. It can be observed that, in the case of SMA RC frame at a higher intensity the maximum demand is concentrated at floor level 4, whereas in the case of the Steel-SMA and the Steel RC frames, the maximum demands are concentrated between floor level 4 and 6. The median demand observed from Figure 4.16 at design intensity are the same as the demand observed from the fractile curves.

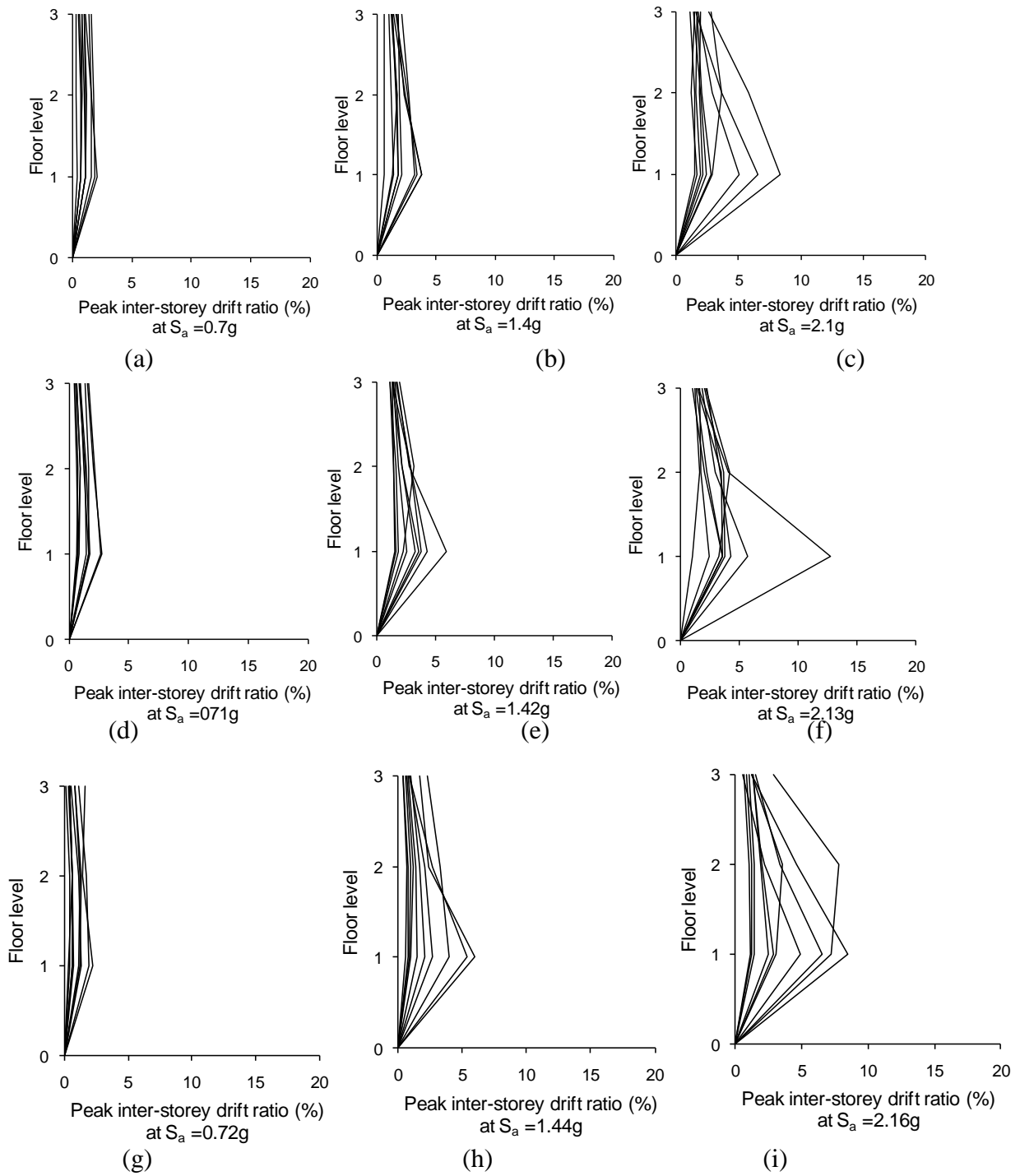


Figure 4.13 Peak inter-storey drift along the height of the 3-storey frames under selected ground motion records at different intensity levels, for SMA RC (a) $S_a = 0.7$ g, (b) $S_a = 1.4$ g, (c) $S_a = 2.1$ g; for Steel-SMA RC (d) $S_a = 0.71$ g, (e) $S_a = 1.42$ g, (f) $S_a = 2.13$ g and for Steel RC (g) $S_a = 0.72$ g, (h) $S_a = 1.44$ g, (i) $S_a = 2.16$ g.

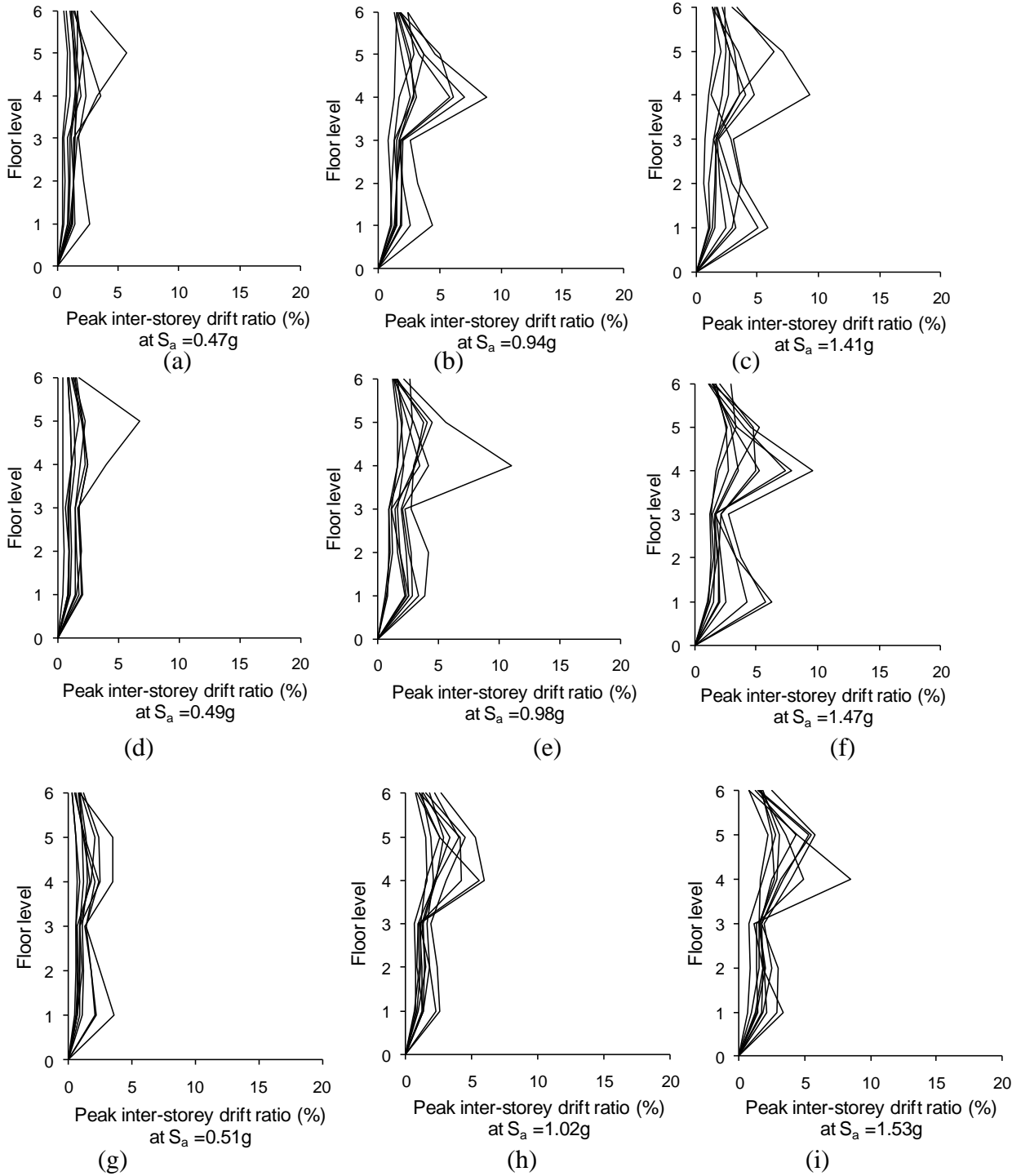


Figure 4.14 Peak inter-storey drift along the height of the 6-storey frames under selected ground motion records at different intensity levels for SMA RC (a) $S_a = 0.47$ g, (b) $S_a = 0.94$ g, (c) $S_a = 1.41$ g; for Steel-SMA RC (d) $S_a = 0.49$ g, (e) $S_a = 0.98$ g, (f) $S_a = 1.47$ g; and for Steel RC (g) $S_a = 0.51$ g, (h) $S_a = 1.02$ g, (i) $S_a = 1.53$ g.

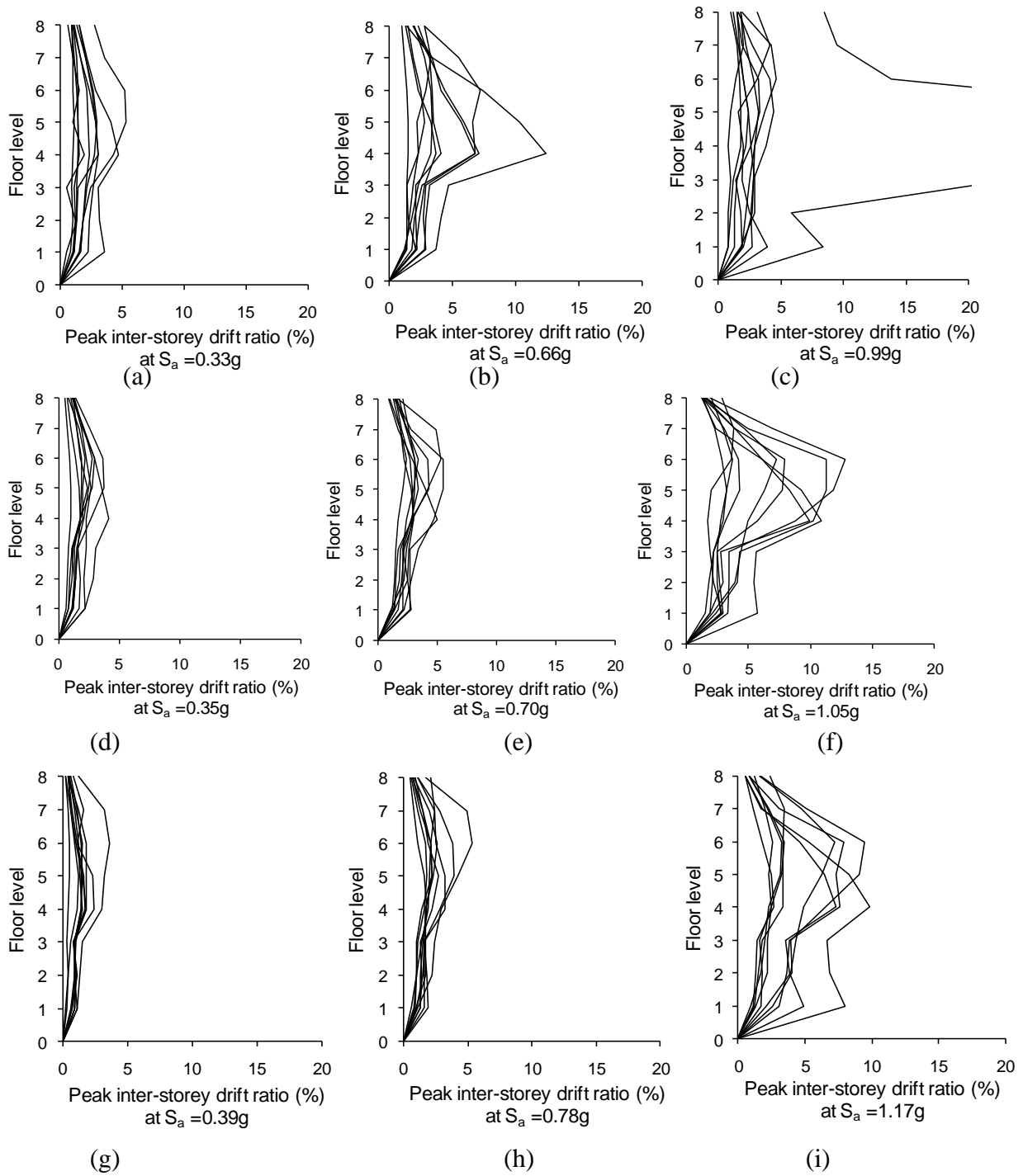


Figure 4.15 Peak inter-storey drift along the height of the 8-storey frames under selected ground motion records at different intensity levels, for SMA RC, (a) $S_a = 0.33$ g, (b) $S_a = 0.66$ g, (c) $S_a = 0.99$ g.; for Steel-SMA RC, (d) $S_a = 0.35$ g, (e) $S_a = 0.70$ g, (f) $S_a = 1.05$ g.; for Steel RC, (g) $S_a = 0.39$ g, (h) $S_a = 0.78$ g, (i) $S_a = 1.17$ g.

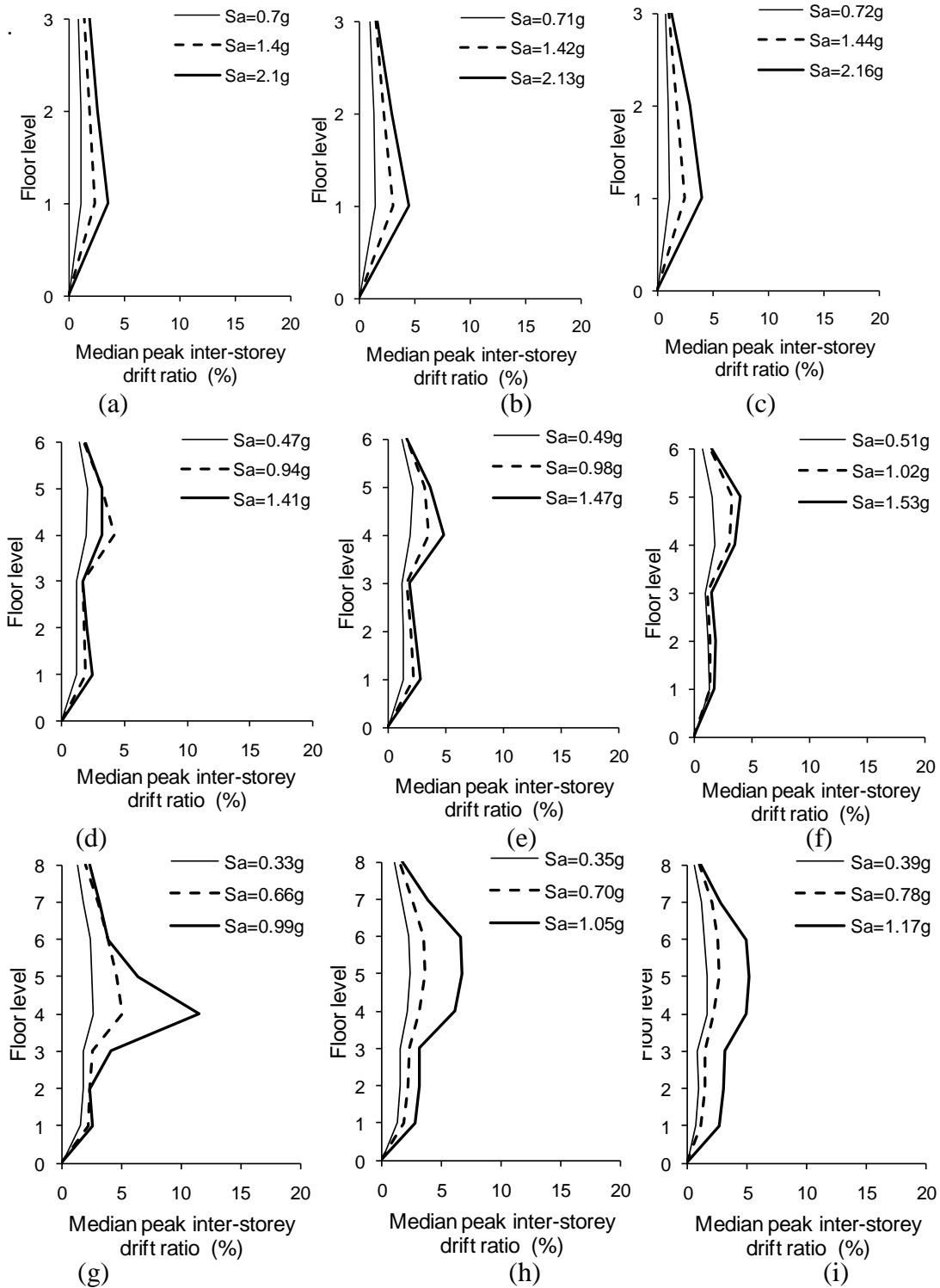


Figure 4.16 Median peak inter-storey drift ratios for all storey levels at different ground motion intensities, for 3-storey (a) SMA RC, (b) Steel-SMA RC, (c) Steel RC; for 6-storey (d) SMA RC, (e) Steel-SMA RC, (f) Steel RC; for 8-storey (g) SMA RC, (h) Steel-SMA RC, (i) Steel RC.

4.6 SUMMARY

The results of this chapter indicated that the inter-storey drift and maximum roof drift demand for SMA reinforced concrete frames was higher than those of the Steel RC frames. This higher inter-storey drift and roof drift may lead to non structural damage and shows that the SMA RC frames will be more vulnerable during a seismic event compared to Steel-SMA and Steel RC frames.

CHAPTER 5: PERFORMANCE OF SHAPE MEMORY ALLOY REINFORCED CONCRETE FRAME UNDER PROGRESSIVE COLLAPSE

5.1 GENERAL

After the collapse of the Ronan Point apartment in England due to a gas explosion in 1968, the progressive collapse phenomenon was identified as a critical component in structural analysis and design (Sasani and Kropelnicki 2008). Since the terrorist attack on the Twin Tower and the Pentagon building in the US in 2001, the security and safety of a structure and its occupants has become a major concern among engineers, building owners, and government organizations. It has received much attention in the structural engineering practice and research. Nowadays the consideration of the progressive collapse phenomenon has become an integral part of structural analysis and design for any important structure. The term progressive collapse generally refers to the extent of an initial local failure within a structure. The local failure is triggered by the loss of one or more load carrying members, leading to a partial or total collapse of the structure in a manner similar to a chain reaction (Ellingwood 2006). Following the initial event, the structure seeks alternative load paths to transfer the load, originally carried by the adjacent damaged portions. Since the latter may or may not have adequate resistance to withstand the additional loads, further failures of overloaded structural elements are likely to occur, which in turn will cause more redistribution of loads until a state of equilibrium is reached. However, due to the magnitude of the loads involved and the dynamic nature of the entire process, equilibrium may only be achieved when a substantial part of the structure has already collapsed (Vlassis 2007). Research is going on to increase the resistance of structures against progressive

collapse (Sasani and Kropelnicki 2008). Ellingwood and Dusenberry (2005) highlighted the challenges for further improvement of design practices to prevent progressive collapse. Most codes stipulate that structures are designed with continuity and structural integrity so that there might be a partial collapse, but not a total collapse (CSA A23.3-04). Some researchers have shown that seismic design improves the resistance of a structure against progressive collapse (Baldrige and Humay 2003). In a study done recently by Ioani and Cucu (2010), they analytically assessed the vulnerability to progressive collapse of seismically designed reinforced concrete (RC) frame structures and illustrated that seismic design reduces the possibility of progressive collapse. Researchers are also investigating how to reduce the progressive collapse failure of structures by strengthening and also incorporating new members into an existing structure. Yagob et al. (2009) performed a thorough review on progressive collapse analyses of structures and emphasized the development of new techniques for protecting structures against progressive collapse.

Superelastic SMAs are unique materials with the ability to undergo large deformation and return to a predetermined shape upon unloading (Alam et al. 2007), which makes SMA a smart material. Although the superelasticity of SMA may have a great potential to resist a progressive collapse failure of a frame structure, the use of such material to prevent progressive collapse remains unexplored. Therefore, the objective of this research is to explore the possibility of utilizing superelasticity of SMA bar in resisting any partial or full collapse of a RC frame structure. Numerical analyses are carried out to determine and compare the failure modes and behaviours of different types of frame (reinforced with and without SMA reinforcement) buildings under progressive collapse. The description of the considered frames was given in Chapter 3.

5.2 PREVIOUS WORK

In the recent years, especially after the terrorist attack on the Twin Towers and the Pentagon, progressive collapse behaviour of structures has become an important subject not only within the structural engineering community and industry, but also among politicians, governments and even the general public. Since 2001 experimental and analytical research on progressive collapse has increased substantially. Several researchers have conducted experimental studies on the progressive collapse behaviour of frame structures; for instances, Yi et al. (2008) investigated the progressive collapse behaviour of a 4-bay, 3-story RC frame due to the loss of the interior lower storey column, and Sasani et al. (2007) experimentally and analytically evaluated the potential progressive collapse in a 10-storey RC structure following the explosion of an exterior column. Likewise, Sasani and Kropelnicki (2008) conducted experimental and analytical studies to evaluate the progressive collapse of a 7-storey reinforced concrete (RC) frame building. Tsitos et al. (2008) conducted an experimental investigation on a seismically designed 3-storey special moment-resisting steel frame and a post tensioned energy dissipating steel frame to determine their resistance against progressive collapse by quasi-static push-down tests. Both frames exhibited sufficient strength and ductility after the central column was removed. Razaqpur et al. (2007) retrofitted a concrete slab with glass fibre reinforced polymer, then applied a blast load, and concluded that the performance of the retrofitted slab was better compared to that of the original one. Fujikura et al. (2008) proposed a multi-column pier-bent with concrete filled steel tube columns for highway bridge type structures for preventing its potential progressive collapse under blast loading. Luccioni et al. (2004) conducted an analytical study to simulate a real blast-induced damaged RC

building. Hayes Jr. et al. (2005) performed an analytical study on seismically retrofitted buildings and observed that their progressive collapse resistance increased significantly. Pilehchianlangroodi et al. (2008) performed an analytical investigation on the blast resistance of a RC building with a front wall as a fuse, which proved to be very effective in resisting blast loads. Saatcioglu et al. (2009) analytically evaluated the progressive collapse performance of a 10-storey seismically designed RC moment resisting frame with and without a shear wall. They suggested that seismic design detail of beams, columns, and existence of shear walls provide substantial progressive collapse resistance against blast loads. Marjanishvili (2004) and later Marjanishvili and Agnew (2006) systematically demonstrated four successively more sophisticated procedures to perform progressive collapse evaluation of frame structures with examples and step by step analysis procedures. Tsai and Lin (2008) constructed capacity curves from a nonlinear static analysis, which is capable of predicting the progressive collapse resistance of an RC building. Khandelwal and El-Tawil (2008) presented a pushdown analysis technique to determine the collapse modes and ultimate load carrying capacity of a frame structure with lost or damaged critical members. Ellingwood et al. (2007) developed a guideline to prevent the progressive collapse of buildings. Khandelwal et al. (2008) developed a macro model-based simulation procedure to evaluate the performance of steel frames under progressive collapse. Grierson et al. (2005) described the procedure of progressive failure analyses of buildings subjected to abnormal loading.

There are several building codes and specifications that provide guidelines to protect buildings against progressive collapse. The National Building Code of Canada (NBCC) has addressed progressive collapse in some form in its 1975 edition. The recent edition of

NBCC (NBCC-2005) has addressed progressive collapse in the commentary B under the title “Structural Integrity.” Although NBCC-2005 has addressed progressive collapse, it has failed to provide any firm guideline regarding progressive collapse resistance design. Detailed information regarding the methodology to resist progressive collapse is provided by the US General Service Administration (GSA 2003) and the US Department of Defense (DoD 2005). Besides GSA (2003) and DoD (2005), progressive collapse analysis procedures are also addressed by the U.S. Department of Army (DA) FM 3-19.30, the Federal Emergency Management Agency (FEMA) (426,427,428 [2003]), the British Standards Institution (BSI 8110: Part 2:1985), and the unified facilities criteria (UFC4-023-03, 2005). In the current study the GSA (2003) standard has been considered to evaluate the progressive collapse behaviour of the seismically designed SMA RC, Steel-SMA RC and Steel RC buildings. The GSA standard is appropriate for evaluating the progressive collapse performance of buildings up to 10-storey, a condition which is satisfied in this study. The definition of progressive collapse is presented here in a schematic diagram (Figure 5.1).

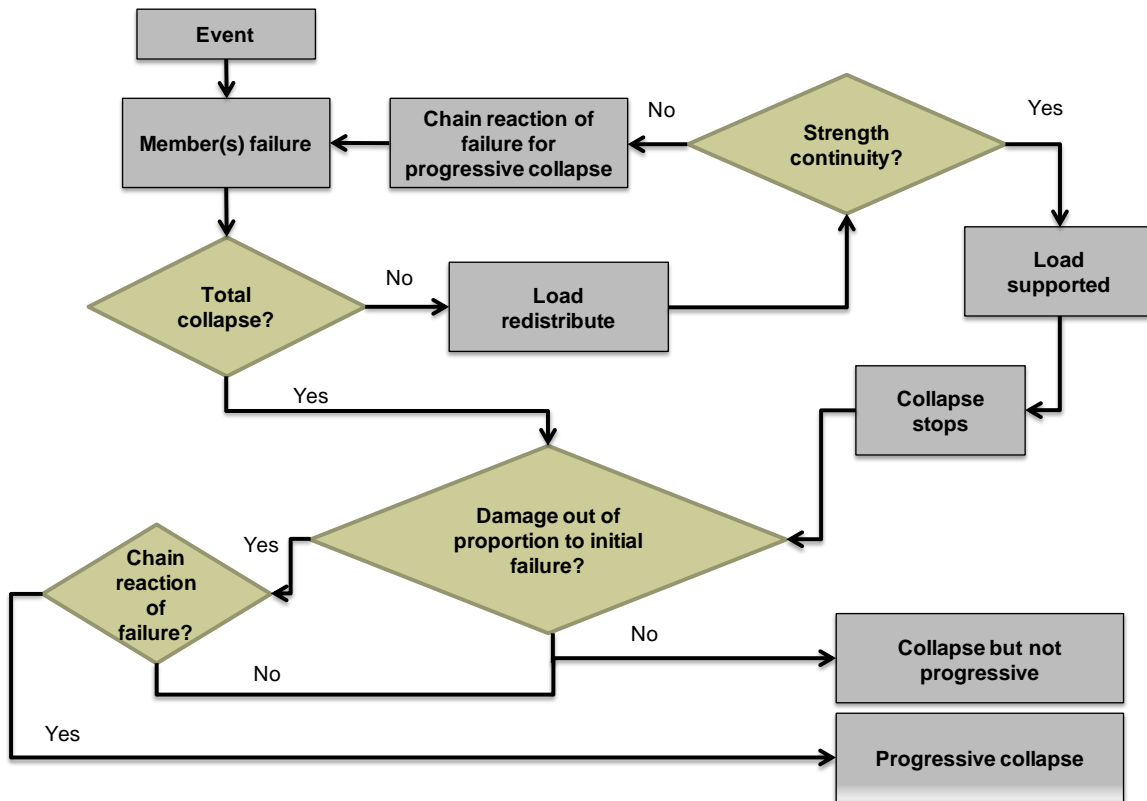


Figure 5.1 Definition of progressive collapse of a structure (Adapted from GSA 2003).

From this figure it can be observed that the progressive collapse can either be the total collapse or partial collapse of a structure. If the failure occurs like a chain reaction then the failure is called progressive collapse. If the total structure fails but there is no chain reaction then the failure is known as collapse, but not progressive collapse. GSA (2003) recommends performing both linear and nonlinear analyses as well as static and dynamic analyses to evaluate the performance of buildings under progressive collapse.

5.3 PROGRESSIVE COLLAPSE ANALYSIS METHOD

The objective of this research is to explore the possibility of utilizing superelasticity of SMA bar in resisting any partial or full collapse of a building. In order to achieve the objectives the steps taken into consideration include: designing a building considering

earthquake load and wind load as per NBCC-2005 and CSA A23.3-04, modeling an exterior 2D frame in SeismoStruct (2010), and conducting linear and nonlinear static and dynamic analyses as per GSA 2003 for evaluating the performance.

5.4 FRAME CHARACTERISTICS AND MODELLING

Three different frame stories (3, 6 and 8) have been considered in this study where each building has three different types of rebar arrangements in their beams, i.e. Steel, Steel-SMA and SMA, as described in Chapter 3. Detailed design procedures for these buildings have been described in chapter 3. The plan of each building is kept similar and is shown in Figure 5.1(a), and the elevation of 3, 6, and 8-storey buildings are shown in Figure 5.1(b), (c) and (d), respectively. The storey heights are 3m for all the buildings. The reinforcement of the building has been detailed as per Canadian standards (CSA A23.3-04). Table 3.2 and 3.3 show the member sizes and the reinforcement detailing of columns and beams. Figure 3.5 illustrates the reinforcement detailing of a typical beam.

In order to predict the progressive collapse behaviour of RC frame structures all analyses have been performed using a FE program (SeismoStruct 2010). The fibre modelling approach has been considered to perform both static and dynamic linear analyses. For linear analyses the beam column element has been assigned as an elastic frame element. The fibre modelling approach has also been implemented to represent the distribution of material nonlinearity along the length and cross-sectional area of the member for nonlinear analyses. Here, inelastic displacement-based 3D beam-column elements have been used for modelling the beam and column. The sectional stress-strain state of the elements is obtained through the integration of the nonlinear uniaxial stress-

strain response of the individual fibres in which the section has been subdivided. Concrete has been represented using the Mander et al. (1988) constitutive relationship and the cyclic response by Martinez-Rueda and Elnashai (1997), and a bilinear kinematic strain hardening model was used for steel. SMA has been modelled according to the model of Auricchio and Sacco (1997). The parameters used to define the material model were discussed in the Section 3.4. In the case of the Steel-SMA RC frame, the beam-column joint is represented by the model of Alam et al. (2008) to consider the slippage of the SMA rebar inside the coupler.

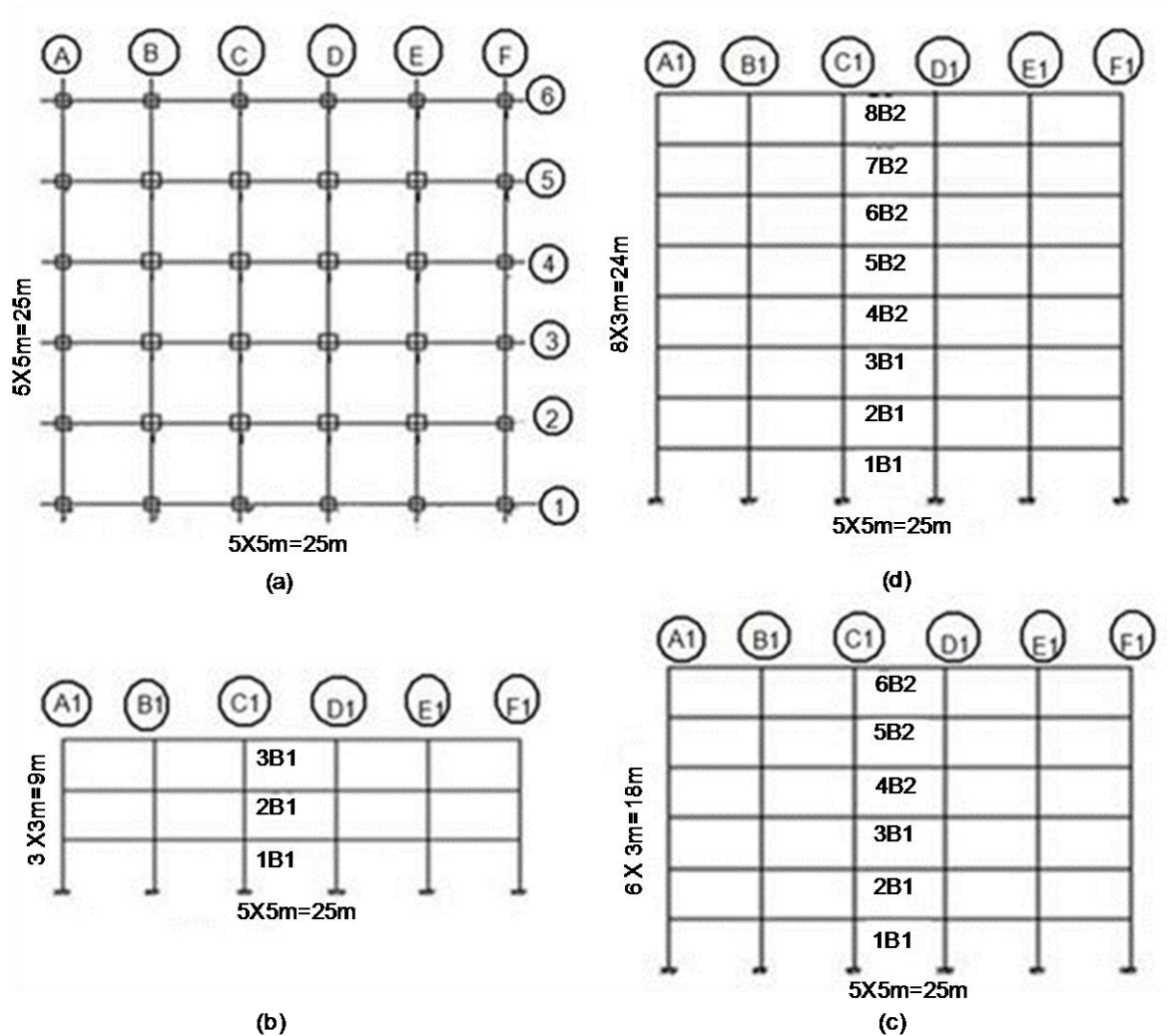


Figure 5.2 Configuration of building geometry: (a) Plan, (b) Elevation of 3-storey, (c) Elevation of 6-storey and (d) Elevation of 8-storey building.

5.5 PROGRESSIVE COLLAPSE ANALYSES

To evaluate the vulnerability of a progressive collapse in a regular building structure, GSA 2003 recommends performing structural analyses in which the instantaneous loss of one of the following first floor columns at a time is assumed:

- A column located at the corner of the building.
- An exterior column near the middle of the longer side of the building.
- An exterior column near the middle of the shorter side of the building.
- A column interior to the perimeter column lines for facilities that have underground parking and/or uncontrolled public ground floor areas.

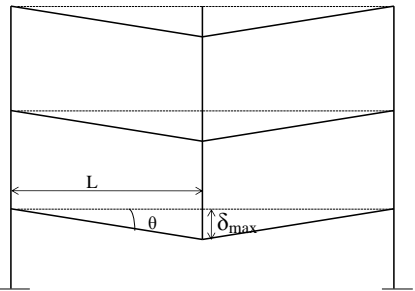
The buildings considered in this study have symmetric plan geometry and have the same number of bay in each direction. Therefore, a bottom storey corner column removal was considered (Figure 5.3 a). The other case considered in this study was the bottom storey exterior bay intermediate column removal (Figure 5.3 b). Although GSA 2003 recommends evaluating the performances of structures using linear elastic static analysis or non-linear dynamic analysis, this study also considers nonlinear static and linear dynamic analysis.

For any structure the flexural demand capacity ratio (*DCR*), in terms of moment plays an important role in its performance evaluation when the structure is in the elastic state. When the structure undergoes into nonlinear phase, support rotation, θ , and vertical ductility, μ , play critical roles to evaluate its performance. The rotation, θ , is the ratio of the maximum vertical displacement of the point from which the column is removed to the horizontal distance of the adjacent column (Table 5.1). The vertical ductility, μ , is the ratio of the maximum inelastic vertical displacement of the point from which the column is

removed to the yield displacement of this point (Table 5.1). Here the yield displacement (δ_e) is defined as the displacement occurring at the time of a local yield of any adjacent member from which the column is removed. The GSA (2003) has provided some analyses response limits to evaluate the progressive collapse. These limiting values are given in Table 5.1.

Table 5.1 Response Limit.

Analysis Types	Performance Indicator
Linear	$DCR \leq 2.0$
Nonlinear	Support rotation, $\theta \leq 12^\circ$ Ductility, $\mu \leq 20$



The GSA guidelines recommend static analysis under the following load combination (Eq. 5.1), which would be applied to the structure in the gravity direction:

$$Load = 2 * (DL + 0.25LL) \quad [5.1]$$

In the case of dynamic analysis the following load combination (Eq. 5.2) is applied to the structure in the gravity direction:

$$Load = DL + 0.25LL \quad [5.2]$$

Here, the dead load (DL) includes self weight of the column, beam and slab as well as the load of floor finish (FF), partition wall (PW) and machine load. The floor finish is assumed 1.0 kN/m^2 and the partition wall and machine load are assumed to be 1.0 kN/m^2 . The slab thickness is considered as 0.15 m . The live load (LL) is assumed to be 2.4 kN/m^2 .

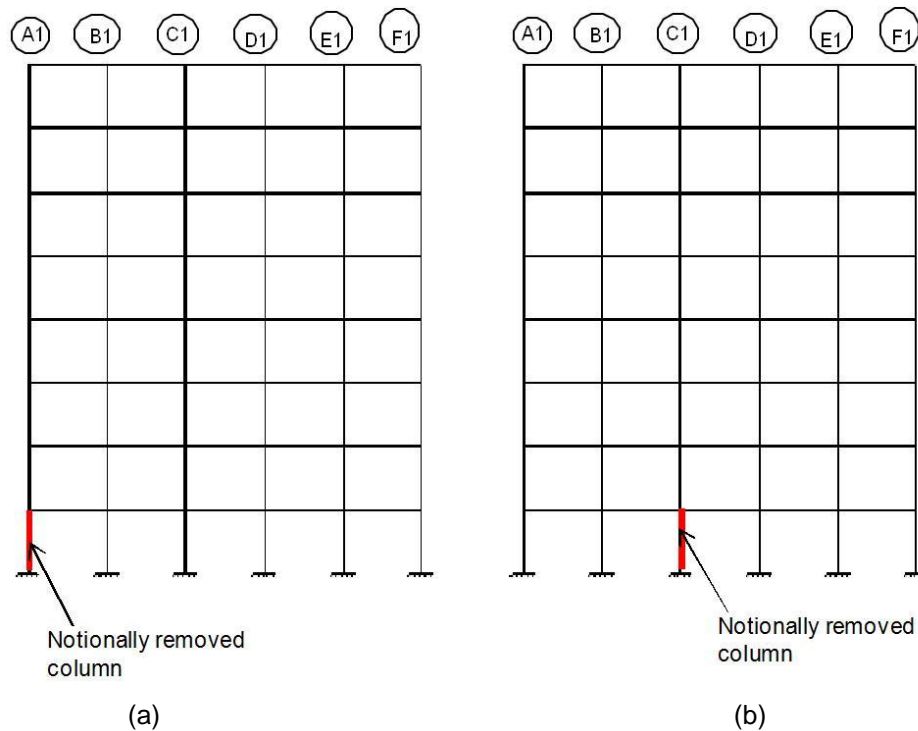


Figure 5.3 Typical column removal for 8-storey (a) exterior bay corner column and (b) exterior bay intermediate column.

5.5.1 Linear static analyses

To perform linear static analyses the beam and column elements have been assigned as elastic frame elements. The material linearity has been considered by utilizing an elastic material model for the steel and the SMA. Linear static analyses were performed by using an amplified combination of service loads, such as dead and live load, as per Eq. 5.1. For each type of frame the exterior bay was considered for this comparative study. Two scenarios were considered: In the first scenario, the corner column of the bottom storey was

removed, and in the second scenario a bottom storey intermediate column closer to the middle column of the exterior bay was removed, as shown in Figure 5.3 (a) and (b). After completing the analyses, the *DCR* values for flexure were computed. *DCR* is the ratio of the maximum negative moment of the beam at its supports due to column removal and amplified DL and LL to the ultimate negative moment capacity of the corresponding beam. *DCR* values are also calculated for the positive moment of the beam. After calculating the *DCR* values for both the negative and positive moments, the largest value was considered to evaluate the performance of the frame (Table 5.2).

Table 5.2 *DCR* values for corner column removal from linear static analyses.

Corner Column Removal								
Building ID	RC Frame Types	Beam ID	Positive Moment Demand (kN-m)	Negative Moment Demand (kN-m)	Positive Moment Capacity (kN-m)	Negative Moment Capacity (kN-m)	DCR_{pos}	DCR_{neg}
3	SMA	1B1	144	231	134	134	1.07	1.72
	Steel-SMA	1B1	144	231	134	134	1.07	1.72
	Steel	1B1	144	231	134	134	1.07	1.72
6	SMA	1B1	145	255	245	335	0.59	0.76
		4B2	134	216	151	151	0.89	1.43
	Steel-SMA	1B1	147	236	245	335	0.6	0.70
		4B2	134	217	151	151	0.89	1.44
	Steel	1B1	147	236	245	335	0.60	0.70
		4B2	134	217	151	151	0.89	1.44
8	SMA	1B1	144	238	245	335	0.59	0.71
		4B2	137	221	151	151	0.91	1.46
	Steel-SMA	1B1	141	238	245	335	0.58	0.71
		4B2	137	221	151	151	0.91	1.46
	Steel	1B1	141	238	245	335	0.58	0.71
		4B2	137	221	151	151	0.91	1.46

Table 5.2 presents the *DCR* values for corner column removal cases obtained from linear static analyses where the values are less than 2.0 for all different frame types and stories. Except the 3-storey frame, for each frame type 2 maximum values have been reported for two different beam types B1 and B2 as shown in Figure 5.2.

The maximum *DCR* value is observed for the 3-storey frames, which is 1.72 irrespective of the frame type. In the case of the 6 and 8-storey frames, the *DCR* values for beam 1B1s are less than those of beam 4B2s because of 4B2s' has lower capacity. The SMA, Steel-SMA and Steel RC frames performed in similar fashion. In the case of the 3-storey frames the *DCR* value is slightly higher for the SMA RC frame compared to those of the Steel-SMA and Steel RC frames. From the results of linear static analyses it can be concluded that the reinforcement type is not a governing issue for progressive collapse prevention. Although SMAs may have greater recovering capabilities, simple the linear static analyses will not be able to capture the advantages of utilizing SMA in the case of progressive collapse. The *DCR* values obtained from the linear static analyses by removing exterior bay intermediate columns are presented in Table 5.3. The *DCR* values are comparatively lower for interior column removal than those for a corner column removal (Figure 5.4). Figure 5.4 depicts that the loss of the corner column increases the possibility of progressive collapse failure of a structure more than that of the intermediate column.

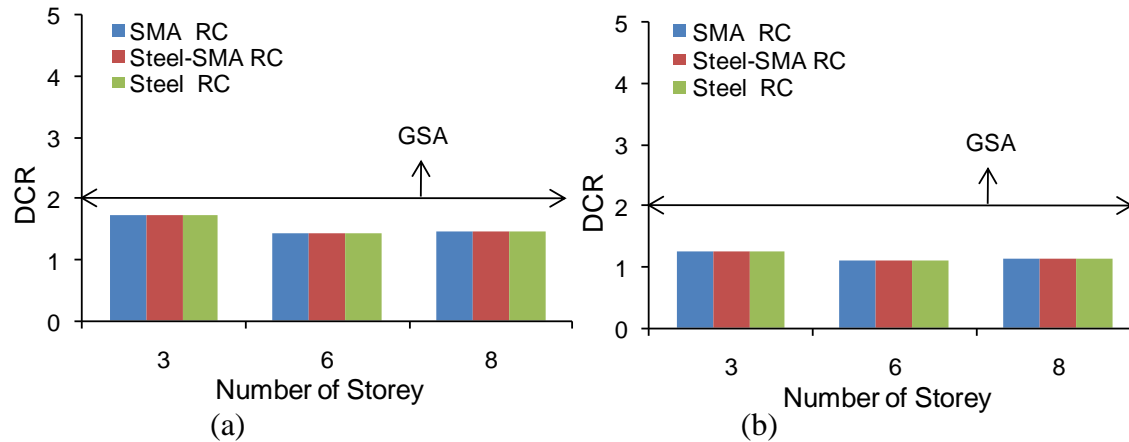


Figure 5.4 Comparison of DCR values due to (a) corner column removal and (b) exterior bay interior column removal from linear static analyses.

Table 5.3 *DCR* values for exterior bay intermediate column removal for linear static analyses.

Exterior bay intermediate column removal								
Building ID	RC Frame Types	Beam ID	Positive Moment Demand (kN-m)	Negative Moment Demand (kN-m)	Positive Moment Capacity (kN-m)	Negative Moment Capacity (kN-m)	DCR_{pos}	DCR_{neg}
3	SMA	1B1	95	166	134	134	0.71	1.24
	Steel-SMA	1B1	95	166	134	134	0.71	1.24
	Steel	1B1	95	166	134	134	0.71	1.24
6	SMA	2B1	104	179	245	335	0.42	0.53
		4B2	93	164	151	151	0.62	1.09
	Steel-SMA	2B1	104	179	245	335	0.42	0.53
		4B2	93	164	151	151	0.62	1.09
	Steel	2B1	104	179	245	335	0.42	0.53
		4B2	93	164	151	151	0.62	1.09
8	SMA	2B1	109	186	245	335	0.44	0.56
		4B2	98	171	151	151	0.65	1.13
	Steel-SMA	2B1	109	186	245	335	0.44	0.56
		4B2	98	171	151	151	0.65	1.13
	Steel	2B1	109	186	245	335	0.44	0.56
		4B2	98	171	151	151	0.65	1.13

5.5.2 Nonlinear static analyses

To perform nonlinear static analyses, both material and geometric nonlinearity have been considered. The beam column elements were modeled as an inelastic displacement based frame element. To evaluate the performance, the maximum load resisted by the frames as well as the maximum rotation and vertical ductility, are determined by applying the load as per Eq. 5.1. The results obtained from the nonlinear static analyses by removing the bottom storey corner column and the intermediate column are presented in Table 5.4 and 5.5, respectively. From Table 5.4 it can be observed that in the case of the 3-storey SMA RC frame, the vertical deflection of the point from which the corner column is removed is 261 mm and the adjacent column distance is 5000 mm, thus the maximum rotation is 2.99 degrees.

Table 5.4 Ductility and support rotation due to corner column removal from nonlinear static analyses.

Corner Column Removal						
Building ID	RC Frame Types	θ°	δ_e (mm)	δ_{max} (mm)	μ	% load at collapse
3	SMA	2.99	40.0	261.0	6.5	90%
	Steel-SMA	2.51	42.0	219.0	5.2	90%
	Steel	2.43	40.0	212.0	5.3	80%
6	SMA	0.88	20.0	77.0	3.9	91 %
	Steel-SMA	0.74	40.0	65.0	1.6	100%
	Steel	0.45	38.0	39.0	1.0	100
8	SMA	0.76	30	66	2.2	100%
	Steel-SMA	0.70	30	61	2.0	100%
	Steel	0.22	19	19	1.0	100%

Figures 5.5 (a) and (b) show the ductility of various frame types from the nonlinear static analyses due to the corner and the intermediate column removal, respectively. In the case of the 3-storey Steel RC frame the maximum vertical displacement of the point is 212mm, and the yield displacement is 40mm. Therefore the vertical ductility for the 3-storey Steel RC frame is 5.3. The results obtained from the nonlinear static analyses by removing the ground floor intermediate column are presented in Table 5.5. From Table 5.4 and Table 5.5 it is evident that none of the 3-storey RC frames could carry the amplified loads (Eq.5. 2) before collapse. Among the 6 and 8-storey buildings, only the 6-storey SMA RC frame was unable to carry the applied loads before collapse.

Table 5.5 Ductility and support rotation due to exterior bay intermediate column removal from nonlinear static analyses.

Intermediate Column Removal						
Building ID	RC Frame Types	θ°	δ_e (mm)	δ_{max} (mm)	μ	% load at collapse
3	SMA	1.61	30.0	88.0	2.9	77 %
	Steel-SMA	1.51	45.0	132.0	2.9	77%
	Steel	1.15	40.0	100.0	2.5	100%
6	SMA	0.74	30.0	65.0	2.2	100%
	Steel-SMA	0.60	20.0	52.0	2.6	100%
	Steel	0.29	21.0	25.0	1.2	100%
8	SMA	0.76	30	66	2.2	100%
	Steel-SMA	0.60	30	52	1.7	100%
	Steel	0.30	29	26	0.9	100%

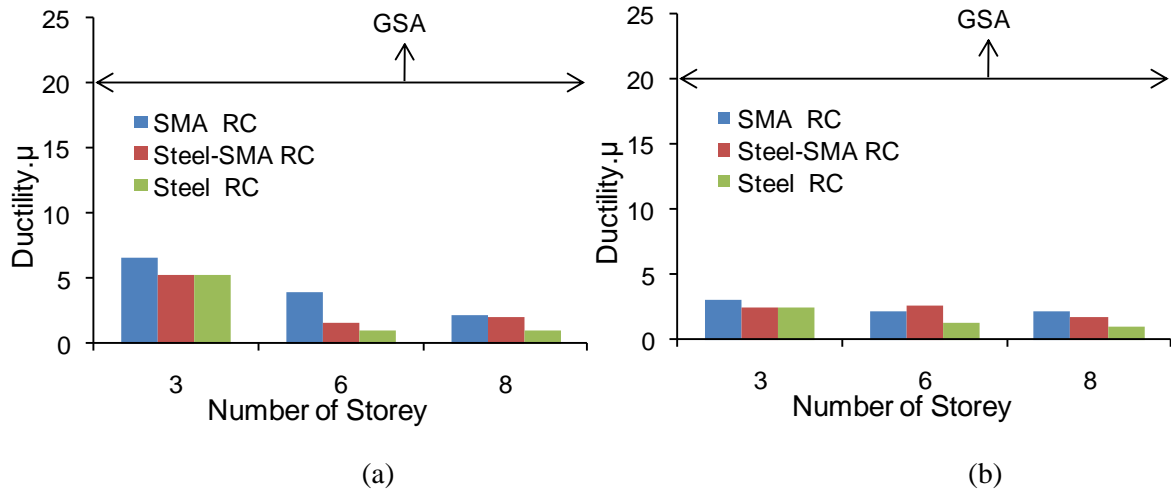


Figure 5.5 Comparison of ductility from nonlinear static analyses due to (a) corner column removal, and (b) exterior bay intermediate column removal.

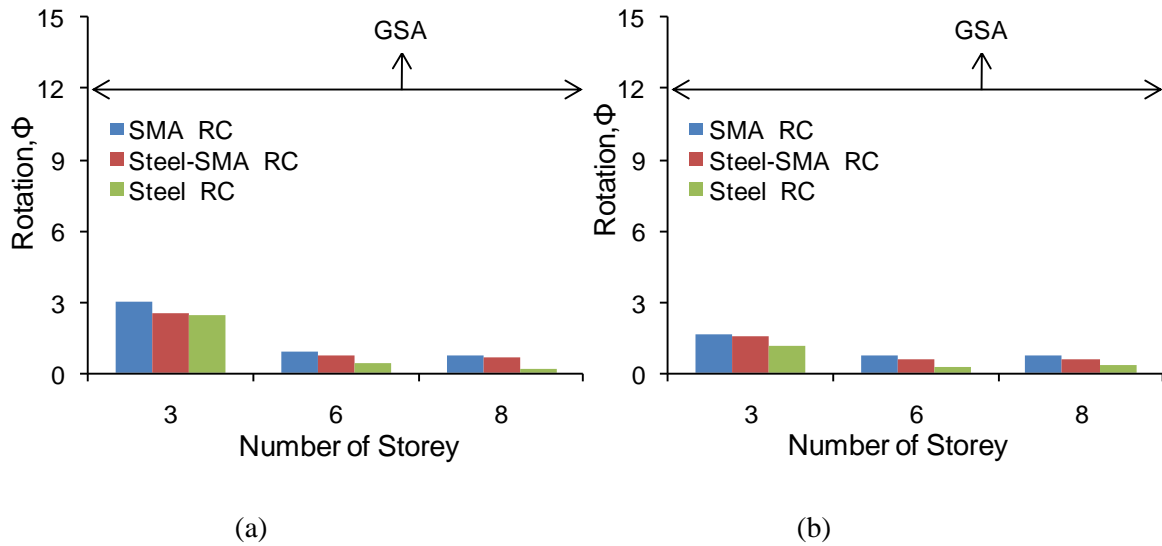


Figure 5.6 Comparison of rotation due to (a) corner column removal, and (b) exterior bay intermediate column removal.

Figure 5.5 and 5.6 show the variation of ductility and rotation, respectively. According to GSA-2003 if the ductility value is larger than 20 then the structure is susceptible to progressive collapse. The SMA RC frame suffered more ductility compared to that of the Steel-SMA and the Steel RC frames, which indicates that the SMA RC frame is more

susceptible to progressive collapse compared to the others. For all types of frames the value of the vertical ductility is higher for the corner column removal than that for the intermediate column removal.

The rotation value permitted by the GSA (2003) is 12. From nonlinear static analyses it is observed that the support rotation value did not exceed the limiting value for all cases. One interesting observation is, with the increase of storey numbers, the support rotation values decrease. As the storey number increases the loads can be redistributed over a larger path in the building frame during a column removal event, and thus, it can experience lesser deformation compared to those frames which have a lower number of storeys.

5.5.3 Linear dynamic analyses

To perform the linear dynamic analyses, the models developed for linear static analyses have been used. First the dynamic load combination was applied, as mentioned in Eq. (5.2). The loading (reaction at the removed column) for the linear dynamic analyses to simulate column removal is shown in Figure 5.7.

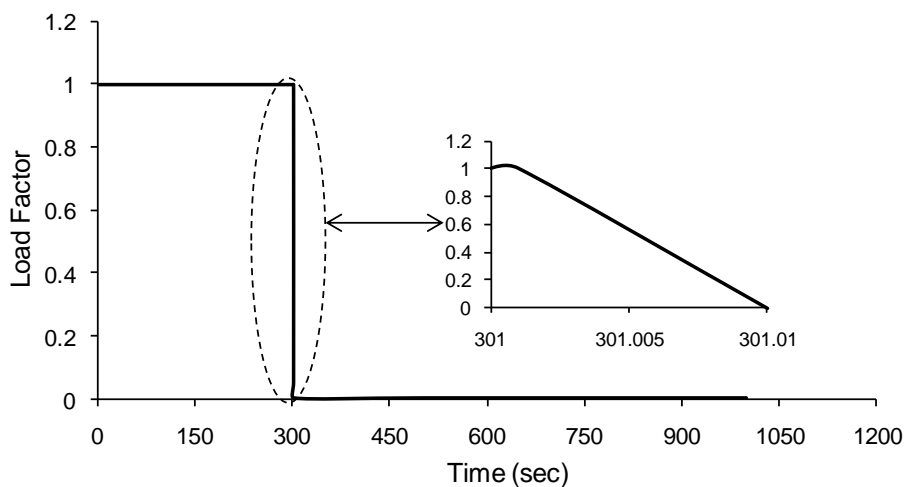


Figure 5.7 Time history loading (reaction at removed column) for linear and nonlinear dynamic analyses.

After conducting the dynamic time history analyses, the performance of various frames were evaluated by calculating the flexural demand to capacity ratio (DCR). The demand observed from the time history analyses are presented in Table 5.6 and Table 5.7 for the corner column and exterior bay intermediate column removal cases, respectively. Figure 5.8(a) and (b) show the DCR values obtained from the linear dynamic analyses for corner and intermediate column removal, respectively.

Table 5.6 DCR values for corner column removal from linear dynamic analyses.

Corner Column Removal								
Building ID	RC Frame Types	Beam ID	Positive Moment Demand (kN-m)	Negative Moment Demand (kN-m)	Positive Moment Capacity (kN-m)	Negative Moment Capacity (kN-m)	DCR_{pos}	DCR_{neg}
3	SMA	1B1	184	276	134	134	1.37	2.06
	Steel-SMA	1B1	184	276	134	134	1.37	2.06
	Steel	1B1	184	276	134	134	1.37	2.06
6	SMA	1B1	191	286	245	335	0.78	0.85
		4B2	167	252	151	151	1.11	1.67
	Steel-SMA	1B1	191	286	245	335	0.78	0.85
		4B2	167	252	151	151	1.11	1.67
	Steel	1B1	191	286	245	335	0.78	0.85
		4B2	167	252	151	151	1.11	1.67
8	SMA	1B1	188	283	245	335	0.77	0.84
		4B2	177	266	151	151	1.17	1.76
	Steel-SMA	1B1	188	283	245	335	0.77	0.84
		4B2	177	266	151	151	1.17	1.76
	Steel	1B1	188	283	245	335	0.77	0.84
		4B2	177	266	151	151	1.17	1.76

Table 5.7 *DCR* values for exterior bay intermediate column removal from linear dynamic analyses.

Intermediate column removal								
Building ID	RC Frame Types	Beam ID	Positive Moment Demand (kN-m)	Negative Moment Demand (kN-m)	Positive Moment Capacity (kN-m)	Negative Moment Capacity (kN-m)	DCR_{pos}	DCR_{neg}
3	SMA	1B1	104	169	134	134	0.78	1.26
	Steel-SMA	1B1	104	169	134	134	0.78	1.26
	Steel	1B1	104	169	134	134	0.78	1.26
6	SMA	2B1	107	174	245	335	0.44	0.52
		4B2	102	166	151	151	0.68	1.10
	Steel-SMA	2B1	107	174	245	335	0.44	0.52
		4B2	102	166	151	151	0.68	1.10
	Steel	2B1	107	174	245	335	0.44	0.52
		4B2	102	166	151	151	0.68	1.10
8	SMA	2B1	114	182	245	335	0.47	0.54
		4B2	106	172	151	151	0.70	1.14
	Steel-SMA	2B1	114	182	245	335	0.47	0.54
		4B2	106	172	151	151	0.70	1.14
	Steel	2B1	114	182	245	335	0.47	0.54
		4B2	106	172	151	151	0.70	1.14

It can be observed that the *DCR* values obtained from the dynamic analyses are more than those from the static analyses. Although the *DCR* values observed from the static linear analyses for the 3-storey SMA, Steel-SMA, and Steel RC frames were less than 2.0 for both the positive and the negative moments, in the case of the linear dynamic analyses the *DCR* valued slightly exceeded 2.0 for negative moment while removing the corner column. Similar to the static analyses results, linear dynamic analysis also indicates that the corner column is a more critical location than the intermediate column for progressive collapse failure. Figure 5.8 also illustrates that the vulnerability of progressive failure for low rise building is higher compared to mid-rise buildings.

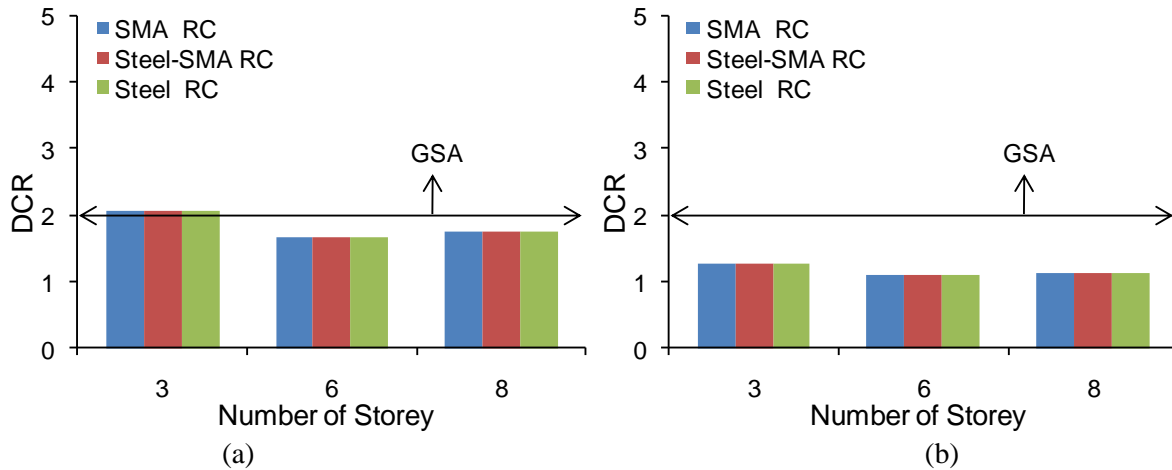


Figure 5.8 Comparison of *DCR* values from linear dynamic analyses due to (a) corner column removal, and (b) exterior bay intermediate column removal.

5.5.4 Nonlinear dynamic analyses

The previously developed model for the nonlinear static analyses was used to perform nonlinear dynamic analyses where both geometric and material nonlinearity were considered and the load was applied as per Eq. (5.2). The loading used to perform the nonlinear dynamic analyses is shown in the Figure 5.7. From the nonlinear dynamic time history analyses, the support rotation and ductility are calculated, and the results are provided in Table 5.8 and 5.9, for the corner column and the exterior bay intermediate column removal cases, respectively. The support rotation and the ductility observed from the dynamic analyses are comparatively less than the values obtained from the static analyses. It has been observed that for all frame types, the ductility and rotation values are within the GSA (2003) limits (Figure 5.9 and 5.10).

Table 5.8 Ductility and support rotation due to corner column removal from nonlinear dynamic analyses.

Corner column removal					
Building ID	RC Frame Types	θ°	δ_e (mm)	δ_{max} (mm)	μ
3	SMA	2.21	92.0	193.0	2.1
	Steel-SMA	2.01	95.0	175.0	1.8
	Steel	0.20	9.3	17.5	1.9
6	SMA	0.92	60.0	80.0	1.3
	Steel-SMA	0.86	50.0	75.0	1.5
	Steel	0.52	35.0	45.0	1.3
8	SMA	0.89	72	78	1.1
	Steel-SMA	0.83	39	72	1.8
	Steel	0.40	29	35	1.2

Table 5.9 Ductility and support rotation due to intermediate column removal from dynamic analyses.

Intermediate column removal					
Building ID	RC Frame Types	θ°	δ_e (mm)	δ_{max} (mm)	μ
3	SMA	1.72	39.0	150.0	3.8
	Steel-SMA	0.89	36.0	78.0	2.2
	Steel	0.58	33.0	51.0	1.5
6	SMA	0.80	37.0	70.0	1.9
	Steel-SMA	0.71	36.0	62.0	1.7
	Steel	0.31	19.0	27.0	1.4
8	SMA	0.86	26	75	2.9
	Steel-SMA	0.72	25	63	2.5
	Steel	0.33	19	29	1.5

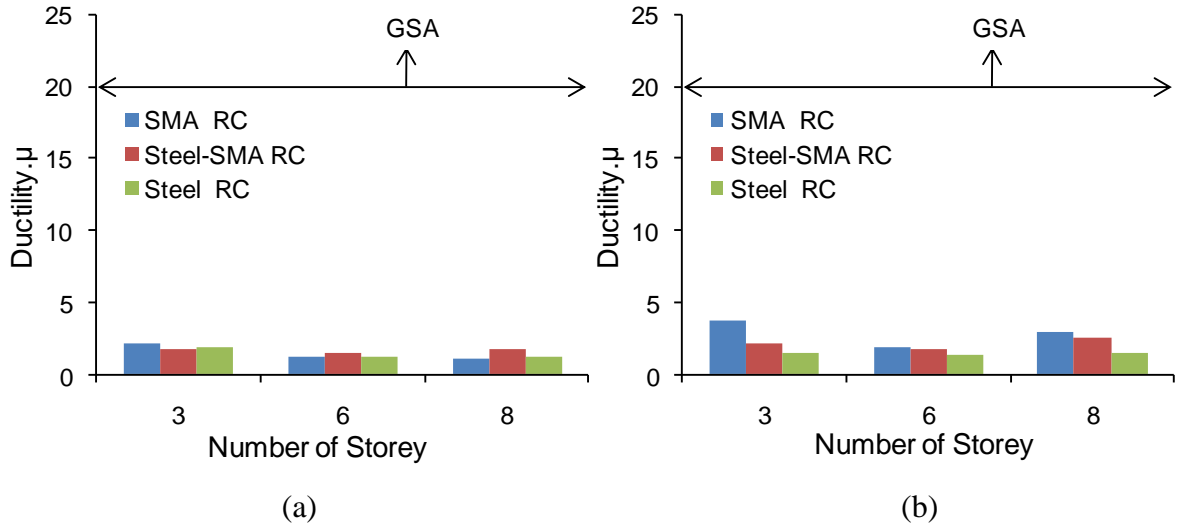


Figure 5.9 Comparison of ductility due to (a) corner column removal, and (b) exterior bay intermediate column removal.

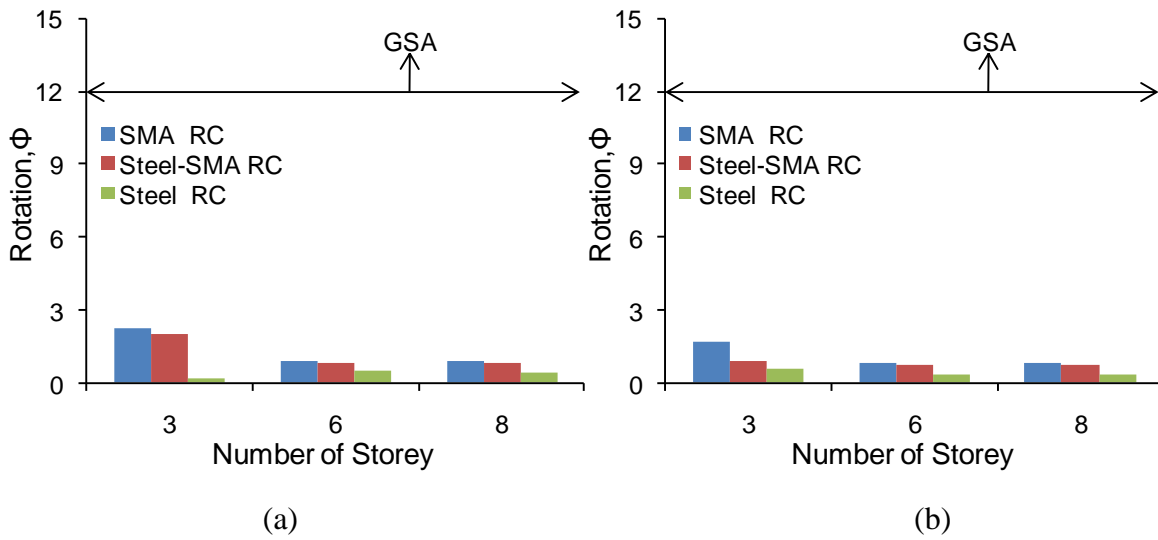


Figure 5.10 Comparison of rotation due to (a) corner column removal, and (b) exterior bay intermediate column removal.

The results indicate that the SMA RC frames are more prone to progressive collapse failure than the Steel RC frames.

5.5.4.1 Vertical displacement

In addition to the GSA evaluation techniques, the performance of the SMA RC, Steel-SMA RC and Steel RC frames are also compared by considering the vertical deflection of the joint at which the column is removed. The vertical deflection results are shown in Figures 5.11, 5.12, and 5.13 for the 3, 6, and 8-storey frames, respectively. For all cases, the SMA RC frames were subjected to larger deflections compared to those of the Steel-SMA and Steel RC frames. The residual drifts were also higher for the SMA RC frames. However, the percentage of recovering the deflection is higher for the SMA RC frames compared to the other framing systems. In the case of the 3-storey frames, the recovery rates are 17%, 18% and 12% for the SMA, Steel-SMA and Steel RC frames, respectively, when the corner column is removed. In the cases of the 6 and 8-storey frames, the recovery rates are 33% 31%, 28% and 32%, 31% and 25% for the SMA, Steel-SMA and Steel RC frames, respectively. When an exterior bay intermediate column is removed from the SMA, Steel-SMA, and Steel RC frames, the recovery rates are 46%, 39%, and 22% for the 3-storey frames, 41%, 42% and 36% for the 6-storey frames, and 36%, 42%, and 32% for the 8-storey frames, respectively.

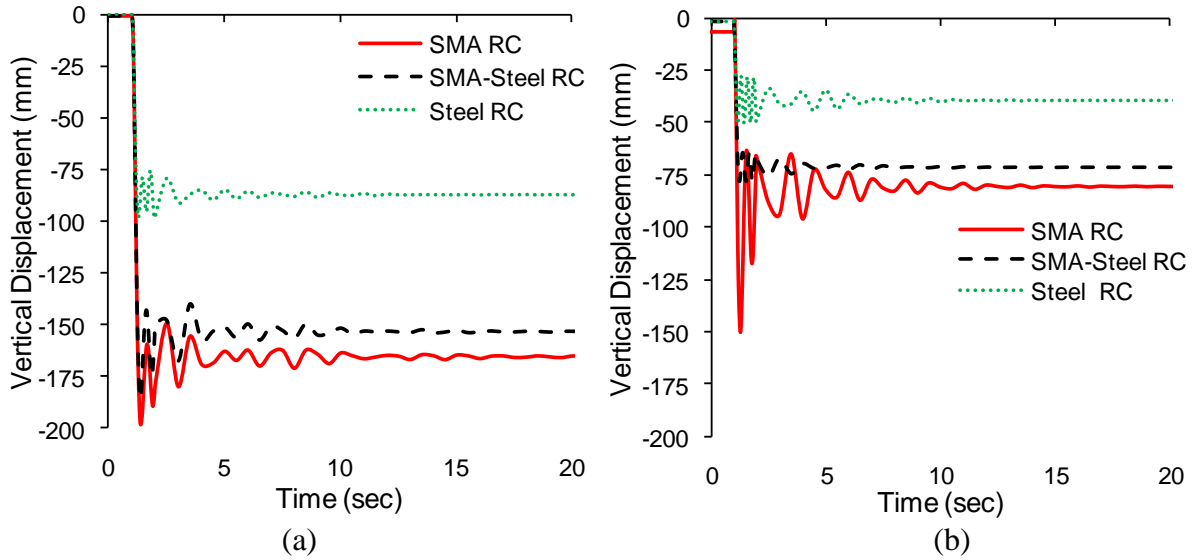


Figure 5.11 Vertical displacement of the point at which the bottom storey column is removed from 3-storey frames due to: (a) corner column removal, and (b) exterior bay intermediate column removal.

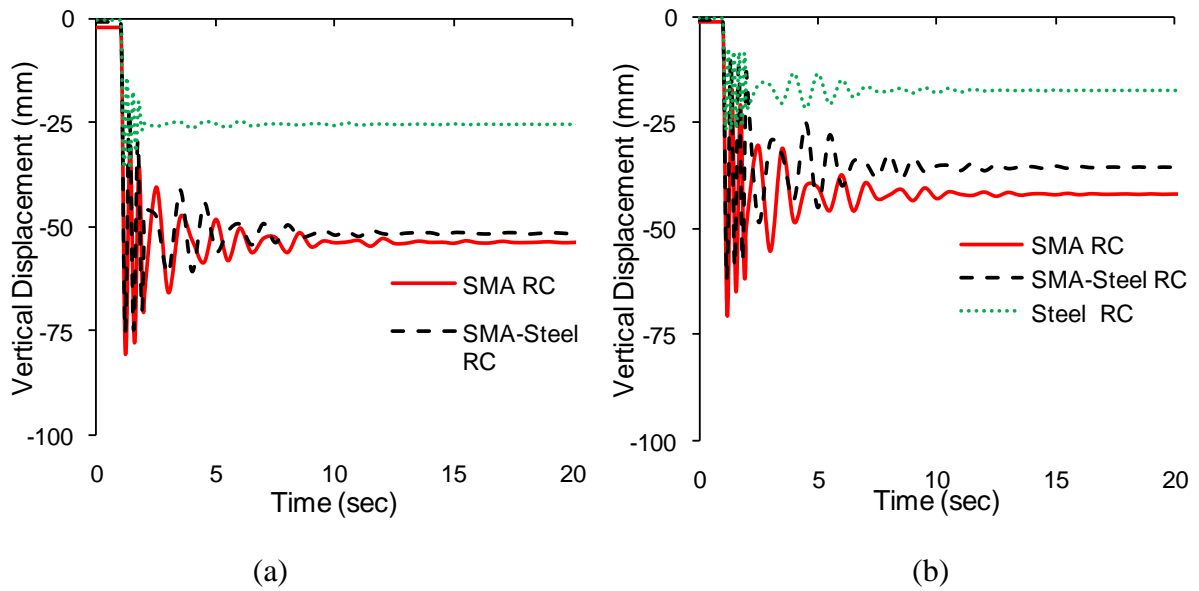


Figure 5.12 Vertical displacement of the point at which the bottom storey column is removed from 6-storey frames due to: (a) corner column removal, and (b) exterior bay intermediate column removal.

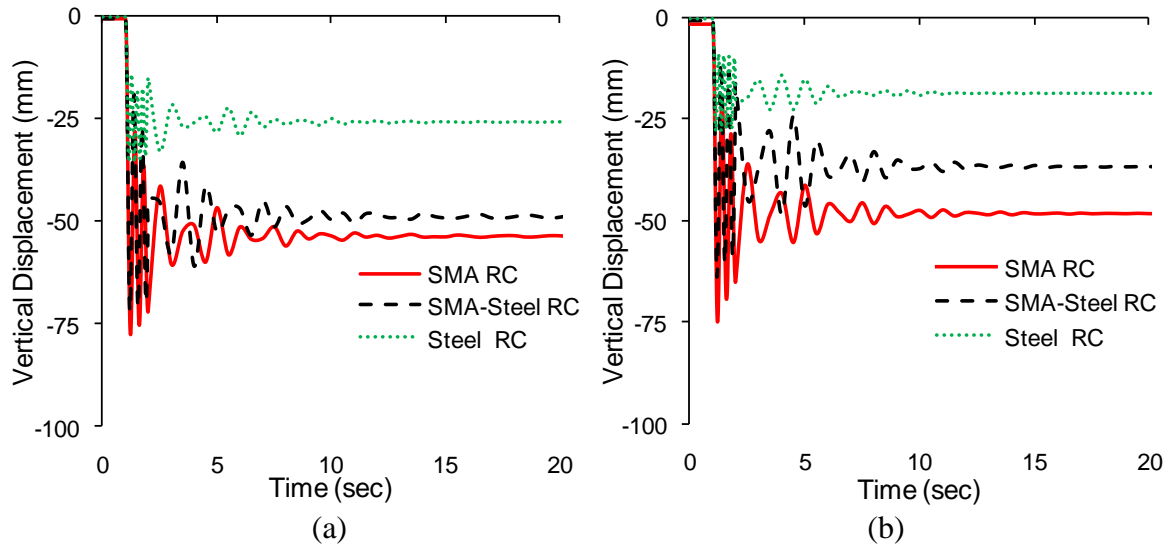


Figure 5.13 Vertical displacement of the point at which the bottom storey column is removed from 8-storey frames due to: (a) corner column removal, and (b) exterior bay intermediate column removal.

When an exterior bay intermediate column is removed from the SMA, Steel-SMA, and Steel RC frames, the recovery rates are 46%, 39%, and 22% for the 3-storey frames, and 41%, 42%, 36% for the 6-storey frames, and 36%, 42%, 32% for the 8-storey frames, respectively.

5.5.4.2 Variation of axial forces

The variations in axial forces in columns due to the sudden removal of a column have been observed from nonlinear dynamic time history analyses. The results are presented in Figures 5.14, 5.15 and 5.16 for the 3, 6, and 8-storey frames, respectively. It can be observed that the axial force in the adjacent column of the removed corner column is higher for the 3-storey Steel RC frame compared to that of the SMA and Steel-SMA RC frames. However, in the case of the intermediate column removal, the 3-storey SMA RC frame

experienced higher axial force (Figure 5.14b). In the case of the 6 and 8-storey frames, the Steel RC frames experienced lesser axial forces compared to the other framing systems.

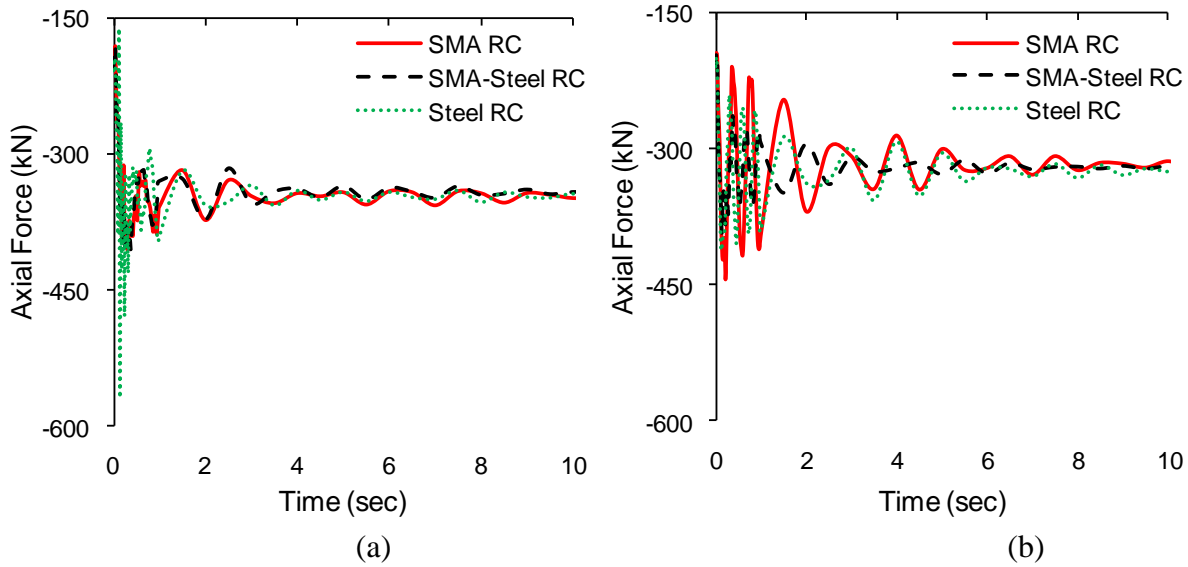


Figure 5.14 Column axial force variation adjacent to the removed column (bottom storey B1) for 3-storey frames due to: (a) corner column removal, and (b) exterior bay intermediate column removal.

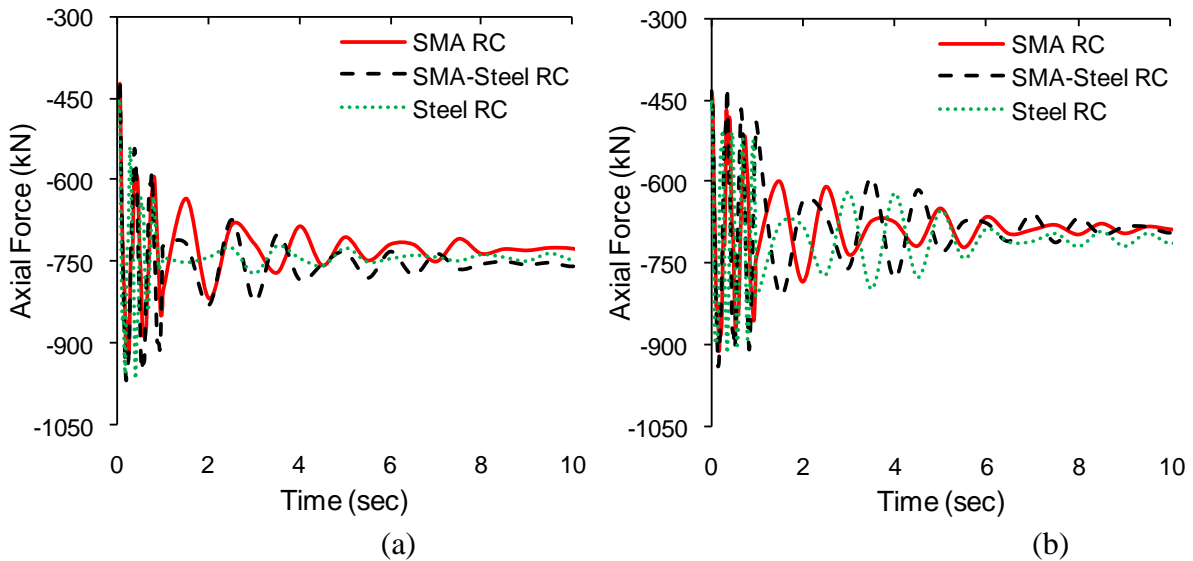


Figure 5.15 Column axial force variation adjacent to the removed column (bottom storey of B1) for 6-storey frames due to: (a) corner column removal, and (b) exterior bay intermediate column removal.

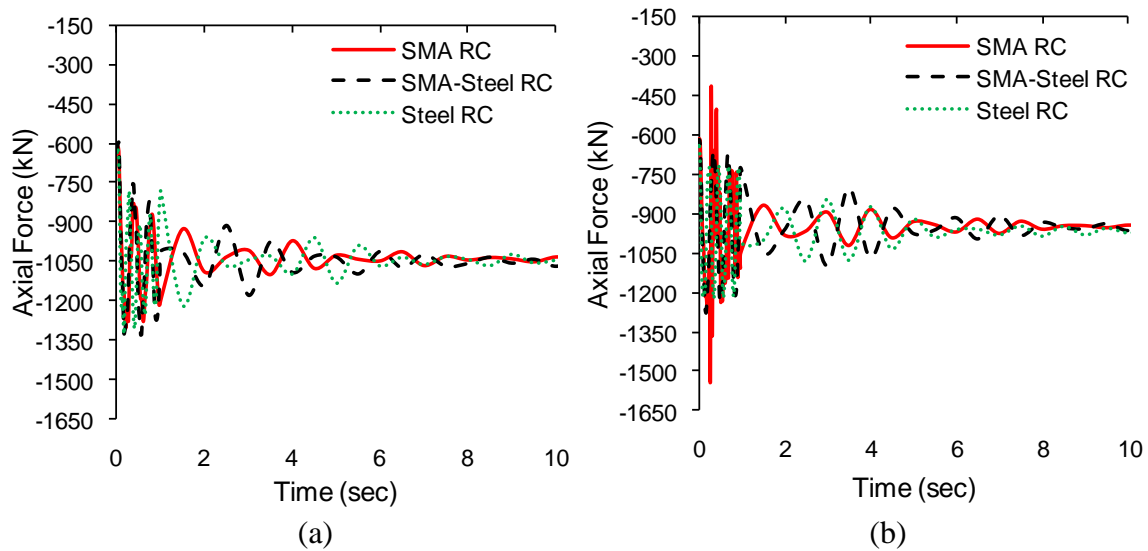


Figure 5.16 Column axial force variation adjacent to the removed column (bottom storey of B1) for 8-storey frame due to (a) corner column removal, and (b) exterior bay intermediate column removal.

Figures 5.17 shows how the axial forces along the height of the frame change for the 3, 6, and 8-storey frames when the corner and intermediate columns are removed under nonlinear dynamic analyses. From these results it is observed that for all cases column B1 has adequate capacity to carry the increased axial load due to the removal of the corner or intermediate column. In the case of the corner column removal of the 3-storey frame, the SMA RC frame is subjected to less axial force compared to that of the Steel RC frame along the height of the frame. But when the intermediate column was removed, the SMA RC frames (except for the 6-storey) are subjected to higher axial forces compared to those of other frames. However, in most cases the results are comparable except for the 3-storey frames (Figures 5.17 a and b) where there was no particular trend in the axial force variations at different storey levels for different frame types (Figures 5.17 c to f). During a sudden column removal event, the response of a 3-storey structure is different compared to a 6 and 8-storey frame structures because of its smaller path along its height for uniform

distribution of forces. The variations in results were also because of SMA's lower modulus of elasticity compared to steel.

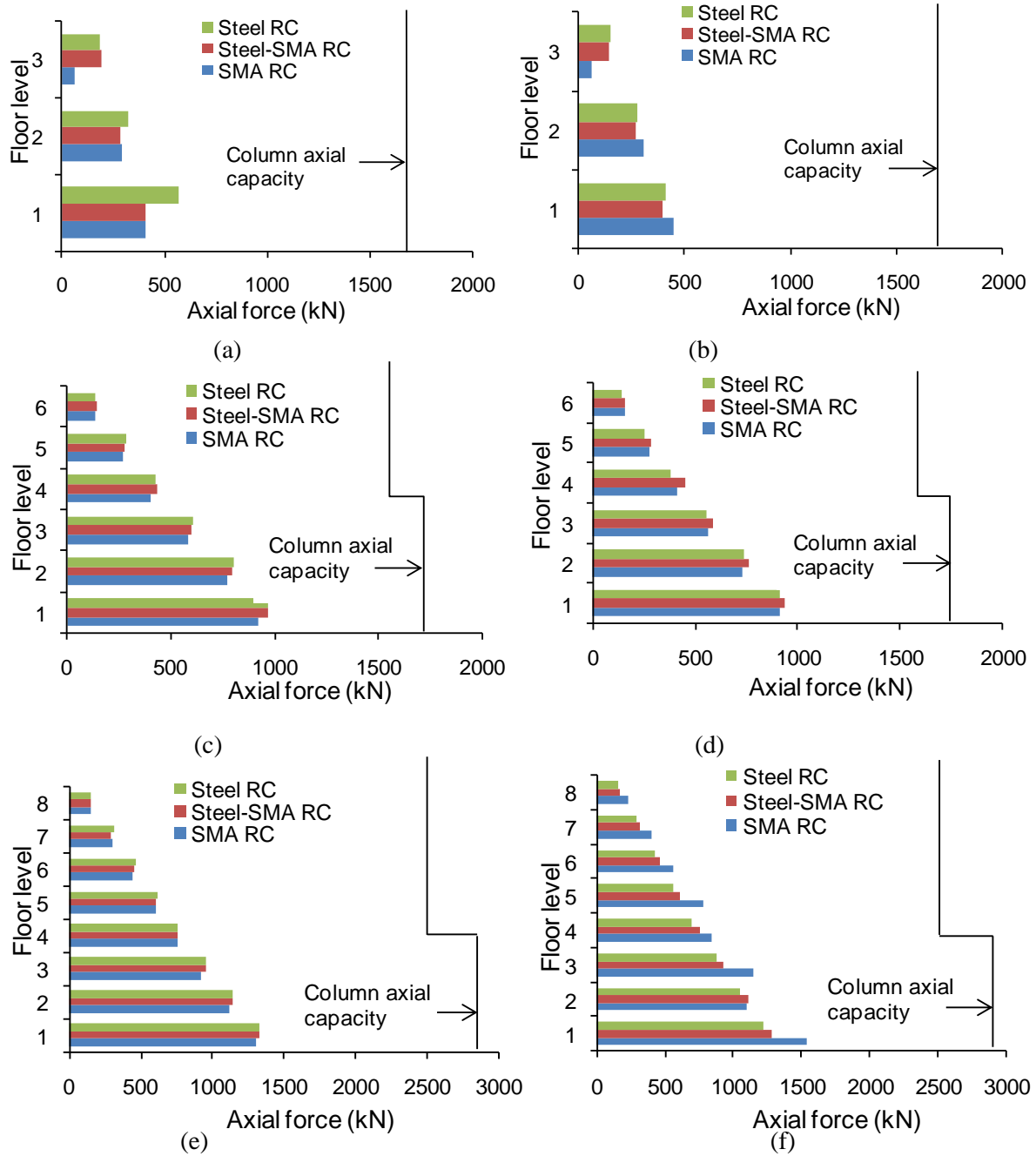


Figure 5.17 Variation of axial forces in column B1 due to: (a) corner column removal from 3 storey, (b) intermediate column removal from 3-storey, (c) corner column removal from 6-storey, (d) intermediate column removal from 6-storey, (e) corner column removal from 8-storey, and (f) intermediate column removal from 8-storey frames.

5.5.4.3 Variation of maximum shear forces

The variations in shear forces in the first floor beams at the joint locations of the column removal are also presented in Figures 5.18, 5.19 and 5.20, for the 3, 6, and 8-storey frames, respectively.

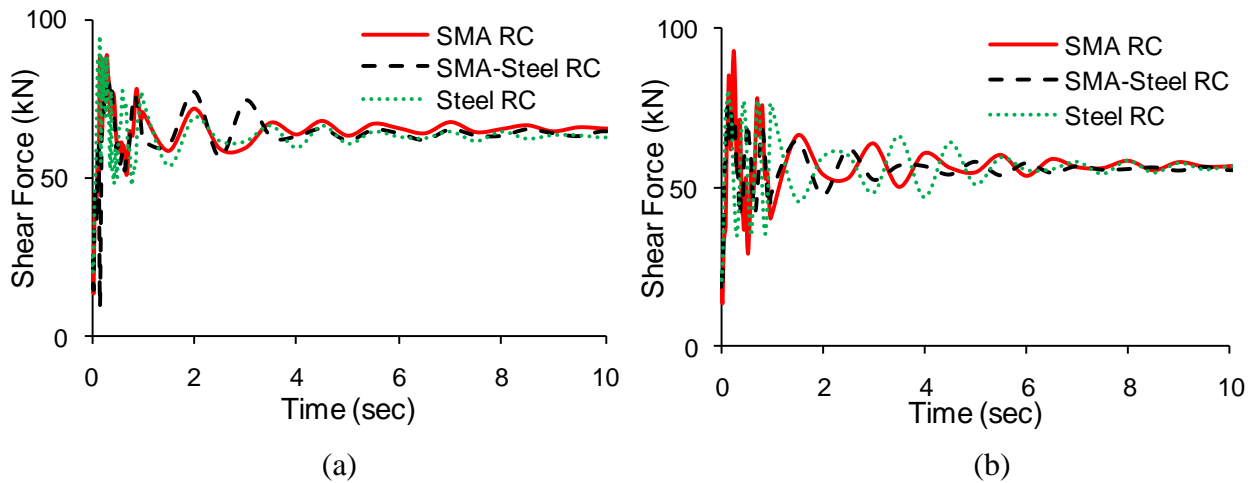


Figure 5.18 Shear forces in beams for 3 storey frames due to: (a) corner column removal, and (b) exterior bay intermediate column removal.

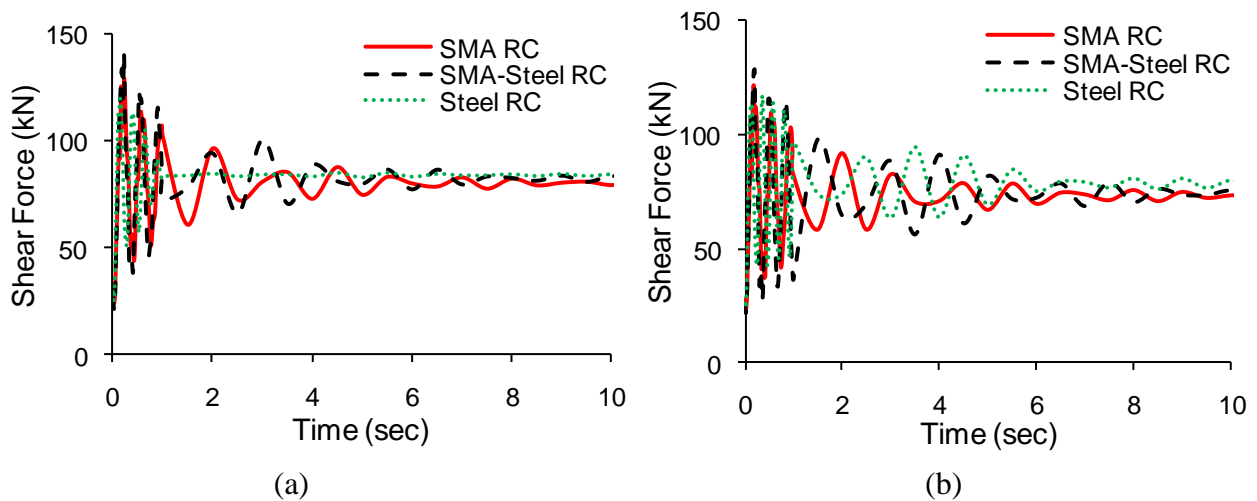


Figure 5.19 Shear forces in beams for 6 storey frames due to: (a) corner column removal, and (b) exterior bay intermediate column removal.

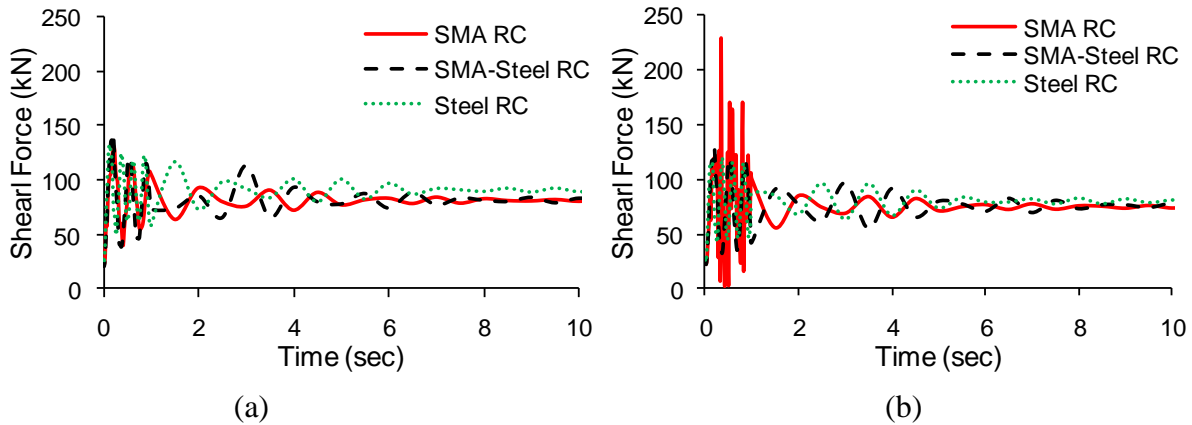


Figure 5.20 Shear forces in beams for 8 storey frames due to: (a) corner column removal, and (b) exterior bay intermediate column removal.

5.6 PERFORMANCE COMPARISON AMONG DIFFERENT ANALYSES TECHNIQUES

Tables 5.10 and 5.11 show the variations in the axial forces for the 3, 6, and 8-storey frames using the different analysis techniques. For all the frames it is observed that the axial force demand is higher when the corner column is removed compared to the intermediate column removal. When the corner column is removed the common scenario is that column B1 of the Steel RC frames are subjected to more axial forces compared to the SMA RC frames. The results obtained by removing an intermediate column of an exterior bay are not consistent like the corner column removal condition. The maximum variations of the axial forces are obtained for the 3-storey frame when the corner column is removed under linear static analyses. This variation is 6.06 times the initial condition for the SMA RC, Steel-SMA and Steel RC frames. For the 6 and 8-storey frames the maximum variation is also obtained when linear static analyses are performed.

Table 5.10 Ratio of the maximum axial force to its initial condition in column B1 due to corner column removal.

Analysis type	Building ID	RC Frame Type		
		SMA RC	Steel-SMA RC	Steel RC
Linear static analyses	3	6.06	6.06	6.06
	6	5.92	6.26	6.26
	8	3.74	3.74	3.74
Nonlinear static analyses	3	5.02	5.06	4.67
	6	5.18	5.52	5.57
	8	3.51	3.52	3.67
Linear dynamic analyses	3	3.86	5.52	5.52
	6	5.15	5.10	5.47
	8	3.23	3.23	3.23
Nonlinear dynamic analyses	3	4.06	4.05	5.69
	6	4.46	4.70	4.69
	8	2.89	2.98	2.98

Table 5.11 Ratio of the maximum axial force to its initial condition in column B1 due to an exterior bay intermediate column removal.

Analysis type	Building ID	RC Frame Type		
		SMA RC	Steel-SMA RC	Steel RC
Linear static analyses	3	2.56	2.56	2.11
	6	2.31	2.05	2.49
	8	1.60	1.60	1.60
Nonlinear static analyses	3	2.02	2.39	2.44
	6	2.38	2.34	2.40
	8	1.68	1.67	1.68
Linear dynamic analyses	3	2.11	2.11	2.11
	6	1.96	1.92	2.00
	8	1.39	1.39	1.39
Nonlinear dynamic analyses	3	2.12	1.87	1.96
	6	1.98	2.03	1.98
	8	1.78	1.44	1.36

The variations of shear forces for the different frames which are obtained from different analyses are presented in Tables 5.12 and 5.13. Tables 5.12 and 5.13 present the variations in shear forces when the corner and intermediate columns are removed, respectively using

different analysis techniques. In almost every case the Steel RC frames are subjected to a large shear forces ratio compared to the SMA RC frames.

Table 5.12 Ratio of the beam maximum shear force to its initial condition due to corner column removal.

Analysis type	Building ID	RC Frame Type		
		SMA RC	Steel-SMA RC	Steel RC
Linear Static Analyses	3	2.25	2.25	2.25
	6	1.37	1.37	1.38
	8	1.40	1.40	1.40
Nonlinear Static Analyses	3	1.98	2.00	1.81
	6	1.51	1.62	1.63
	8	1.61	1.71	1.74
Linear Dynamic Analyses	3	2.00	2.46	2.46
	6	1.53	1.53	1.61
	8	1.53	1.53	1.53
Nonlinear Dynamic Analyses	3	1.80	1.70	1.93
	6	1.57	1.73	1.46
	8	1.59	1.68	1.62

Table 5.13 Ratio of the beam maximum shear force to its initial condition due to an exterior bay intermediate column removal.

Analysis type	Building ID	RC Frame Type		
		SMA RC	Steel-SMA RC	Steel RC
Linear Static Analyses	3	1.87	1.87	1.87
	6	1.14	1.08	1.19
	8	1.16	1.16	1.16
Nonlinear Static Analyses	3	1.60	1.73	1.94
	6	1.49	1.47	1.50
	8	1.49	1.50	1.52
Linear Dynamic Analyses	3	1.75	1.75	1.75
	6	1.05	1.04	1.09
	8	1.06	1.06	1.06
Nonlinear Dynamic Analyses	3	1.89	1.54	1.64
	6	1.49	1.57	1.43
	8	1.58	1.57	1.46

In the current study linear and nonlinear static and dynamic analyses are performed. The buildings considered here are regular in nature. The linear static analyses are suitable when

both the nonlinear response and dynamic effects can be predicted. In order to estimate the dynamic influence, an amplified load factor of 2 [Eq. (5.1)] is used. The linear dynamic analyses can be used when the nonlinear behaviour of structures are easily predicted. The *DCR* values obtained from the linear dynamic analyses are higher than the values obtained from the linear static analyses. By analyzing the results from Tables 5.10 to 5.13, it can be observed that linear dynamic analyses are more reliable than other analyses techniques in predicting the variation in axial forces of different types of frames under progressive collapse. For instance, in the case of corner column removal, the ratio of the maximum axial force to its initial reaction values obtained from nonlinear static analyses are on an average 15% higher when compared to the nonlinear dynamic analyses whereas this prediction in the case of linear dynamic analyses were within 5% to those of nonlinear dynamic analyses. However, while predicting the vertical displacement during progressive collapse, nonlinear static analyses produced more accurate predictions compared to other techniques. For instance, the vertical displacement values obtained from nonlinear static analyses were on an average only 3% offset from those obtained from nonlinear dynamic analyses.

5.7 SUMMARY

The results of this chapter indicated that the resistance to progressive collapse of seismically designed Steel RC frames are much better compared to SMA RC frames during a progressive collapse load event.

CHAPTER 6: CONCLUSIONS

6.1 SUMMARY

This thesis explores the possibility of utilizing shape memory alloys (SMAs) as longitudinal reinforcement in beams in reinforced concrete frame buildings. This study provides literature review on shape memory alloys where its mechanical behaviour, various factors influencing their mechanical properties and its constitutive material models has been discussed. The use of SMAs in repairing deficient structures and constructing new civil engineering structures has been broadly presented.

This study determines the seismic response modification factor (R) supply and demand for the Steel RC, Steel-SMA RC and SMA RC frame buildings designed as per NBCC (2005) and CSA A23.3-04. The performance of these building in terms of seismic response modification factors supply and demand ratio has been evaluated. This study also evaluates the seismic vulnerability of these buildings and their resistance against progressive collapse.

6.2 LIMITATIONS OF THIS STUDY

The main limitations of the current study are

- The slab and transverse beams contribution were not considered.
- Vertical irregularity and Irregularity in bay length were not considered.
- Two out of the ten earthquake records considered in this study produced elastic base shear, which were having large deviation from the other records, however, no statistical analyses were performed except the arithmetic mean.

- To evaluate the progressive collapse performance only the exterior bay bottom storey corner and intermediate column were removed in this.

6.3 CONCLUSIONS

A major part of this study examines the overstrength factor, the ductility reduction factor supply and demand, and the response modification factor supply and demand for Steel-SMA and SMA RC frames. The results are then compared to those obtained from a regular Steel RC frames. Three different (3, 6 and 8) storey RC frames have been designed where each frame has three different types of reinforcement configurations in their beams. All the buildings are located in a high seismic zone in Vancouver, and are designed according to CSA standards (A 23.3-04). Nonlinear static pushover analyses have been performed to determine the overstrength factor and the ductility of all the frames. All the frames have been analyzed under selected and scaled seismic loading using a finite element program. Nine real and one artificial earthquake record have been considered in this study. Nonlinear incremental dynamic time history analyses and linear dynamic time history analyses have been performed to obtain the ductility reduction factors and the response modification factors.

From the pushover analyses it is observed that

- The lateral base shear capacities for Steel-SMA and SMA RC frames are similar to those of Steel RC frames. For each storey type, the initial stiffness of the Steel RC, the Steel-SMA RC and the SMA RC frame was similar. Once concrete cracked, the SMA RC frame shows much reduced stiffness compared to the Steel RC frames

because of SMA's lower modulus of elasticity compared to steel, which is also the cause of SMA's higher inter-storey drift compared to Steel RC frames.

- The overstrength factor was also calculated for the Steel, the Steel-SMA and the SMA RC frames, which is found to be very close to each other.
- The displacement ductility for each frame type was calculated from the pushover analyses based on the idealized elasto-plastic behaviour. From this study it was observed that the Steel RC frames are more ductile for all 3, 6, and 8-storey frames by at least 20%.

Nonlinear incremental dynamic time-history analyses and linear dynamic time history analyses were also performed for all the frames to determine their ductility reduction factor and their response modification factor supply.

- The ductility reduction factor increased with the increase of storey numbers.
- The ductility reduction factor demand and the response modification factor demand were also calculated by using empirical equations.
- The supply-demand ratio for the ductility reduction factor was also compared among the considered frames.
- From the results of this study it can be concluded that the response modification factor supply and demand for the SMA RC frames are similar to the Steel RC frames.

- The NBCC (2005) provided response modification factor can be used for the SMA RC and Steel-SMA RC frames.

Seismic vulnerability of the considered frames is also assessed in this study. The vulnerability of a building can be a function of plastic rotations, member forces and inter-storey drift, which can be controlled by controlling the overall capacity of the building. The building subjected to an earthquake ground motion causes a building response resulting in drifts and member forces, all of which can express demands. If both the ground motion demand and the building's capacity to resist this demand could be estimated with some confidence, then buildings could be designed with some level of assurance in performing as desired.

The performance and response of the considered frames have been evaluated by developing nonlinear analytical models of the frames and performing seismic analyses with an ensemble of 10 earthquake ground motions scaled to different intensity levels. The spectral acceleration at the structure's fundamental mode period was used to scale each record, thus allowing a reduction in record-to-record variability. The corresponding peak ground acceleration (*PGA*) was also used as a seismic hazard representation for comparing the performance of the SMA RC frame system. The height-wise distribution and record-to-record variability of the maximum drift demands were also studied. The general conclusions drawn from the results of this study are summarized below:

- At the design level ground motion intensity for the 3 and 6-storey SMA RC frames, the calculated roof and maximum inter-storey drift demands based on the median

ground motions provide satisfactory performance on the basis of the NBCC drift limits. The 8-storey SMA RC frame exceeded the NBCC drift limit.

- The allocation of the inter-storey drift demand along the height of the frames differs from record to record in terms of magnitude, but follows a very similar pattern. The maximum drift demands in the elastic range of response normally occur at the upper-story levels. In the inelastic range of response, there is a high concentration of inelasticity, mainly in the 4th-storey level for the 8-storey SMA RC frames.
- The median capacities for the Steel RC frames in terms of maximum inter-storey drift based on collapse prevention levels are between 1.5 to 3.3 times the NBCC drift limit.
- The median capacities for the Steel-SMA RC frames in terms of the maximum inter-story drift based on collapse prevention levels are between 1.1 to 2.1 times the NBCC drift limit.
- The median capacities for SMA RC frames in terms of the maximum inter-storey drift based on collapse prevention levels are between 0.94 to 2.31 times the NBCC drift limit.
- When residual roof drift and maximum residual inter-storey drift were considered, the SMA and the Steel-SMA RC frames performed better than the Steel RC frames.
- SMA RC frames can be used for low-rise buildings of up to 6-storeys. With the increase in building height, SMA RC frames become unsafe. The main reason behind this was the low modulus of elasticity of the SMA material. Therefore, the current reinforced concrete design approach is not applicable for medium rise SMA

RC frames. New design methodology is necessary for SMA RC frames that are 8-storeys or higher.

To evaluate the performance of 9 frames, four different analysis techniques were used: linear static and dynamic, and nonlinear static and dynamic analyses. GSA 2003 guidelines were followed for performance comparison. From the results of the linear static analyses the following observations were made:

- Irrespective of the frame type and storey height, the *DCR* value in each case was less than 2.0.
- The maximum *DCR* value was observed for 3 storey frames where the value was 1.72.
- For the 6 and 8-storey frames the *DCR* value for beam B1 was less than beam B2 where beam B2 is located at the 4th floor level for both the 6 and 8-storey frames. This is due to the lower reinforcement ratio of beam B2 compared to that of beam B1, which reduced the capacity of beam B2 compared to its demand.
- The *DCR* values for the SMA RC, Steel-SMA and Steel RC frames were similar for all stories.

From the results obtained from linear static analyses it was observed that the reinforcement types did not affect the behaviour of the frame structures significantly under progressive collapse. The seismically designed building as per CSA A23.3-04 and NBCC-2005, exhibited satisfactory performance in preventing progressive collapse, when performing the static linear analysis.

On the basis of the nonlinear static analyses results the following conclusions can be drawn:

- Steel RC frames offer less ductility than the other frame systems during sudden removal of a column. In the case of the SMA RC frame, it offered more ductility compared to the Steel-SMA and the Steel RC frames, which implies more susceptibility to progressive collapse compared to others.
- When the exterior bay intermediate column was removed, the Steel RC frame could carry the full load where as the other frames could not.

The following conclusions were drawn on the basis of the linear dynamic analyses results:

- The *DCR* values observed from the linear dynamic analyses were more than those from the linear static analyses. Although the *DCR* values obtained from the linear static analyses for the 3-storey SMA, Steel-SMA, and Steel RC frame are less than 2.0 for both positive and negative moments, in the case of linear dynamic analyses the *DCR* values for these frames exceeded 2.0 for the negative moment when the corner column was removed.
- The *DCR* values are always greater when the corner column is removed, which implies that the corner columns are more critical than the exterior bay intermediate columns for progressive collapse.

From the nonlinear dynamic time history analyses the following conclusions are drawn:

- The support rotation and the ductility observed from the nonlinear dynamic analyses are comparatively less than those obtained from the static analyses.
- For all types of frames the ductility and the rotation values are less than the GSA (2003) recommended values.

- From the nonlinear dynamic analyses it is observed that the SMA RC frames are more susceptible to progressive collapse than the Steel RC frames.

Although SMAs have unique properties like superelasticity, their performance under progressive collapse is similar to regular Steel RC frames. In most cases their performance was rather inferior as they experienced larger vertical displacement, axial and shear forces for 6 and 8-storey frames compared to those of the regular Steel RC frames. All the analyses results showed that the corner columns are more vulnerable to progressive collapse. Therefore, care should be taken by engineers while designing new structures and strengthening the existing structures against progressive collapse. From the static linear analyses it was observed that all types of frame structures are safe under progressive collapse. However, the linear dynamic analyses showed that the 3-storey frames are not safe against progressive collapse, which clearly indicates that more rigid guidelines should be incorporated in building design codes for preventing progressive collapse.

6.4 RECOMMENDATIONS FOR FUTURE RESEARCH

Further research is necessary to investigate the seismic performance of SMA and Steel-SMA RC frames under shake table loading. Different moment resisting frames can be considered for the test, for instance, ductile, moderately ductile and gravity load designed frames with regular and irregular framing. Such experimental investigations will confirm the results demonstrated in this study on the seismic performance of the ductile SMA and Steel-SMA RC frames. Research is also needed to study the effect of slab and transverse beams on the performance of SMA and Steel-SMA frames under seismic loading (i.e 3-Dimensional analyses). Design code provisions for the seismic design of Steel RC

structures need to be re-examined for SMA and Steel-SMA RC structures considering its relatively lower modulus of elasticity and energy dissipation capacity, large deformation capability, negligible residual strain, and recentering capability. Future research may include understanding the behaviour of SMA RC shear walls, interior SMA RC beam-column joint, top storey interior and top-storey corner joint. Since the strength and failure mechanisms of interior and top-storey corner joints might be different than that of an exterior beam-column joint, it is important to carry out further research on these particular elements. Such elements can substantially affect the overall seismic performance of a structure, which may consequently change the force modification factors for seismic design.

BIBLIOGRAPHY

- Adachi Y, Unjoh S, Kondoh M. 2000 Development of a shape memory alloy damper for intelligent bridge systems. *Materials Science Forum (Shape Memory Materials)*; 327(3):31–34.
- Alam, M.S.; Youssef, M. A.; Nehdi, .; 2007. Utilizing shape memory alloys to enhance the performance and safety of civil infrastructure: a review, *Can. J. Civ. Eng.* 34: 1075–1086.
- Alam, M.S., Youssef, M.A. and Nehdi, M. 2007. Seismic behaviour of concrete beam-column joints reinforced with superelastic shape memory alloys. *9th Canadian Conference on Earthquake Engineering*, June, ON, Canada 2007, Paper no. 1125, 10 p.
- Alam, M.S., Youssef, M.A., and Nehdi, M. 2008. Analytical prediction of the seismic behaviour of superelastic shape memory alloy reinforced concrete elements. *Engineering Structures*, 30: 3399-3411.
- Alam, M.S., Nehdi, M., and Youssef, M.A. 2009. Seismic performance of concrete frame structures reinforced with superelastic shape memory alloys. *Smart structures and systems*, 5(5):565-585.
- Alam, M.S., Youssef, M.A., and Nehdi, M. 2010. Exploratory investigation on mechanical anchors for connecting SMA bars to steel or FRP bars. *Materials and Structures*, available online at <http://www.springerlink.com/content/tu8546r8021x6451/>.
- Annan, C.D.; Youssef, M.A.; and El Naggar., M.H. 2009. Seismic vulnerability assessment of modular steel buildings. *Journal of Earthquake Engineering* 13.8, 1065-1088
- ANSYS, Inc. Version 10.0. 2005. *Southpointe, Canonsburg, PA, USA*.
- Asai, M., and Suzuk, Y. 2000. “Applications of shape memory alloys in Japan.” *Mater. Sci. Forum*, 327–328, 17–22.
- ATC-3-06 (1985) Tentative Provisions for the Development of Seismic Regulations for Buildings, Applied Technology Council 555 Twin Dolphin Drive, Suite 550, Redwood City, CA 94065.
- ATC-19 (1995) Structural Response Modification Factors, Applied Technology Council 555 Twin Dolphin Drive, Suite 550, Redwood City, CA 94065.

- ATC-34 (1995) A Critical Review of Current Approaches to Earthquake-Resistant Design, Applied Technology Council 555 Twin Dolphin Drive, Suite 550, Redwood City, CA 94065.
- Atkinson, G.M. 2009. Earthquake time histories compatible with the 2005 National building code of Canada uniform hazard spectrum. *Canadian Journal of Civil Engineering*, 36: 991–1000.
- Auricchio, F., and Taylor, R.L. 1996. Shape memory alloy superelastic behavior: 3D finite element simulations. Proceedings of SPIE - *The International Society for Optical Engineering*, Vol. 2779, pp. 487-492.
- Auricchio F, Taylor RL, Lubliner J. 1997. Shape-memory alloys: macromodelling and numerical simulations of the superelastic behaviour. *Computer Methods in Applied Mechanics and Engineering*; 146(3-4):281-312.
- Auricchio, F. and Lubliner, J. 1997. Uniaxial model for shape-memory alloys. *International Journal of Solids and Structures*, 34: 3601-3618.
- Auricchio, F., and Sacco, E. 1997. Superelastic shape-memory-alloy beam model. *Journal of Intelligent Material Systems and Structures*, 8: 489-501.
- Auricchio, F. and Sacco E. 1997. “A One-Dimensional Model for Superelastic Shape Memory Alloys with Different Elastic Properties Between Austenite and Martensite,” *International Journal of Non-Linear Mechanics*, 32(6):1101–1114.
- Bauer, C, Martin, W. and Siegling, H. F. 1998. An adaptive composite structure to control the sonic shock of transport aircraft wings. *Proc. 4th European Conference of Smart Structures and Materials, Harrogate, UK*, pp. 25-32.
- Beauchamp, C. H. 1992. “Shape memory alloy adjustable camber (SMAAC) control surfaces.” *Proc., 1st European Conf. on Smart Structures and Materials, Glasgow, U.K.*, 189–192.
- Bertran, A. 1982. “Thermo-Mechanical Constitutive Equations for the Description of Shape Memory Effects in Alloys,” *Nuclear Engineering and Design*, 74:173–182.
- Boyd, J.G. and Lagoudas, D.C. 1994. “Constitutive Model for Simultaneous Transformation and Reorientation in Shape Memory Alloys.” *In: Brinson, L.C. and Moran, B. (eds)*,

Mechanics of Phase Transformation and Shape Memory Alloys, pp. 159–177, ASME, New York.

Baldrige, S.M.; and Humay, F. K.; 2003. Preventing Progressive Collapse in Concrete Buildings, concrete international.

Brinson, L.C. 1993. One-dimensional constitutive behavior of shape memory alloys: Thermomechanical derivation with non-constant material functions and redefined martensite internal variable. *Journal of Intelligent Material Systems and Structures*, 4: 229-242.

Brocca, M., Brinson, L.C, and Bazant, Z.P. 2002. Three-dimensional constitutive model for shape memory alloys based on microplane model. *Journal of the Mechanics and Physics of Solids*, 50: 1051-1077.

Bruno, S., and Valente, C. 2002. Comparative response analysis of conventional and innovative seismic protection strategies. *Earthquake Engineering and Structural Dynamics*, 31: 1067-1092

BS 8110. "Structural use of Concrete Part 1. Code of Practice for Design and Construction." *The British Standards Institute*, 1997.

Buscemi, N.; Marjanishvili, S.M.; 2005. SDOF model for progressive collapse analyses, *Proc. SEI structures Congress, ASCE, Reston Va.*

CSA A23.3-04 2004. Design of Concrete Structures (Canadian Standards Association, *Rexdale, Ontario, Canada*).

Chandra, R. 2001. "Active shape control of composite blades using shape memory actuation." *Smart Mater. Struct.*, 10, 1018–1024.

Choi, E.; Cho, S. C.; Hu, J. W., Park, T.; and Chung, Y. S.; 2010. Recovery and residual stress of SMA wires and applications for concrete structures, *Smart Mater. Struct.* 19, 094013 (10pp)

Clark, P.W., Aiken, I.D., Kelly, J.M., Higashino, M. and Krumme, R. 1995. Experimental and analytical studies of shape-memory alloy dampers for structural control. Proceedings of SPIE, *Smart Structures and Materials 1995: Passive Damping*, Vol. 2445, pp.241-251.

- Czaderski, C, Hahnebach, B., and Motavalli, M. 2006. RC beam with variable stiffness and strength. *Construction and Building Materials*, 20: 824-833.
- Delgadillo-Holtfort, I., Kaack, M., Yohannes, T., Pelzl, J., and Khalil-Allafi, J. 2004. Ultrasonic investigation of multistage martensitic transformations in aged Ni-rich Ni- Ti shape memory alloys. *Materials Science and Engineering A*, 378: 76-80.
- Deng Z C, Li Q B, Jiu A and Li L 2003. Behavior of concrete driven by uniaxially embedded shape memory alloy actuators, *J. Eng. Mech.* 129 697–703.
- DesRoches, R.; McCormick, J; and Delemont, M.; 2004. Cyclic Properties of Superelastic Shape Memory Alloy Wires and Bars, *Journal of Structural Engineering*, Vol. 130, No. 1
- DesRoches, R., and Smith, B. 2004. Shape memory alloys in seismic resistant design and retrofit: a critical review of their potential and limitations. *Journal of Earthquake Engineering*, 8: 415-429.
- DesRoches, R., McCormick, J., and Delemont, M. 2004. Cyclic properties of superelastic shape memory alloy wires and bars. *Journal of Structural Engineering, ASCE*, 130: 38-46.
- DesRoches, R.; and McCormick, J.; 2007. Application of shape memory alloys in control of buildings under seismic loads, *Proceedings of SMSST'07, World Forum on Smart Materials and Smart Structures Technology (SMSST'07), China*, 22-27
- DoD. "Unified Facilities Criteria (UFC) 4-010-10, DoD Minimum Antiterrorism Standoff Distances for Buildings." *Department of Defence of the United States of America*.
- DoD. "DoD Ammunition and Explosive Safety Standards . 6055.9-STD." *Department of Defence of the United States of America*. July, 1999.
- Dolce, M. 1994. "Passive Control of Structure", Proc. *10th European Conference on Earthquake Engineering, Vienna*, 10 pp
- Dolce, M., Cardone, D., and Marnetto, R. 2000. Implementation and testing of passive control devices based on shape memory alloys. *Earthquake Engineering and Structural Dynamics*, 29: 945-968.

- Dolce, M. and Cardone, D. 2001a. Mechanical behaviour of shape memory alloys for seismic applications 1. *Martensite and austenite Ni-Ti bars subjected to torsion. International Journal of Mechanical Sciences*, 43: 2631-2656.
- Dolce, M., Cardone, D., Marnetto, R., Mucciarelli, M., Nigro, D., Ponzo, F.C., and Santarsiero, G. 2004. Experimental Static and Dynamic Response of a Real RC Frame Upgraded with SMA Re-Centering and Dissipating Braces. *Proceedings of the 13th World Conference on Earthquake Engineering, Canada, Paper no. 2878.*
- Duerig, T.; Melton, K.; Stockel, D.; Wayman C. 1990. Engineering Aspects of Shape Memory Alloys, *Butterworth-Heinemann, London.*
- Duval, L, Noori MN, Hou Z, Davoodi H, Seelecke S. 2000. Random vibration studies of an SDOF system with shape memory restoring force. *Physica B*; 275(1–3):138–141.
- Elbahy YI, Youssef MA, and Nehdi M. 2009. Stress block parameters for flexural members reinforced with shape memory alloys. *Mat & Struct* 42(10): 1335-135.
- Elbahy YI, Youssef MA, and Nehdi M. 2010. Deflection of superelastic shape memory alloy reinforced concrete beams: assessment of existing models, *Can. J. Civ. Eng.* 2010; 37(6): 855–865
- El Howary, H. A. and Mehanny, S. S. F. 2010. “Seismic vulnerability evaluation of RC moment frame buildings in moderate seismic zones” *journal of Earthquake Engng Struct. Dyn.* 40:215–235
- Ellingwood, B.R.; and Dusenberry, D.O.; 2005. Building Design for Abnormal Loads and Progressive Collapse, *Computer-Aided Civil and Infrastructure Engineering* 20, 194–205
- Ellingwood, B.R., Smilowitz, R., Dusenberry, D.O., Duthinh, D., Lew, H.S., Carino, N.J., 2007. Best practices for reducing the potential for progressive collapse in buildings. NIST 7396, 194p.
- Elnashai, A.S. and Mwafy, A.M. 2002. Overstrength and force reduction factors of multi-storey reinforced-concrete buildings. *Structural Design of Tall Building*, 11: 329–351
- El-Tawil, S., and Ortega-Rosales, J. 2004. Prestressing concrete using shape memory alloy tendons. *ACI Structural Journal*, 101: 846-851.

- Elwood , K.J.; and Eberhard, M.O.; 2006. Effective Stiffness of Reinforced Concrete Columns, *PEER Research Digest 2006-1*.
- Erduran, E. and Yakut , A.; 2007. “Vulnerability Assessment of Reinforced Concrete Moment Resisting Frame Buildings” *Journal of Structural Engineering, Vol. 133, No. 4, ASCE, ISSN 0733-9445/2007/4-576–586*.
- Falk, F. 1980. “Model Free-Energy, Mechanics and Thermodynamics of Shape Memory Alloys,” *ACTA Metallurgica, 28:1773–1780*.
- FEMA 2000a. Recommended seismic design criteria for new steel moment frame buildings, FEMA-350, SAC Joint Venture, *Federal Emergency Management Agency, Washington, D.C.*
- FEMA 2000b. Recommended seismic evaluation and upgrade criteria for existing welded steel moment frame buildings, FEMA-351, SAC Joint Venture, *Federal Emergency Management Agency, Washington, D.C.*
- FEMA 356, 2000. NEHRP Guidelines for the seismic rehabilitation of buildings. *Federal Emergency Management Agency. Washington DC.*
- FEMA 386-7. 2003. "Integrating Mad-Made Hazard into Mitigation Planning." Federal Emergency Management Agency (FEMA). *The U.S. Department of Homeland Security, September.*
- FEMA 426. 2003. "Reference Manual to Mitigate Potential Terrorist Attacks Against Buildings." Federal Emergency Management Agency (FEMA). *The U.S. Department of Homeland Security, December.*
- FEMA 427. 2003. "Primer for Design of Commercial Buildings to Mitigate Terrorist Attacks." Federal Emergency Management Agency (FEMA). *The U.S. Department of Homeland Security, December.*
- FEMA 428. 2003. "Primer to Design Safe School Projects in Case of Terrorist Attacks." Federal Emergency Management Agency (FEMA). *The U.S. Department of Homeland Security, December .*

- Ford DS, White SR. 1996. Thermomechanical Behavior of 55Ni45Ti Nitinol. *Acta Materialia*;44:2295.
- Frick, C.P., Ortega, A.M., Tyber, J., Gall, K., and Maier, H.J. 2004. Multiscale structure and properties of cast and deformation processed polycrystalline NiTi shape-memory alloys. *Metallurgical and Materials Transactions A: Physical Metallurgy and Materials Science*, 35: 2013-2025.
- Fujikura, S., Bruneau, M., Lopez-Garcia, D. 2008. Experimental investigation of multihazard resistant bridge piers having concrete-filled steel tube under blast loading. *Journal of Bridge Engineering, ASCE*, 13(6), 586-594.
- Fukuta, T., and Iiba, M. 2002. Experimental results on stress-strain relation Ti-Ni shape memory alloy bars and their application to seismic control of buildings. Summary, Resolution and Recommendations of the Seventh Management Panel on Collaboration Research Activities between JRC-IPSC J-NILIM and J-BRI, Japan, available at: http://www.nilim.go.jp/lab/bcg/siryou/tnn/tnnO_104pdf/ks010406.pdf, viewed on 11 May'06.
- Funakubo H. 1987. Shape Memory Alloys, *Gordon and Breach Science Publishers*.
- Furukawa, A., Takagi, T., Matsuki, H., Luo, Y., Hayashi, J., Yambe, T., Kamiyama, T., Amae, S., and Wada, M. 2006. Artificial sphincter. *United States Patent no. 6997952*.
- General Services Administration (GSA 2003). Progressive collapse analyses and design guideline for new federal office buildings and major modernization projects, GSA.
- Ghobarah, A. 2001. Performance-based design in earthquake engineering: state of development. *Engineering Structures*, 23(8): 878-884. Heidebrecht, A.C. 2003.
- Overview of seismic provisions of the proposed 2005 edition of the National Building Code of Canada. *Canadian Journal of Civil Engineering*, 30: 241–254.
- Goo, B.C., and LExcellent, C. 1997. Micromechanics-based modeling of two-way memory effect of a single crystalline shape-memory alloy, *Acta Materialia*, 45: 727-737.

- Govindjee, S. and Kasper, E. 1997. “A Shape Memory Alloy Model for Uranium-Niobium Accounting for Plasticity,” *Journal of Intelligent Material Systems and Structures*, 8:815–826.
- Govindjee, S. and Hall, G.J. 2000. “A Computational Model for Shape Memory Alloys,” *International Journal of Solids and Structures*, 37:735–760.
- Grierson, D.F.; Xu, L.; and Liu, Y.; 2005. Progressive-failure analysis of buildings subjected to abnormal loading, *Computer-Aided Civil and Infrastructure Engineering* 20 ; 155–171
- Hayes Jr.,J.R., Woodson,S.C., Pekelnicky,R.G., Poland,C.D., Corley,W.G., Sozen,M., (2005), Can strengthening for earthquake improve blast and progressive collapse resistance? *J. of Struct Eng.*, 131(8):1157-1177.
- Hibbet, Karlsson, and Sorensen, Inc., 2003. ABAQUS, version 6.4, <http://www.hks.com>.
- Hsu, S. E., Yeh, M. T., Hsu, I. C., Chang, S. K., Dai, Y. C., and Wang, J. Y. (2000). “Pseudo-elasticity and shape memory effect on the TiNi- CoV alloy.” *Mater. Sci. Forum*, 327–328, 119–122
- Huang, M., and Brinson, L.C. 1998. Multivariant model for single crystal shape memory alloy behaviour. *Journal of the Mechanics and Physics of Solids*, 46: 1379-1409.
- Humbeeck, V. J.; and Liu, Y. 2000. Shape memory alloys as damping materials. *Materials Science Forum (Shape Memory Materials)*, 327(3):331–338.
- Indirli, M., Castellano, M.G., Clemente, P., and Martelli, A. 2001. Demo-application of shape memory alloy devices: The rehabilitation of the S. Giorgio Church Bell-Tower. *Proceedings of SPIE, Vol. 4330, pp. 262-272.*
- Inel, M., Ozmen, H.B., and Bilgin, H. 2008. Re-evaluation of building damage during recent earthquakes in Turkey, *Engineering Structures*, 30(2): 412-427.
- Ioani, A.M.; and Cucu, H.L. 2010. Vulnerability to progressive collapse of seismically designed RC framed structures: corner column case, *Bul. Inst. Polit. Iași, t. LVI (LX), f. 4*
- Ivshin, Y. and Pence, T.J. 1994. “A Constitutive Model for Hysteretic Phase Transition Behavior,” *International Journal Engineering Science*, 32:681–704.

- Jackson, C. M.; Wagner, H. J.; Wasilewski, R. J. 1972. 55-Nitinol—The alloy with a memory: Its physical metallurgy, properties and applications, *Tech. Rep. NASA SP-5110, NASA Technology Utilization Office, Washington, D.C.*
- James, R.D. 2000. “New Materials from Theory: Trends in the Development of Active Materials,” *International Journal of Solids and Structures*, 37:239–250.
- Janke, L., Czaderski, C, Motavalli, M., and Ruth, J. 2005. Applications of shape memory alloys in civil engineering structures - overview, limits and new ideas. *Materials and Structures/Materiaux et Constructions*, 38: 578-592.
- Jian,Z.; and Ping, T.; 2009. A displacement base seismic vulnerability of RC buildings in SCE, *International conference on engineering computation (ICEC) 978-0-7695-3655*.
- Jung, M.S. 2006. Microactuator and fluid transfer apparatus using the same. *United States Patent no. 7128403*.
- Kim, J. and Choi, H. 2005. Response modification factors of chevron braced frames, *Engineering structures* 27:285-300
- Kannel, J., French, C, and Stolarski, H. 1997. Release methodology of strands to reduce end cracking in pretensioned concrete girders. *PCI Journal*, 42: 42-54.
- Khandelwal, K., El-Tawil, S. 2008. Assessment of progressive collapse residual capacity using pushdown analysis, *Crossing the Borders*, 314.
- Khandelwal, K., El-Tawil, S., Kunnath, S.K., Lew, H.S., 2008. Macromodel-based simulation of progressive collapse: Steel frame structures. *J. of Struct. Eng.*, 134(7):1070-1078.
- Kumar, P. K. ; and Lagoudas, D. C., 2008. Introduction to Shape Memory Alloys, Shape memory Alloys, DOI: 10.1007/978-0-387-47685-8 1, © Springer Science+Business Media, LLC
- Kuribayashi, K., Tsuchiya, K., You, Z., Tomus, D., Umemoto, M., Ito, T., Sasaki, M., 2006. Self-deployable origami stent grafts as a biomedical application of Nitinol shape memory alloy foil. *Materials Science and Engineering A* 419 (1–2), 131–137.
- Leclerq, S., Bourbon, G. and Lexcellent, C. 1995. “Plasticity Like Model of Martensite Phase Transition in Shape Memory Alloys,” *Journal de Physique IV*, 5:513–518.

- Lee, L.H., Han, S.W., and OH, Y.H. 1999. Determination of ductility factor considering different hysteretic models. *Earthquake engineering & structural dynamics*, 28(9):957-977.
- Liang, C, and Rogers, CA. 1990. One-dimensional thermomechanical constitutive relations for shape memory materials. Collection of Technical Papers AIAA/ASME/ASCE/AHS Structures, Structural Dynamics & Materials Conference, pp.16-28.
- Liang, C. and Rogers, C.A. 1990. “One-Dimensional Thermomechanical Constitutive Relations for Shape Memory Materials,” *Journal of Intelligent Material Systems and Structures*, 1:207–234.
- Liao, W. I.; and Mo, Y.L.; 2006. Shake table tests of rc frame with shape memory alloys bracings bars, *4th International Conference on Earthquake Engineering Taipei, Taiwan*
- Lim, T. J., and McDowell, D.L. 1999. Mechanical behaviour of an Ni-Ti shape memory alloy under axial-torsional proportional and nonproportional loading. *Journal of Engineering Materials and Technology, Transactions of the ASME*, 121: 9-18.
- Liu, Y., Xie, Z., Humbeeck, J.V. and Delaey, L. 1998. Asymmetry of stress-strain curves under tension and compression for NiTi shape memory alloys. *Acta Materialia*, 46: 4325-4338.
- Liu, Y., Xie, Z., and Van Humbeeck, J. 1999. Cyclic deformation of NiTi shape memory alloys. *Materials Science and Engineering A: Structural Materials: Properties, Microstructure and Processing*, A273-275: 673-678.
- Liu, Y., and Favier, D. 2000. Stabilisation of martensite due to shear deformation via variant reorientation in polycrystalline NiTi. *Acta Materialia*, 48: 3489-3499.
- Liu, Y. 2003. Mechanical and thermomechanical properties of a Ti50Ni25Cu25 melt spun ribbon. *Materials Science and Engineering A*, 354: 286-291.
- Luccioni, B.M., Ambrosini, R.D., Danesi, R.F. 2004. Analysis of building collapse under blast loads. *Engineering Structures*, 26(1), 63-71.
- Luco, N. and Cornell, C.A., 1998. “Effects of Random Connection Fractures on the Demands and Reliability for a 3-Story Pre-Northridge SMRF Structure”, *Proc. 6th U.S. National Conference on Earthquake Engineering, Seattle, Washington, June, 1998*.

- Ma, N., Song, G., and Tarefder, R.A. 2004. Vibration control of a frame structure using shape memory alloy braces. *Proceedings of the 3rd International Conference on Earthquake Engineering, Nanjing University of Technology, China, Chapter 4, Paper No. 12.*
- Ma, N., and Song, G. 2005. Study of damping capacities of nitinol shape memory alloys in martensite, austenite, and martensite-austenite co-existence phases. *Proceedings of SPIE~the international society for optical engineering, Vol. 5760, pp. 142-151.*
- Maji, A.K., and Negret, I. 1998. Smart prestressing with shape memory alloy. *Journal of Engineering Mechanics, 124: 1121-1128.*
- Manach, P.-Y., and Favier, D. 1997. Shear and tensile thermomechanical behavior of near equiatomic NiTi alloy. *Materials Science & Engineering A: Structural Materials: Properties, Microstructure and Processing, A222: 45-57.*
- Mander J.B., Priestley M.J.N., Park R. 1988. "Theoretical stress-strain model for confined concrete," *Journal of Structural Engineering, Vol. 114, No. 8, pp. 1804-1826.*
- Mao, C, and Li, H. 2004. Experimental investigation of shape memory alloy as passive energy dissipation device for seismic response reduction of buildings. *Proceedings of the Third International Conference on Earthquake Engineering, Nanjing, China, 2004, Chapter no. 4, Paper no. 22.*
- Marjanishvili, S.M. 2004. Progressive analysis procedure for progressive collapse; *Journal of Performance of Constructed Facilities, 18(2), 79-85.*
- Marjanishvili, S.; Agnew, E.,2006. Comparison of various procedures for progressive collapse analysis. *Journal of Performance of Constructed Facilities, 20(4), 365-374.*
- Martinez-Rueda J.E., Elnashai A.S. 1997. "Confined concrete model under cyclic load," *Materials and Structures, Vol. 30, No. 197, pp. 139-147.*
- Mazzolani, F.M., and Mandara, A. 2002. Modern trends in the use of special metals for the improvement of historical and monumental structures. *Engineering Structures, 24: 843-856.*

- McCormick, J.; DesRoches, R.; Fugazza, D.; and Auricchio, F.; 2007. Seismic assessment of concentrically braced steel frames with shape memory alloy braces, *Journal of structural engineering @ASCE*, Vol. 133, No. 6 ISSN 0733-9445/2007/6-862–870
- McNaney, J.M., Imbeni, V., Jung, Y., Papadopoulos, P., and Ritchie, R.O. 2003. An experimental study of the superelastic effect in a shape-memory nitinol alloy under biaxial loading. *Mechanics of Materials*, 35: 969-986.
- Melton, K.N. 1990. Ni-Ti based shape memory alloys. Duerig TW, Melton KN, Stoeckel D, Wayman CM, editors. *Engineering aspects of shape memory alloys*. London: Butterworth-Heinemann Ltd, pp. 21-35.
- Melton, K.R.; 1999. General applications of shape memory alloys and smart materials, in: K. Otsuka, C. M. Wayman (Eds.), *Shape Memory Materials*, Cambridge University Press, Cambridge, Ch. 10, pp. 220–239.
- Miller, A. 2005. Multi-fastener surgical apparatus and method. *United States Patent no. 6837893*.
- Miranda, E. and Bertero, V. V. 1994 "Evaluation of strength reduction factors for earthquakeresistant design," *Earthq. Spectra* 10(2), 357-379.
- Mitchell, D, Tremblay, R, Karacabeyli, E, Paultre, P, Saatcioglu M, and Anderson, D.L. 2003. Seismic force modification factors for the proposed 2005 edition of the National Building Code of Canada. *Canadian Journal of Civil Engineering*, 30: 308–327.
- Mitchell, D. and Paulter, P. 1994. Ductility and overstrength in seismic design of reinforced concrete structures. *Canadian Journal of Civil Engineering*, 21: 1049–1060.
- Miyazaki, S., Imai, T., Igo, Y., and Otsuka, K. 1986. Effect of cyclic deformation on the pseudoelasticity characteristics of Ti-Ni alloys. *Metallurgical Transactions. A*, 17A: 115-120.
- Mwafy AM, Elnashai AS. 2002. Calibration of force reduction factors of RC buildings, *Journal of Earthquake Engineering*, Vol. 6, No. 2 . 234-273, @ Imperial College Press
- Moser, K.; Bergamini, A; Christen R and Czaderski C 2005. Feasibility of concrete prestressed by shape memory alloy short fibers, *Mater. Struct.* 38 593–600

- Motta, L.B., Guille´n, L.L., Mamiya, E.N. and Vianna, D.M. 1999. ‘‘A Study on the Hardening in Particular Model for Pseudoelastic Materials,’’ *In: Proceedings of the 15th Brazilian Congress of Mechanical Engineering.*
- Muller, I. and Xu, H. 1991. ‘‘On the Pseudo-Elastic Hysteresis,’’ *ACTA Metallurgical Materials*, 39(3):263–271.
- Naumoski, N., Tso, W.K. & Heidebrecht, A.C., A selection of representative strong motion earthquake records having different A/V ratios, *EERG Report 88-01, Earthquake Engineering Research Group, Dept. of Civil Engg., McMaster University, Hamilton, ON Canada 1988.*
- NBCC 2005. National Building Code of Canada, Canadian Commission on Building and Fire Codes. *National Research Council of Canada, Ottawa.*
- Norton, K.H. 1998. Disk drives. United States Patent no. 5808837.
- Ocel, J., DesRoches, R., Leon, R.T., Hess, W.G., Krumme, R., Hayes, J.R. and Sweeney, S. 2004. Steel beam column connections using shape memory alloys. *ASCE Journal of Structural Engineering*, 130(5): 732-740.
- Orgeas, L., and Favier, D. 1995. Non-symmetric tension-compression behaviour of NiTi alloy. *Journal De Physique. IV: JP, 5: 605-610.*
- Orgeas, L., Liu, Y., and Favier, D. 1997. Experimental study of mechanical hysteresis of NiTi during ferroelastic and superelastic deformation. *Journal De Physique. IV : JP, 7:C5-477-C5-482.*
- Otani S, Hiraishi H, Midorikawa M. 2000. Development of smart systems for building structures. *Proceedings of SPIE ;3988:2–9.*
- Otsuka, K. and Wayman, CM. 1999. Shape memory materials, 1st Paperback Edition, *Cambridge University Press, Cambridge.*
- Parra-Montesinos, G.J., Canbolat, B.A., and Jeyaraman, G.R. 2006. Relaxation of confinement reinforcement in structural walls through the use of fiber reinforced cement composites. *Proceedings of the 8th U.S. National Conference on Earthquake Engineering, Paper No. 1394.*

- Patoor, E., Eberhardt, A., and Berveiller, M. 1994. Micromechanical modelling of the shape behaviour. American Society of Mechanical Engineers, *Applied Mechanics Division, AMD, Mechanics of Phase Transformations and Shape Memory Alloys, Vol. 189, pp. 23-37.*
- Patoor, E., Eberhardt, A., and Berveiller, M. 1996. Micromechanical modelling of superelasticity in shape memory alloys. *Journal De Physique. IV: JP, 6: C1-277-C1-292.*
- Paulay T, Priestley M N J. Seismic Design of Reinforced Concrete and Masonry Buildings. *John Wiley & Sons, Inc., New York, 1992.*
- Perkins, J. 1975. Shape Memory Effects in Alloys, *Plenum Press, New York,*
- Pilehchianlangroodi, B., Mirnezami, A., Zakeri, A.A., 2008. Utilizing front wall of blast resistant building as an entrance fuse of energy. *Proc. of the 2008 Struct Congress, ASCE, 314:10p.*
- Priestley MJN 1998. Displacement based approaches to rational limit states of new structures. *Proceeding of the 11th European conference on earthquake engineering, Rotterdam.AA.Blakema.*
- Razaqpur, A.G. Tolba, A. Contestabile, E., 2007. Blast loading response of reinforced concrete panels reinforced with externally bonded GFRP laminates. *Composites Part B: Eng, 38(5-6):535-546.*
- Rejzner, J., Lexcellent, C, and Raniecki, B. 2002. Pseudoelastic behaviour of shape memory alloy beams under pure bending: Experiments and modelling. *International Journal of Mechanical Sciences, 44: 665-686.*
- Rossetto, T.; and Elnashai, A.; 2005. Analytical procedure for the deviation of displacement based vulnerability for populations of RC structures, *Engineering structure 27-397-409*
- Rossettoa, T.; and Elnashai, A.; 2005. “A new analytical procedure for the derivation of displacement-based vulnerability curves for populations of RC structures” *Journal of Engineering Structures 27,P397–409*
- Saatcioglu, M., Ozbakkaloglu, T., Naumoski, N., Lloyd, A., 2009. Response of earthquake-resistant reinforced-concrete buildings to blast loading. *Canadian J. of Civil Eng., 36(8):1378-1390.*

- Sabelli, R. 2001. Research on improving the design and analysis of earthquake-resistant steel-braced frames, *The 2000 NEHRP Professional Fellowship Report, Earthquake Engineering Research Institute, USA*.
- Saiidi, M.S. and Wang, H. 2006. Exploratory study of seismic response of concrete columns with shape memory alloys reinforcement. *ACI Structural Journal*, 103(3): 435-442.
- Saiidi MS, Zadeh MS, Ayoub C, and Itani A. 2007. Pilot study of behavior of concrete beams reinforced with shape memory alloys. *J Mater Civil Eng, ASCE*; 19(6):454-46
- Sakai, Y., Kitagawa, Y., Fukuta, T., and Iiba, M. 2003. Experimental study on enhancement of self-restoration of concrete beams using SMA wire. Proceedings of SPIE – *The International Society for Optical Engineering*, Vol. 5057, pp. 178-186.
- Salichs, J., Hou, Z., and Noori, M. 2001. Vibration suppression of structures using passive shape memory alloy energy dissipation devices. *Journal of Intelligent Material Systems and Structures*, 12: 671-680.
- SAP 2000 Advanced 14.0 structural analysis program, computers and structures, Inc. 1995 *University Ave. Berkeley, CA, 94704*.
- Sasani, M.; Bazan, M., Sagioglu, S. 2007. Experimental and analytical progressive collapse evaluation of actual reinforced concrete structure. *ACI Structural Journal*, 104(6), 731- 739.
- Sasani, M.; and Kropelnicki, J.; 2008. Progressive collapse analyses of an RC structure, *Journal of Structural Design of Tall and Special Building*. DOI: 10.1002/tal.375, 17, 757–771
- Sawaguchi, T., Sahu, P., Kikuchi, T., Ogawa, K., Kajiwara, S., Kushibe, A., Higashino, M., Ogawa, T., 2006. Vibration mitigation by the reversible fcc/ hcp martensitic transformation during cyclic tension-compression loading of an Fe–Mn–Si-based shape memory alloy. *Scripta Mater*. 54 (9), 1885– 1890.
- SeismoStruct Help file. 2004. Version 3.1.0. accessed on Jan, 2006, available at <http://www.seismosoft.com/SeismoStruct/index.htm>.
- Shome, N., Cornell, C. A., Bazzurro, P., and Carballo, J. 1998. “Earthquake, records, and nonlinear MDOF responses,” *Earthquake Spectra* 14(3), 469–500.

- Shome, N. and Cornell, C. A. 1999. Probabilistic seismic demand analysis of nonlinear structures, *RMS Report-35, Reliability of Marine Structures Group, Stanford University, Stanford.*
- Silva, E.P. 1995. “Mechanical Modeling of Stress Induced Phase Transformation in Solids,” M.Sc. Dissertation, University of Brasilia – *Department of Mechanical Engineering (in portuguese).*
- Shahin, A. R., Meckl, P. H., and Jones, J. D. 1997. Modeling of SMA tendons for active control of structures. *Journal of Intelligent Material Systems and Structures*, 8: 51-70.
- Shirmohamadi, M. 2005. Sag compensating device for suspended lines. *Unites States Patent no.6864421.*
- Song, G., Mo, Y.L., Otero, K. and Gu, H. 2005. Develop intelligent reinforced concrete structures using shape memory alloys and piezoceramics. *Proceedings of the 3rd International Conference on Earthquake Engineering, China, Chapter 5, Paper No. 11*
- Song, G., Ma, N., and Li, H.-N. 2006. Application of shape memory alloys in civil structures. *Engineering Structures*, 28: 1266-1274.
- Souza, A.C., Mamiya, E.N. and Zouain, N. 1998. “Three-Dimensional Model for Solids Undergoing Stress-Induced Phase Transformations,” *European Journal of Mechanics A – Solids*, 17:789–806.
- Soroushian, P., Ostowari, K., Nossoni, A., and Chowdhury, H. 2001. Repair and strengthening of concrete structures through application of corrective posttensioning forces with shape memory alloys. *Transportation Research Record*, 1770: 20-26.
- Strnadel, B., Ohashi, S., Ishihara, T., Ohtsuka, H., and Miyazaki, S. 1995. Cyclic stress-strain characteristics of Ti-Ni and Ti-Ni-Cu shape memory alloys. *Materials Science and Engineering: A*, 202: 148-156.
- Sun, Q.P., and Hwang, K.C. 1993. Micromechanics modelling for the constitutive behavior of polycrystalline shape memory alloys. I. Derivation of general relations. *Journal of the Mechanics and Physics of Solids*, 41: 1-17.

- Sun, S.; and Rajapakse, R.K.N.D.; 2003. Dynamic response of a frame with SMA bracing, *Smart Structures and Materials: Active Materials: Behavior and Mechanics, Proceedings of SPIE Vol. 5053*
- Sawaguchi T, Kikuchi T, Ogawa K, Kajiwara S, Ikeo Y, Kojima M and Ogawa T 2006. Development of prestressed concrete using Fe–Mn–Si-based shape memory alloys containing NbC Mater. *Trans.* 47 580–3
- Tamai, H., and Kitagawa, Y. 2002. Pseudoelastic behaviour of shape memory alloy wire and its application to seismic resistance member for building. *Computational Materials Science*, 25:218-227.
- Tamai, H., Miura, K., Kitagawa, Y., and Fukuta, T. 2003. Application of SMA rod to exposed-type column base in smart structural system. *Proceedings of SPIE -Structures and Materials 2003: Smart Systems and Nondestructive Evaluation, Vol.5057, pp. 169-177.*
- Tanaka, K., and Nagaki, S. 1982. Thermomechanical description of materials with internal variables in the process of phase transitions. *Ingenieur-Archiv*, 51: 287-299.
- Todoroki, A.; Kumagai, K.; Matsuzaki, R.; 2009. Self-deployable space structure using partially flexible CFRP with SMA wires, *Journal of Intelligent Material Systems and Structures* August 2009 vol. 20 no. 12 1415-1424
- Tsai, M.-H., and Lin, B.-H. 2008. Investigation of progressive collapse resistance and inelastic response for an earthquake-resistant RC building subjected to column failure. *Engineering Structures*, 30(12), 3619-3628.
- Tsitos, A.; Mosqueda, G.; Filiatrault, A.; and Reinhorn, A. M.; 2008. Experimental investigation of progressive collapse of steel frames under multi-hazard extreme loading. *The 14th World Conference on Earthquake Engineering October 12-17, 2008, Beijing, China*
- Uang, C.M. 1991. Establishing R (or R_w) and C_d factors for building seismic provisions. *ASCE Journal of Structural Engineering*, 117(1): 19–28.
- UFC 4-023-03, Design of Buildings to resist progressive collapse 2005. Unified Facilities Criteria, US 2005.

- Ullakko, K. 1996. Magnetically controlled shape memory alloys: a new class of actuator materials. *Journal of Materials Engineering and Performance, ASM International*, 5:405-409.
- Uniform Building Code (UBC), 1997. was first enacted by the International Conference of Building Officials (ICBO)
- Uriz, P. and Mahin, S. A. 2004. "Seismic Performance assessment of concentrically braced steel frames," *Proc. of the 13th World Conf. on Earthquake Eng., Vancouver, Canada, Paper No. 1639.*
- U.S. Department of Army (DA) FM 3-19.30 "Physical Security" Document,
- Vamvatsikos, D. and Cornell, C. A. 2002. "Incremental dynamic analysis," *Earthquake Engineering & Structural Dynamics* 31(3), 491–514.
- Vamvatsikos, D. and Cornell, C. A. 2004. "Applied incremental dynamic analysis," *Earthquake Spectra* 20(2), 523–553.
- Vivet, A., Orgeas, L., Lexcellent, C, Favier, D., and Bernardini, J. 2001. Shear and tensile pseudoelastic behaviours of CuZnAl single crystals. *Scripta Materialia*, 45: 33-40.
- Vlassis, A.G. 2007. Progressive collapse assessment of tall buildings. *PhD thesis, Department of Civil Engineering, University of London.*
- Vokoun D and Stalmans R 1999. Recovery stresses generated by NiTi shape memory wires SPIE's 6th Annu. Int. Symp. on Smart Structures and Materials (Newport Beach, CA, 1999) (Bellingham,WA: SPIE Optical Engineering Press)
- Wang, H., 2004. A study of RC columns with shape memory alloy and engineered cementitious composites. *M.Sc. Thesis, University of Nevada, Reno, USA.*
- Wilde, K., Gardoni, P. and Fujino, Y. 2000. Base isolation system with shape memory alloy device for elevated highway bridges. *Engineering Structures*, 22: 222–229.
- Wilson, J.C. and Wesolowsky, M.J. 2005. Shape memory alloys for seismic response modification: A state-of-the-art review. *Earthquake Spectra*, 21: 569-601
- Yagob, O., Galal, K., Naumoski, N., 2009. Progressive collapse of reinforced concrete structures. *J. of Struct. Eng. and Mechanics*, 32(6): 771-786.

- Yi, W.J., He, Q. F., Xiao, Y., Kunnath, S. K. 2008. Experimental study on progressive collapse-resistant behavior of reinforced concrete frame structures. *ACI Structural Journal*, 105(4), 433- 439.
- Youssef MA, Alam MS, Nehdi M. 2007. Experimental investigation on the seismic behaviour of beam-column joints reinforced with superelastic shape memory alloys. *Journal of Earthquake Engineering*, submitted for publication April.
- Yun, S., Hamburger, R. O., Cornell, C. A., and Foutch, D. A. (2002) ‘‘Seismic performance evaluation for steel moment frames,’’ *Journal of Structural Engineering* 128(4), 534–545.
- Zak, A.J., Cartmell, M.P., Ostachowicz, W.M., and Wiercigroch, M. 2003. One-dimensional shape memory alloy models for use with reinforced composite structures. *Smart Materials and Structures*, 12: 338-346.